

**Rutherford Scattering and GeLi Detection**

A Major Qualifying Project Report

submitted to the Faculty

of the

WORCESTER POLYTECHNIC INSTITUTE

in partial fulfillment of the requirements for the

Degree of Bachelor of Science

by

---

Joseph Mullin

---

Dericc Orso

---

Matthew Silva Sa

Date: January 16, 2009

Approved:

---

Professor Rafael Garcia, Advisor

---

Professor Germano Iannacchione, Advisor

---

Professor Suzanne L. Weekes, Advisor

### **Abstract**

Radiation detection is an important part of understanding our physical world. After repairing the WPI GeLi gamma ray detector, we tested soil samples from around campus for the effective radiation doses sustained by an average person, showing that the WPI dose is below the national average. The Rutherford scattering experiment explores the interaction of  $\alpha$ -particles with nuclei and the basic scientific principles involved. We used a mathematical model of the Rutherford experiment and obtained results using the classical Runge-Kutta method and the Dormand-Prince embedded pair method with MATLAB. Comparing the simulated data with known results unites the mathematical theories with experimental practice.

## **Acknowledgments**

Dericc, Joseph, and Matthew would like to thank Professors Garcia, Iannacchione, and Weekes for their support during this project. In addition they would like to thank graduate student Marco Kaltofen for his advice and sample contributions.

Individually Dericc would like to thank all those who helped him through his MQP and time at WPI as well as his parents and friends for helping him make it here. Joseph would like to thank his parents, Joseph Mullin and Kathleen Mullin for their love. Joseph would also like to thank all of his friends, most notably Chad Mondor. Matthew would like to thank his fiancée, Michaela Prouty, his parents, Margaret and Edilson Silva Sa, family, and friends for their constant love and support through the project and his time at WPI. Matthew would also like to thank Dericc and Joseph for their hard work and contributions to this project.

# Contents

<b>1</b>	<b>Introduction</b>	<b>1</b>
<b>2</b>	<b>Background</b>	<b>3</b>
2.1	Rutherford's Scattering Experiment . . . . .	3
2.2	Alpha Decay and Detection . . . . .	4
2.3	Rutherford Scattering . . . . .	5
2.4	Gamma Ray Emission and Detection . . . . .	6
<b>3</b>	<b>Experiment</b>	<b>8</b>
3.1	Rutherford Scattering . . . . .	8
3.2	Coulomb Scattering Model Derivation . . . . .	9
3.2.1	Nondimensionalization . . . . .	10
3.2.2	System of First Order Differential Equations . . . . .	11
3.2.3	Numerical Modeling with MATLAB . . . . .	12
3.3	Numerical Experiment: Process and Methods . . . . .	14
3.3.1	Rutherford Scattering Numerical Experiment . . . . .	14
3.3.2	AlphaScat.m . . . . .	15
3.3.3	AlphaCount.m and AlphaCount.m . . . . .	19
3.4	Numerical Rutherford Scattering Experiment Procedure . . . . .	26
3.4.1	'Atom' Numerical Experiment . . . . .	26
3.4.2	'Foil' Numerical Experiment . . . . .	26
3.5	GeLi Detection . . . . .	27
<b>4</b>	<b>Analysis</b>	<b>31</b>
4.1	Total Radiation Effect . . . . .	31
4.2	Radioactive Object Results . . . . .	35
4.3	Rutherford Theoretical Data Analysis . . . . .	40
<b>5</b>	<b>Conclusions</b>	<b>47</b>
<b>6</b>	<b>Appendices</b>	<b>49</b>
6.1	Alpha Scattering Experiment Setup in Pictures . . . . .	49
6.2	Alpha Scattering Lab Procedure . . . . .	55
6.2.1	Rutherford Scattering Experiment . . . . .	55
6.2.2	Alpha Detector Experimental Procedure . . . . .	55
6.3	Dirt Sample Graphs . . . . .	57

6.4	GeLi Instructions . . . . .	76
6.5	Radioactive Sample Data . . . . .	76
6.6	MATLAB Code . . . . .	82
6.6.1	AlphaScat.m . . . . .	82
6.6.2	AlphaCount.m . . . . .	93
6.6.3	AlphaPlot.m . . . . .	96
6.6.4	Depth Calculation Code . . . . .	104

# List of Tables

3.1	These are the constants used to adapt the model to the nondimensionalized form. . . . .	10
3.2	Target material characteristics used in AlphaScat.m. . . . .	15
3.3	Default values for the arguments of AlphaScat.m . . . . .	16
3.4	This table shows the run times for both the 'Atom' experiments and 'Foil' experiments. . . .	18
3.5	This shows the times per particle for each experiment depicted in Table 3.4. . . . .	19
3.6	MultiNuclide Test Data - 50 Hours . . . . .	28
4.1	Calculated Dirt Sample Data . . . . .	36
6.1	Peak data for Chernobyl button. . . . .	77
6.2	Peak data for the Columbia River sand sample. . . . .	77
6.3	Peak data for the Ganges River sediment sample. . . . .	78
6.4	Peak data for the LAO 1175 sample from Los Alamos. . . . .	78
6.5	Peak data for the mesa soil sample from Los Alamos. . . . .	79
6.6	Peak data for Takedu Solods sample from Los Alamos. . . . .	80
6.7	Peak data for trailer dust sample from Los Alamos. . . . .	81

# List of Figures

2.1	Alpha particle scattering Top: plum pudding model. Bottom: Rutherford Scattering model[9]	4
2.2	The trajectory of an $\alpha$ -particle experiencing Rutherford scattering [14]	5
3.1	This figure, time step size versus the magnitude of the $x$ -position, shows how the step size changes as an $\alpha$ -particle moves through the foil.	18
3.2	This is an example of a 'Foil' experiment trajectories plot, where 499 particles are incident upon a 47 layers of 97 Gold nuclei.	20
3.3	This is an example of a 'Foil' experiment angle distribution plot, where 997 particles are incident upon a 21 layers of 21 Gold nuclei.	21
3.4	This is an example of a 'Atom' experiment trajectories plot, where 25 particles are incident upon an Aluminum nucleus.	22
3.5	This is an example of a 'Atom' experiment magnitudes plot, where 25 particles are incident upon an Aluminum nucleus.	23
3.6	This is an example of a 'Atom' experiment energies plot, where 25 particles are incident upon an Aluminum nucleus.	24
3.7	This is an example of a 'Atom' experiment angle distribution plot, where 101 particles are incident upon an Aluminum nucleus.	25
3.8	Measured Efficiency Curve for GeLi Detector.	28
3.9	Soil Sample Locations	29
4.1	Graph of percent error in the linear assumption of energy conversion.	32
4.2	Radiation Levels around WPI Campus in mSieverts. The average yearly total from external radiation is 3.00	37
4.3	Effective doses of radiation before correction for each area along with national and WPI averages.	38
4.4	Actual Radiation absorbed by a person using efficiency corrections along with national and WPI averages.	39
4.5	Plot of Counts per angle for 997 incident particles on Au Foil. The theoretical data is represented by the solid red line and the the experimental data is represented by the blue circles.	41
4.6	Plot of counts per atomic number <sup>2</sup>	42
4.7	Plot of counts per number of incident particles for all different foils.	43
4.8	Trajectory of particles for 449 incident particles on Au foil that is 29 atoms thick.	43
4.9	Trajectory of particles for 449 incident particles on Au foil that is 47 atoms thick.	44
4.10	Plot of counts per thickness for all foils.	45
4.11	Trajectory of particles for 499 incident particles on Au that is 37 atoms wide.	45
4.12	Trajectory of particles for 499 incident particles on Au that is 79 atoms wide.	46

4.13	Plot of counts per width for all foils. . . . .	46
6.1	Full setup of the Rutherford Scattering Experiment. On the left there is a standard Ortec electronic counter. In the middle is the control box for the setup. There is a switch for rotating the sample wheel, and a switch for moving the detector through a range of angles. . . . .	49
6.2	Rutherford Control Switch. The left switch rotates the thin film wheel, while the right switch moves the detector through a range of angles. . . . .	50
6.3	The counter and control box are connected to the main section of the experiment setup via cables into the following connector. . . . .	50
6.4	The back part of this connector shown below, is connected to the main detector housing, and the wiring on the back was removed and re-soldered to ensure that it is working. . . . .	51
6.5	These connections are connected into the vacuum chamber through a contact plate on the under side seen here. . . . .	51
6.6	All the connections lead to the main region of the connector which contains a wheel to hold thin material samples, a detector to detect alpha rays, and a holder for the alpha ray sample. . . . .	52
6.7	The Sample is held in place by this plate with two screws to project the $\alpha$ -particles directly forward through the thin film wheel. . . . .	52
6.8	The sample wheel seen here is used to hold thin material films a few atoms thick in order to measure the deflection created by the nuclei of the atom. In addition the protractor is used in relation to the detector arm to determine the angle of deflection being measured. . . . .	53
6.9	The detector connections were also re-soldered to ensure that they were working properly. . . . .	53
6.10	This is connected to the previous region via a BNC connection and registers when an $\alpha$ -particle hits it. This is the section of the device that we have determined to be malfunctioning. . . . .	54
6.11	When the entire device is assembled a bell jar is placed over the detection devices, and a light dampening cover is placed on top of that. The setup is hooked to a vacuum pump and a vacuum is created in order to ensure that there are no loose particles floating around. . . . .	54

# Chapter 1

## Introduction

The goal of this project is to repair, calibrate and test the nuclear equipment we have taken from the old WPI Nuclear reactor. We will obtain an experimental setup that is intended to showcase Ernest Rutherford's Alpha Scattering principles as well as a Germanium-Lithium (GeLi) detector that is used to measure gamma radiation. We will explore the theoretical and experiment sides of these phenomena in an attempt to gain further understanding of them, and will provide lab procedures and documentation on how to run them.

To approach the experiments, both will be considered independently, each in their own laboratories and each different experiment in their own rights. For the Rutherford scattering experiment, we will put the assembly together and test it. We will troubleshoot errors and complications in a scientific manner. We will create a lab experiment for use in courses once the equipment is fully operational. In addition, we will create a mathematical model of how Rutherford scattering should work, using various numerical methods, such that any experimental data can be tested against the model for accuracy. The data from this model will also be tested against Rutherford's theories to determine its accuracy. Both the model data and the procedure of how to conduct the experiment will prove useful in future experiments.

In terms of the GeLi detector, we plan to get the device entirely running and calibrate its energy detection system. We will collect soils samples from around campus in order to measure the various radiation levels, and use this data to calculate the average radiation dosage a person receives from that soil. By combining this data with the efficiency data for the detector, we will find the effective dose a person receives. In addition to these samples, we will test various international radiation samples to identify notable, unique isotopes in each one.

The GeLi device is in perfect working order with instructions on how to use it as it is now and how it could be made better in the future. The Rutherford device, though still not operational, is in a state where it could easily be made operational and all data can be verified through the use of the model. The paper that follows is a clear demonstration of nuclear physics theories and experimental procedure.

In Chapter 2 we introduce the theory and practice behind Rutherford scattering and GeLi detection. We discuss the nature of alpha and gamma particles as well as a brief history of the Rutherford scattering experiment. In Chapter 3 we discuss the methods and procedures for both Rutherford scattering and GeLi detection. We develop the mathematical model used for the numerical Rutherford scattering experiment, and describe the numerical methods used. This chapter establishes the basis for the analysis and results of the report. In Chapter 4 we analyze the collected data from both the numerical Rutherford scattering experiment as well as the GeLi gamma ray detection. Here, the radiation detected from the WPI soil samples are determined to be well within the national averages, while data from several international samples reveal interesting radioactive isotopes. We use the data from the numerical Rutherford scattering experiment, to

verify and repeat Rutherford's original findings. In Chapter 5, we explain what we have accomplished and determine steps that can be made in the future on this project. We analyze any errors or assumptions that we might have made. Finally we evaluate whether or not we have achieved our goals.

## Chapter 2

# Background

This chapter of our report contains background information to introduce the theory and practice that will occur in later chapters. We discuss the nature of alpha and gamma particles as well as a brief history of the Rutherford scattering experiment.

### 2.1 Rutherford's Scattering Experiment

In this section we will discuss the history of the experiment created by Ernest Rutherford and the scientific context associated with it. We will see how it helped revolutionize the idea of an atom.

In the early 1900s scientists discovered the particle that we call the electron. Until this time there was little understanding of the structure of an atom. The primarily accepted model was the plum pudding model, as proposed by physicist J.J. Thompson [9]. In this model the negatively charged electrons were distributed throughout a positively charged sphere which led to an overall charge balance. The idea was that it was very similar to a plum pudding, where plums (electrons) are distributed throughout the pudding (protons) in order to have no charge [9].

Ernest Rutherford, a nuclear scientist who worked around the same time as Thompson, carried out experiments to further understand the nature of the atom. Under the direction of Rutherford, Hans Geiger and Ernest Marsden performed an experiment in 1909 that helped disprove the plum pudding theory of the atom [9]. In this experiment,  $\alpha$ -particles, which are positively charged, through a piece of gold leaf that was only atoms thick. If the plum pudding model was correct, these positively charged particles should encounter minor scattering throughout the whole of the positive shell around the electrons. Yet, the result of the experiment had most of these  $\alpha$ -particles going through unaltered, while some were scattered backwards at angles above 90 degrees [10]. See Figure 2.1. From this, Rutherford concluded that there must be some single massive positively charged particle somewhere in the atom.

This discovery led to the Rutherford model of the atom, which consists of a large positively charged nucleus surrounded by an equally charged number of electrons which orbit around it. In 1913 this model was further refined by scientist Niels Bohr. Using advanced combinations of classical and quantum mechanics he was able to provide an accurate model of the way that electrons would be able to orbit this massively charged nucleus and not decay. The Bohr model is still popularly used today as a conceptual way to model the hydrogen atom.

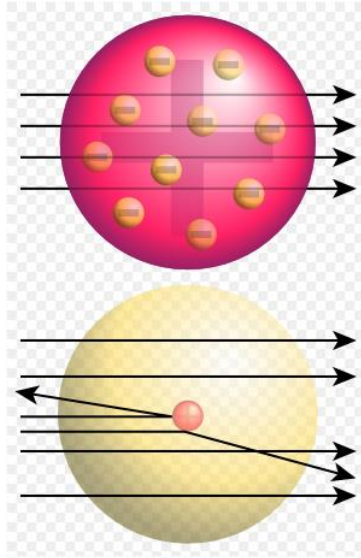


Figure 2.1: Alpha particle scattering Top: plum pudding model. Bottom: Rutherford Scattering model[9]

## 2.2 Alpha Decay and Detection

In this section, we will discuss what an alpha particle is. We will determine the nature of an alpha particle as well as how it is created. Finally we will discuss how Rutherford detected alpha particles as well as how we will detect them in the lab.

At the time Rutherford conducted his experiment, there were only three known emitted subatomic particles, the alpha particle or helium nucleus, the beta particle or high energy electron, and the gamma particle or high energy photon. Alpha particles are naturally occurring and therefore easily obtained. For this reason, Rutherford made use of  $\alpha$ -particles in his experiment.

An  $\alpha$ -particle consists of two protons and two neutrons equivalent to a Helium nucleus. An  $\alpha$ -particle has a mass of  $6.644656 \times 10^{-27}$  kg and carries a charge of  $3.204353 \times 10^{-19}$  C or twice the charge of an electron. Typically,  $\alpha$ -particles are emitted with a kinetic energy of 5 MeV and a speed of about 0.05c (or 5 percent of the speed of light,  $3.0 \times 10^8$  m/s). Due to their large mass, high charge and slow speed,  $\alpha$ -particles are very likely to interact with other particles and thus will usually lose all forward motion within centimeters of emission in air. For this reason, Rutherford conduct his experiment in a vacuum.

Alpha particles were known to be emitted by natural sources such as uranium, thorium, actinium, radium or any mineral containing some small combinations; however, in the early 1900's, alpha emission was not understood. When an atom has too many protons and therefore its nucleus is unstable, alpha decay is one way in which it can become more stable. This unstable strong nuclear force creates a small probability of quantum tunneling, a process through which the  $\alpha$ -particle can escape past the electrons. Once the  $\alpha$ -particles are released, the atom decays to a stable form and will cease to emit radiation.

Once emitted, these particles would travel through space interacting with anything in its path. Rutherford placed a thin gold foil in the path of these  $\alpha$ -particles to determine the interaction that would occur. In order to find the  $\alpha$ -particles, Rutherford used a zinc sulfide screen, which emitted a flash whenever struck by  $\alpha$ -particles. In modern laboratory equipment, the  $\alpha$ -particles strike a similar detector that creates an electrical signal, which can then be received by an electronic counter to keep track of the large volume of alpha

particles.

## 2.3 Rutherford Scattering

This section investigates the mathematical theory behind Rutherford scattering. We introduce Rutherford's differential cross section equation, discussing its limitations as well as the limitations of the Rutherford scattering experiment.

Due to the central concentration of positively charged protons in large atoms, Rutherford scattering (or Coulomb scattering) is the dominant mechanism of interaction due to the Coulomb force,  $\vec{F}$ , on the  $\alpha$ -particles. This force is

$$\vec{F} = \frac{zZe^2}{4\pi\epsilon_0} \frac{\vec{r}_\alpha - \vec{r}_A}{|\vec{r}_\alpha - \vec{r}_A|^3}, \quad (2.1)$$

where the  $\alpha$ -particle is located at  $\vec{r}_\alpha$ , the nucleus is located at  $\vec{r}_A$ ,  $z$  is the number of protons in an  $\alpha$ -particle,  $Z$  is the number of protons in the nucleus,  $e$  is the charge of a proton, and  $\epsilon_0$  is the permittivity of free space. Since the target nuclei used in Rutherford's and similar experiments are significantly more massive than the  $\alpha$ -particles, this scattering can be considered completely elastic. This type of scattering is a result of the electrostatic interactions, therefore, modeled by unbounded orbits.

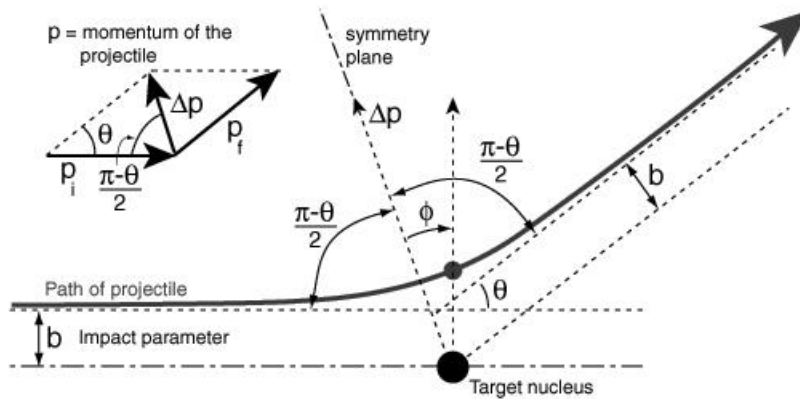


Figure 2.2: The trajectory of an  $\alpha$ -particle experiencing Rutherford scattering [14]

An analysis of these unbounded orbits reveals that an  $\alpha$ -particle, with initial velocity  $v_0$  and mass  $m$  travels past a target nucleus, achieves a minimum separation distance,  $r_{min}$ , from the nucleus before being scattered away. This separation distance depends on the impact parameter,  $b$ , which is the minimum distance from the nucleus the particle would achieve if it did not experience the Coulomb force, as illustrated in Figure 2.2. When an  $\alpha$ -particle, starting at  $\vec{r}_{\alpha 0}$ , is moving directly towards the center of the target nucleus, that is, when  $b = 0$ , we achieve the absolute minimum distance, which is called  $d$ . At this point the particle comes to rest; the difference of the initial kinetic energy,  $KE_0$ , and the initial potential energy,  $PE_0$ , will equal the potential energy,  $PE$ , at that point. These energies are defined as

$$KE_0 = \frac{1}{2}m_\alpha v_0^2, \quad PE_0 = \frac{1}{4\pi\epsilon_0} \frac{zZe^2}{|\vec{r}_{\alpha 0} - \vec{r}_A|}, \quad (2.2)$$

and

$$PE = \frac{1}{4\pi\epsilon_0} \frac{zZe^2}{d}, \quad (2.3)$$

where  $v_0$  is the initial speed of the particle, and  $m_\alpha$  is the mass of an  $\alpha$ -particle.

Solving for  $d$  using Equations 2.2 and 2.3 yields a fundamental limit to investigating the size of an atomic nucleus. That is, for a given initial speed, an  $\alpha$ -particle will only come into direct contact with an atomic nucleus if  $d$ , more precisely,

$$d = \frac{4\pi\epsilon_0}{zZe^2} \left( \frac{1}{2} m_\alpha v_0^2 - \frac{1}{4\pi\epsilon_0} \frac{zZe^2}{|\vec{r}_{\alpha 0} - \vec{r}_A|} \right)$$

is less than the actual atomic radius. However, Rutherford was still able to investigate the properties of atomic nuclei.

Rutherford's target was not a single nucleus; instead, a thin foil was used to limit the number of nuclei the  $\alpha$ -particles interact with. This allows certain assumptions to be made in order to predict the scattering paths of incident  $\alpha$ -particles. Using conservation of energy and the symmetry of the Coulomb force, the differential cross section for Rutherford scattering can be derived as,

$$\frac{\Delta\sigma}{\Delta\Omega} = \left( \frac{zZe^2}{4\pi\epsilon_0} \right)^2 \left( \frac{1}{4KE_0} \right)^2 \frac{1}{\sin^4 \frac{\theta}{2}}, \quad (2.4)$$

where  $\theta$  is the scattered angle, and  $\Delta\sigma$  is the fraction of incident particles scattered within a solid angle interval,  $\Delta\Omega$  [14].

Even though Rutherford's differential cross section formula, (2.4), is derived using simplified conditions and several assumptions, it can be used to investigate experimental results. Rutherford and his coworkers were able to verify the fraction of scattered particles dependence on the number of protons in the target nucleus, the initial kinetic energy, the dependence upon the scattering angle  $\theta$ , and the independence of the azimuthal angle due to the symmetry of the Coulomb force [4].

## 2.4 Gamma Ray Emission and Detection

In this section, we will discuss the nature of gamma rays. We will come to understand how they are emitted and detected and how they are important to GeLi detection.

As previously discussed, in early nuclear physics, there were known to be three forms of atomic radiation. Along with alpha radiation, there is gamma emission. When an atom releases an  $\alpha$ -particle, it is often left in an excited atomic state. As a way of releasing the excess energy, a photon is emitted. Gamma rays are a form of electromagnetic radiation, similar to every other form of photon release, except in wavelength and energy. The main difference between gamma rays and other forms of electromagnetic radiation is that gamma rays have the highest energy and therefore the shortest wavelength.

Gamma rays are dangerous to living cells, because they have the highest energy of all photon emissions. For this reason, it is very important to both detect and locate various natural gamma ray emitters. Some natural radioactive materials found within the earth constantly emit gamma rays as a way to return to a stable form. Similarly, any atomic event will produce gamma rays; the constant nuclear fusion and fission occurring within our sun and other astrological bodies produce waves of gamma ray emission.

With all of these gamma rays bouncing around the universe with such a high level of energy, the only way to detect them is by their interaction with matter. When a gamma ray interacts with matter, it will do

one of two things; it will go through Compton scattering or it will be absorbed. With Compton scattering, the gamma ray collides with an electron. The electron, now charged full of energy, will be liberated from the atom all together. The second option is that the gamma ray will be absorbed by the electron and push it into higher energy states. Once in these higher states, the electron will then release photons to remove the extra energy. These photons will be of significantly less energy and can thus be detected by simply photodiode detectors. Within the GeLi detector, the matter used to intercept the gamma rays is a crystal of Germanium Lithium (GeLi). This crystal is bombarded with gamma rays and then produces less harmful emissions which can then be absorbed by other devices within the detector.

## Chapter 3

# Experiment

In this chapter, we discuss the methods and procedures for both Rutherford scattering and GeLi detection. Here, we develop the mathematical model used for the numerical Rutherford scattering experiment, comparing several different numerical methods. This chapter establishes the basis for the analysis and results of the report.

### 3.1 Rutherford Scattering

In this section we will detail our work with the Rutherford scattering experiment setup at WPI. We will detail the physical setup of the device as well as our attempts to repair faulty parts and the methods used in doing so.

In order to measure the Rutherford scattering, we need to use an alpha source and have it emit positively charged  $\alpha$ -particles through foils only a few atoms thick, to measure the deflection caused by the positively charged nucleus. The WPI Nuclear Lab has an old Rutherford scattering device which consists of a holding location for the alpha source, a rotating wheel that holds different foils for the source to be shot through, and a detection device mounted to a rotating arm for detection at various deflection angles. The device also has a bell jar lid so that air may be pumped out from around the scattering area to limit the number of molecules that can interfere with the scattering. On top of this, a light inhibiting box is placed since the light may cause erroneous readings. There are electrical connections inside the chamber that are connected to a sealed plate, which then relays the connections to the necessary external devices. There are motors for the rotation of the thin foil wheel, as well as for the rotation of the detector through deflection angles. These are wired with 16 gauge insulated wire, internally and externally. They link to a switch box which allows for gradual movement. The detector is wired with BNC cable internally and externally, and this is connected to an Ortec Dual Counter/Timer in order to count the readings from the internal detector.

Upon initial testing of the device we determined that the motors and both of their respective electronics were properly working. We were able to rotate between sheet samples and move the detector through various scattering angles. The detection device did not seem to be working properly. We switched over to a Ludlum Scalar Rate meter which had been previously tested and known to work. After testing at various angles, we saw that there were no repeatable results, so we further inspected the wiring along with this setup. Finding much of the wiring to be very old and poorly soldered, we removed and replaced all the wiring for the detector and its links to the counting device. We then tested to make sure all the connections were working and properly grounded with a WaveTek digital Voltmeter. All links were properly connected and powered. Further testing of the detector itself revealed inconsistent counting. Any time it was attached to the counter,

directly or via cables, it continued to register counts whether the alpha source was in front of it or not. There is no noticeable name on the detecting device, only two unidentifying numbers. Research into these parts yielded electronic devices but none were comparable to the part we had.

Through continued research into  $\alpha$ -particle detectors we discovered that the company Ortec made a model similar to the one we believe is faulty in our setup. We mailed the device to them and they were able to identify what it was and that they do make a similar part, although they did not make this one. Through continued contact with Ortec we attempted to identify a possible replacement device but met some difficulty in response time from the company. We have not yet been able to receive an actual cost quote for the detector and compatible counter. We attempted to get this device up and running.

Through our communications we identified the detector to be a surface barrier detector with a  $25 \text{ mm}^2$  detection area. In our last communication we were told to figure out the depletion depth and the high voltage required in order to determine a suitable detector. We were unable to determine these as there is no documentation on the detection device available. We requested information on a suitable combination of counter and detector that may be used in conjunction to run an alpha scattering experiment but have continued to receive no response from Ortec. We have looked into other options but they continue to be the easiest identifiable provider of the needed equipment.

While we were unable to get the physical setup running, we have created an ideal lab procedure for the use and understanding of the device and the concepts it conveys. These may be compared with the ideal data created in the computer program that we created to model the results of alpha scattering. In addition, a pictorial understanding of the different parts of the experiment may also be seen in the appendix.

## 3.2 Coulomb Scattering Model Derivation

In this section we derive the model used to perform the numerical experiments. We start with the underlying physical laws and develop the mathematical theory, then we nondimensionalize the governing differential equations, and finally we discuss the numerical methods used. nondimensionalization to the numerical methods used in the final experiment.

Rutherford's findings were used to correctly model the interaction between  $\alpha$ -particles and atomic nuclei. Creating a model of this experiment assists in predicting the outcome by depicting the trajectories of the  $\alpha$ -particles. To derive the model certain assumptions need to be clarified. The  $\alpha$ -particles are considered moving point charges each with a charge  $q$ . The nuclei are considered point charges each with a charge  $Q$ . Since the target nuclei are part of a solid foil it is assumed that their positions are fixed. From these assumptions the force experienced between an  $\alpha$ -particle, located at  $\vec{r}_\alpha$ , and a nucleus, located at  $\vec{r}_A$ , is the Coulomb force,

$$\vec{F}(t) = \frac{qQ}{4\pi\epsilon_0} \frac{\vec{r}_\alpha(t) - \vec{r}_A}{|\vec{r}_\alpha(t) - \vec{r}_A|^3}, \quad (3.1)$$

where  $\epsilon_0$  is the constant permittivity of free space,  $8.854 \times 10^{-12} \frac{\text{C}^2\text{s}^2}{\text{m}^2\text{kg}}$ . The forces between the  $\alpha$ -particles are ignored since they are much smaller than the forces due to the nuclei. This assumption also improves the computation time of the model, since in most cases there are many  $\alpha$ -particles. Now the values of  $q$  and  $Q$  are substituted with  $ze$  and  $Ze$  respectively, where  $e$  is the charge of a proton,  $1.602 \times 10^{-19}\text{C}$ . Here,  $z$  represents the number of protons in an  $\alpha$ -particle, and  $Z$  represents the number of protons in the nucleus. Using Newton's second law,  $\vec{F} = m\vec{a}$ , the acceleration,  $\vec{a}$ , of the  $\alpha$ -particle is found as

$$\vec{a} = \frac{zZe^2}{4\pi\epsilon_0 m_\alpha} \frac{\vec{r}_\alpha - \vec{r}_A}{|\vec{r}_\alpha - \vec{r}_A|^3}, \quad (3.2)$$

where  $m_\alpha = 6.645 \times 10^{-27} \text{ kg}$  is the mass of an  $\alpha$ -particle.

Since the position of the  $\alpha$ -particle is a function of time,  $t$ , and  $\vec{a} = \frac{d^2\vec{r}_\alpha}{dt^2}$ , the basis of the model is a second order differential equation that describes an  $\alpha$ -particle's trajectory due to the presence of a nucleus. We give the position and the velocity of the  $\alpha$ -particle at  $t = 0$  as the initial conditions. Thus, we solve

$$\frac{d^2\vec{r}_\alpha}{dt^2} = \frac{zZe^2}{4\pi\epsilon_0 m_\alpha} \frac{\vec{r}_\alpha(t) - \vec{r}_A}{|\vec{r}_\alpha(t) - \vec{r}_A|^3}, \quad (3.3)$$

with  $\vec{r}_\alpha(0) = \vec{r}_{\alpha 0}$  and  $\frac{d\vec{r}_\alpha}{dt}(0) = \vec{v}_{\alpha 0}$  as initial conditions.

### 3.2.1 Nondimensionalization

The magnitudes of the terms used in (3.3) vary from very small to very large and each value has a unit of measure associated with it. Distances between the particles are measured in femtometers ( $10^{-15} \text{ m}$ ), time in seconds, while the speeds are on the order of  $10^7 \frac{\text{m}}{\text{s}}$ . Constants, like the mass of the  $\alpha$ -particle and  $\epsilon_0$ , vary by several orders of magnitude. So it is useful to transform the model to a nondimensionalized form. This process avoids computational error due to such small and large scales. This issue is solved by introducing new variables as follows:

$$\vec{r}_\alpha = [r_\alpha]\vec{r}, \quad (3.4)$$

$$\vec{r}_A = [r_\alpha]\vec{r}_A^*, \quad (3.5)$$

$$\frac{d\vec{r}_\alpha}{dt}(t) = [v_\alpha] \frac{d\vec{r}(t)}{dt}, \quad (3.6)$$

$$t = [t]t^* = \frac{[r_\alpha]}{[v_\alpha]}t^*, \quad (3.7)$$

$$m_\alpha = [m_\alpha]m, \quad (3.8)$$

using the scaling constants shown in Table 3.1.

Scaling Constant	Scaling Value
$[r_\alpha]$	$10^{-15} \text{ m}$
$[v_\alpha]$	$10^7 \frac{\text{m}}{\text{s}}$
$[m_\alpha]$	$6.645 \times 10^{-27} \text{ kg}$
$[t]$	$10^{-22} \text{ s}$

Table 3.1: These are the constants used to adapt the model to the nondimensionalized form.

A new unitless scaling constant, B, must be defined that will replace the constant,  $\frac{zZe^2}{4\pi\epsilon_0 m_\alpha}$ . In the case where the target nuclei is gold, that is,  $Z = 79$ , this is first done by finding the value of this constant and then using dimensional analysis as follows:

$$\frac{zZe^2}{4\pi\epsilon_0 m_\alpha} = \frac{(2)(79)(1.602 \times 10^{-19} \text{ C})^2}{4\pi((8.854 \times 10^{-12}) \frac{\text{C}^2 \text{ s}^2}{\text{m}^2 \text{ kg}})((6.645 \times 10^{-27}) \text{ kg})},$$

$$\frac{zZe^2}{4\pi\epsilon_0m_\alpha} = (5.486)\frac{m^3}{s^2} = B\frac{[r_\alpha]^3}{[t]^2}, \text{ and}$$

$$\implies B = \frac{zZe^2}{4\pi\epsilon_0m_\alpha} \frac{[t]^2}{[r_\alpha]^3} = 54.859. \quad (3.9)$$

Substituting equations (3.4)-(3.8), and (3.9) into (3.4) we get the final dimensionless form along with the new initial conditions:

$$\frac{[r_\alpha]}{[t]^2} \frac{d^2\vec{r}}{dt^2} = \left( B\frac{[r_\alpha]^3}{[t]^2} \right) \frac{[r_\alpha](\vec{r}(t) - \vec{r}_A^*)}{[r_\alpha]^3|\vec{r}(t) - \vec{r}_A^*|^3},$$

$$\frac{d^2\vec{r}}{dt^2} = B \frac{\vec{r}(t) - \vec{r}_A^*}{|\vec{r}(t) - \vec{r}_A^*|^3}, \quad (3.10)$$

with  $\vec{r}(0) = \frac{\vec{r}_{\alpha 0}}{[r_\alpha]} = \vec{r}_0$  and  $\frac{d\vec{r}}{dt}(0) = \frac{\vec{v}_{\alpha 0}}{[v_\alpha]} = \vec{v}_0$  as initial conditions. Note that, for notational convenience, we have dropped the star on  $t^*$  and use  $t$ .

The new differential equation and accompanying initial conditions will depict the same relationships and trajectories; however, the scale will differ from the real trajectories.

### 3.2.2 System of First Order Differential Equations

In order to model the Rutherford scattering the second order nondimensionalized differential equation (3.10) can be rewritten as a system of two first order differential equations. This form clearly shows how the acceleration changes the velocity which in turn changes the position of the  $\alpha$ -particles. Since  $\vec{a} = \frac{d\vec{v}}{dt}$  and  $\vec{v} = \frac{d\vec{r}}{dt}$  the second order differential equation is rewritten as follows:

$$\begin{bmatrix} \vec{v}'(t) \\ \vec{r}'(t) \end{bmatrix} = \begin{bmatrix} B \frac{\vec{r}(t) - \vec{r}_A^*}{|\vec{r}(t) - \vec{r}_A^*|^3} \\ \vec{v}(t) \end{bmatrix}, \quad (3.11)$$

with  $\vec{v}(0) = \vec{v}_0$  and  $\vec{r}(0) = \vec{r}_0$  as initial conditions. An example of these conditions is  $\vec{v}_0 = 1.96$  and  $\vec{r}_0 = -100$ .

So far the model only describes the trajectory of one single  $\alpha$ -particle interacting with only one gold nucleus. Since a Rutherford scattering experiment involves many  $\alpha$ -particles interacting with many nuclei the system of equations must be modified. Let there be  $n$   $\alpha$ -particles interacting with  $N$  gold nuclei. The new system will now be a first order system of  $2n$  differential equations. Since each  $\alpha$ -particle is interacting with  $N$  nuclei, the acceleration depends on the sum of the forces due to all of the nuclei. The governing equations for the  $i^{th}$   $\alpha$ -particle are now given as

$$\begin{bmatrix} \vec{v}'_i(t) \\ \vec{r}'_i(t) \end{bmatrix} = \begin{bmatrix} B \sum_{j=1}^N \frac{\vec{r}_i(t) - \vec{r}_j^*}{|\vec{r}_i(t) - \vec{r}_j^*|^3} \\ \vec{v}_i(t) \end{bmatrix}, \quad (3.12)$$

$$\vec{r}_i(0) = \vec{r}_{i0}, \text{ and } \vec{v}_i(0) = \vec{v}_{i0}. \quad (3.13)$$

### 3.2.3 Numerical Modeling with MATLAB

We can approximate the solution to the system (3.21)-(3.23) using numerical methods, which we implement in MATLAB. The simplest method is Euler's method, which uses a constant stepsize,  $\Delta t$ , to compute the  $(k+1)^{th}$  values of  $\vec{r}$  and  $\vec{v}$  as follows:

$$\vec{r}_i^{(k+1)} = \vec{r}_i^{(k)} + \Delta t \vec{v}_i^{(k)}, \text{ and} \quad (3.14)$$

$$\vec{v}_i^{(k+1)} = \vec{v}_i^{(k)} + \Delta t \mathbf{B} \sum_{j=1}^N \frac{(\vec{r}_i^{(k)} - \vec{r}_j^*)}{|\vec{r}_i^{(k)} - \vec{r}_j^*|^3}. \quad (3.15)$$

This method is used in early versions of the MATLAB code modeling Rutherford scattering because it was quick and easy to code; however, the accuracy is insufficient, that is, there is too much error in the model. A way to illustrate the error is to compare the experimental value of  $d$  with the theoretical value. The Euler method yielded  $d = 24.88130610$ , whereas the theoretical value for that case was  $d = 24.99155548$ . This resulted in a  $4.41 \times 10^{-1}\%$  error, which can be decreased by decreasing the time step size. However, this results in more steps needed, therefore, more processor time used. Another way to get around this problem is to use a more accurate method. The model is improved by using the classical Runge-Kutta fourth order method to find the  $(k+1)^{th}$  values as follows:

$$\begin{aligned} \vec{Y}_i^k &= \begin{bmatrix} \vec{r}_i^k \\ \vec{v}_i^k \\ \vec{r}_i^k \end{bmatrix}, \quad \vec{f}(\vec{Y}_i^k) = \begin{bmatrix} \mathbf{B} \sum_{j=1}^N \frac{(\vec{r}_i^{(k)} - \vec{r}_j^*)}{|\vec{r}_i^{(k)} - \vec{r}_j^*|^3} \\ \vec{v}_i^k \end{bmatrix}, \\ \vec{K}_1 &= \vec{f}(\vec{Y}_i^k), \\ \vec{K}_2 &= \vec{f}\left(\vec{Y}_i^k + \frac{1}{2}\Delta t \vec{K}_1\right), \\ \vec{K}_3 &= \vec{f}\left(\vec{Y}_i^k + \frac{1}{2}\Delta t \vec{K}_2\right), \\ \vec{K}_4 &= \vec{f}\left(\vec{Y}_i^k + \Delta t \vec{K}_3\right), \text{ and} \\ \vec{Y}_i^{(k+1)} &= \vec{Y}_i^{(k)} + \frac{1}{6} \left( \vec{K}_1 + 2\vec{K}_2 + 2\vec{K}_3 + \vec{K}_4 \right). \end{aligned} \quad (3.16)$$

The above classical method provides a better model of  $n$   $\alpha$ -particles interacting with  $N$  target nuclei. This method yields  $d = 24.99159624$ , with a percent error of  $1.63 \times 10^{-4}\%$ . The classical Runge-Kutta method is more accurate than the Euler method by a factor of  $2.70 \times 10^3$ . Since a time step of  $\Delta t = 0.1$  was used, this supports that the Runge-Kutta method and the Euler method are fourth and first order methods respectfully.

The fourth order Runge-Kutta method is much more accurate than the Euler method; however, we can reduce computation time by using variable time steps rather than using a fixed time step. The time it takes to sufficiently model multiple nuclei is much greater than the time it takes to model the interactions with a single nucleus because we have to compute over a much larger domain. This is due to the fact that the distances between the nuclei are three orders of magnitude greater than the scaled distance factor. More

precisely, the distance between nuclei is on the order of  $10^3$  femtometers or  $10^3[r_\alpha]$ . A new method is needed to efficiently compute the data in order to create a more realistic model with multiple layers of several nuclei.

Most of these adjust the time steps as they solve the differential equations in order to decrease the number of computations. One class of methods is the predictor-corrector methods, which predict the solution and then correct this value by a higher order approximation. We use the Dormand-Prince embedded pair method for this model through MATLAB's built in program ode45.m. This method was adapted to represent the system  $\frac{d\vec{Y}_i}{dt} = \vec{f}(\vec{Y}_i)$ , and used to find the  $(k+1)^{th}$  values as follows:

$$\begin{aligned}
\vec{K}_1 &= \vec{f}(\vec{Y}_i^{(k)}), \\
\vec{K}_2 &= \vec{f}\left(\vec{Y}_i^{(k)} + \frac{1}{5}\Delta t\vec{K}_1\right), \\
\vec{K}_3 &= \vec{f}\left(\vec{Y}_i^{(k)} + \Delta t\left(\frac{3}{40}\vec{K}_1 + \frac{9}{40}\vec{K}_2\right)\right), \\
\vec{K}_4 &= \vec{f}\left(\vec{Y}_i^{(k)} + \Delta t\left(\frac{44}{45}\vec{K}_1 - \frac{56}{15}\vec{K}_2 + \frac{32}{9}\vec{K}_3\right)\right), \\
\vec{K}_5 &= \vec{f}\left(\vec{Y}_i^{(k)} + \Delta t\left(\frac{19372}{6561}\vec{K}_1 - \frac{25360}{2187}\vec{K}_2 + \frac{64448}{6561}\vec{K}_3 - \frac{212}{729}\vec{K}_4\right)\right), \\
\vec{K}_6 &= \vec{f}\left(\vec{Y}_i^{(k)} + \Delta t\left(\frac{9017}{3168}\vec{K}_1 - \frac{355}{33}\vec{K}_2 + \frac{46732}{5247}\vec{K}_3 + \frac{49}{176}\vec{K}_4 - \frac{5103}{18656}\vec{K}_5\right)\right), \\
\vec{K}_7 &= \vec{f}\left(\vec{Y}_i^{(k)} + \Delta t\left(\frac{35}{384}\vec{K}_1 + \frac{500}{1113}\vec{K}_3 + \frac{125}{192}\vec{K}_4 - \frac{2187}{6784}\vec{K}_5 + \frac{11}{84}\vec{K}_6\right)\right), \\
\vec{Y}_i^{(k+1)} &= \vec{Y}_i^{(k)} + \Delta t\left(\frac{5179}{57600}\vec{K}_1 + \frac{7571}{16695}\vec{K}_3 + \frac{393}{640}\vec{K}_4 - \frac{92097}{339200}\vec{K}_5 + \frac{187}{2100}\vec{K}_6 + \frac{1}{40}\vec{K}_7\right), \tag{3.17}
\end{aligned}$$

and

$$\vec{Y}_i^{(k+1)} = \vec{Y}_i^{(k)} + \Delta t\left(\frac{35}{384}\vec{K}_1 + \frac{500}{1113}\vec{K}_3 + \frac{125}{192}\vec{K}_4 - \frac{2187}{6784}\vec{K}_5 + \frac{11}{84}\vec{K}_6\right). \tag{3.18}$$

The Dormand-Prince method uses a fourth order Runge-Kutta approximation, (3.17), and a fifth order approximation, (3.18), to find a sufficiently accurate solution. The accuracy is checked by using the fifth order approximation to calculate the error. If the error is too large, a smaller time step is chosen and the fourth order approximation is recalculated until the error is within an acceptable range. This also allows a larger time step to be chosen if the error is below necessary requirements.

MATLAB's ode45.m is optimized for both accuracy and efficiency. It uses the Dormand-Prince method, described above, to adjust the time steps and decrease the total computation time. This allows the model to incorporate many target nuclei. The final version of the model incorporates the manually coded classical Runge-Kutta method for a single target nucleus and the built in function to model a thin foil. There is more discussion on these methods in the next section.

### 3.3 Numerical Experiment: Process and Methods

Here, we discuss the methods used to develop the three MATLAB programs used for the final numerical model. We detail the steps taken during a foil experiment as well as an experiment involving a single nucleus. We also analyze the numerical methods by comparing the classical Runge-Kutta method with the Dormand-Prince embedded pair method.

#### 3.3.1 Rutherford Scattering Numerical Experiment

Even though the results of Rutherford's scattering experiments are well known and have been reproduced many times, the experiment still offers valuable insights to not only the structure of the atom, but the underlying physics and mathematics. By modifying (2.4) to the specific experimental setup used, Rutherford derived that the number of particles scattered at some angle,  $\theta$  is proportional to

$$\frac{NnL}{4R^2} \frac{(Ze^2)^2}{(4\pi\epsilon_0 KE)^2} \frac{1}{\sin^4(\frac{\theta}{2})} \quad (3.19)$$

where  $R$  is the distance from the target to the detector, and  $L$  is the thickness of the target material [14].

The experimental setup, which is given in the Appendix, when operational, easily allows for the investigation of the relationship between the number of particles detected with  $n$ ,  $N$ ,  $L$ ,  $Z$ , and  $\theta$ . The most notable relationships, which Rutherford originally verified, are the atomic numbers, the thickness, the kinetic energy, and the scattered angle [4]. Since investigating these relationships in a lab environment can be difficult (due to setup limitations), it is beneficial to turn to a virtual lab environment to run numerical experiments that model the same relationships. By using the derived model of Coulomb scattering described in the previous section, a MATLAB program can be written that approximates the data measured in the lab, which is used and analyzed in Section 4.3.

To create a convenient program, which is user friendly and does not require a large amount of time to run, more assumptions must be made to further simplify the experiments. These new assumptions are:

- The model is reduced from three dimensions to two.
- The target nuclei are equally spaced.
- The initial  $x$ -positions of all the  $\alpha$ -particles are the same.
- The initial  $y$ -positions of the  $\alpha$ -particles are equally spaced.
- The initial velocity of all the  $\alpha$ -particles are the same, and are only in the  $x$ -direction.

With the above assumptions, we created the programs AlphaScat.m, AlphaCount.m, and AlphaPlot.m, which numerically model certain aspects of the Rutherford scattering experiments. These allow the user to investigate the interaction with a single target nucleus, as well as thin foils comprised of equally spaced nuclei. The goal of the experiment is to numerically show the dependence of the number of  $\alpha$ -particles scattered at an angle  $\theta$  to the atomic number, to the total number of incident particles, to the number of layers of target nuclei (which corresponds to the foil thickness), and to the initial velocity (which corresponds to the kinetic energy).

### 3.3.2 AlphaScat.m

AlphaScat.m uses the nondimensionalized form of the system of differential equations that models Coulomb scattering. It is written as a MATLAB function, with ten possible arguments, that calculates the  $\alpha$ -particle trajectories and other relevant data based on the derived Coulomb model. The first argument, *Exper*, determines whether to investigate the interactions involving one single target nucleus (*Exper*='Atom') or the interactions involving a thin foil of target nuclei (*Exper*='Foil'). It is important to note that the data for the 'Atom' experiment is calculated using the classical fourth order Runge Kutta method while the data for the 'Foil' experiment is calculated using MATLAB's built in differential equation solver, *ode45.m* using the Dormand-Prince embedded pair method. The type of experiment also determines the number of arguments accepted. For the 'Atom' experiment, AlphaScat accepts eight or less arguments -AlphaScat(*Exper*, *Target*, *n*, *AlphaDensity*, *Xdet*, *x0*, *vx0*, *FileName*)- while the 'Foil' experiment accepts ten arguments or less -AlphaScat(*Exper*, *Target*, *n*, *AlphaDensity*, *Xdet*, *layers*, *N*, *x0*, *vx0*, *FileName*). The second argument, *Target*, specifies the target material, and therefore, the atomic number and separation between the nuclei (if multiple nuclei are present). The separation distances are nondimensionalized; the actual distances are in femtometers.

Material	Argument Input	Atomic Number	Nuclei Separation ( $\times 10^3$ )
Aluminum	'Al'	13	236
Copper	'Cu'	29	290
Zinc	'Zn'	30	284
Silver	'Ag'	47	330
Cadmium	'Cd'	48	322
Tin	'Sn'	50	290
Gold	'Au'	79	348
Lead	'Pb'	82	308

Table 3.2: Target material characteristics used in AlphaScat.m.

The separation distances, listed in the Table 3.2 with the material characteristics, are defined here as twice the atomic radius [8]. These were used as a standard; however, since there is no accepted standard other separation definitions could be used, such as the measured radius or the covalent radius. The third argument, *n*, determines the number of incident particles. The initial spacing of the initial y-positions of the particles are determined by the fourth argument, *AlphaDensity*. The particles are equally spaced between  $\frac{n}{2\text{AlphaDensity}}$  and  $-\frac{n}{2\text{AlphaDensity}}$ . This sets the spacing between the particles  $\alpha_i$  and  $\alpha_{i+1}$  as  $\frac{1}{\text{AlphaDensity}}$ .

*Xdet*, the fifth argument, determines how far away from the target the  $\alpha$ -particles are detected. It is important to choose a distance that is appropriate for the given experiment type. A larger *Xdet* is needed for the 'Foil' type experiment since it considers multiple nuclei spaced relatively far apart. The sixth and seventh arguments for the 'Atom' type experiment and the seventh and eighth for the 'Foil' type, *x0* and *vx0*, determine the initial *x*-position and the initial velocity of all of the particles. For the 'Foil' type experiment, the sixth argument determines the number of layers of target nuclei, separated along the *x*-axis by a distance of  $\frac{\sqrt{3}}{2}sep$ , starting at  $x = 0$ . Each layer consists of *N*, the seventh argument, nuclei that are separated vertically by *sep*. The layers are offset such that the distance from one target nucleus to any of the adjacent nuclei is the nuclear separation distance, *sep*, for that material.

The final possible argument for AlphaScat is *FileName*, which determines the name of the MATLAB

.mat data file that will be created to save the data. Any number of arguments may be omitted when running AlphaScat; however, the argument given must match the order described previously. The first section of code AlphaScat.m, lines 110-172, checks the validity of the given arguments and sets the omitted arguments to the default values shown in Table 3.3. Note that, some of these default values are dependent on Exper. This feature allows the user to simply input AlphaScat into the MATLAB command window and run the default gold 'Atom' experiment with 101  $\alpha$ -particles.

Argument	Default	'Foil' Default
Exper	'Atom'	'Foil'
Target	'Au'	'Au'
n	101	101
AlphaDensity	1	1
Xdet	200	$10^8$
layers		21
N		21
x0	-100	-100
vx0	1.96	1.96

Table 3.3: Default values for the arguments of AlphaScat.m

The default file name is based on the argument values. For example, if a lead ('Pb') 'Atom' experiment is run with 211  $\alpha$ -particles, then FileName will be 'PbAtom211'. If a tin ('Sn') 'Foil' experiment is run with 101 particles and 11 layers consisting of 25 nuclei, then FileName is '11-25SnFoil101'. In the instance that the chosen file name already exists, 'c' will be added to the end of the file name.

### 'Atom' Experiment: Classical Runge Kutta Method

After defining the constants and the scaling factor as explained in Section 3.2.3, AlphaScat.m calculates the necessary trajectory data for each  $\alpha$ -particle involved in the 'Atom' experiment with the classical fourth order Runge-Kutta method. Along with the position data for each particle, the velocity, the acceleration, the respective magnitudes, the kinetic energy, the potential energy, and the total energy for each position is calculated at each of the  $K$  steps.  $K$  is defined as  $\frac{Time}{\Delta t}$  where, the time step size,  $\Delta t = 0.1$ , and the total time,  $Time$ , is

$$Time = \left\lceil 1.05 \frac{Xdet + |x0|}{|vx0|} \right\rceil. \quad (3.20)$$

This definition of  $Time$  ensures that the detection distance will be reached since the velocity as an  $\alpha$ -particle repelled by the nuclei exceeds  $|vx0|$ . Prior to finding the numerical approximations for the trajectories of the  $n$   $\alpha$ -particles, three  $K \times 2 \times n$  data arrays are created to store the position, velocity, and acceleration data. Space for six data  $K \times n$  arrays are preallocated for the other data. This decreases computation time by preventing the arrays from growing inside the loop when each step is calculated.

### 'Foil' Experiment: Dormand-Prince Embedded Pair Method through ODE45.m

For 'Foil' type experiments, some of the data arrays are preallocated in the same manner; however, we only collect the trajectory and scattering angle data for the 'Foil' experiment since the magnitude and energy

data would be similar to the 'Atom' experiment. The positions of the nuclei are defined by using modular arithmetic to shift the individual layers of  $N$  equally spaced nuclei vertically up and down such that the  $y$ -positions of the  $i^{th}$  and the  $(i+2)^{th}$  layer are the same (See Code in Appendix Section 6.6.1). The total time in this case is defined as

$$Time = \frac{\min(3\sqrt{3}layers \quad Xdet) + |x0|}{|vx0|}. \quad (3.21)$$

This definition of total time ensures that efficiency is maintained while avoiding significant error. This approach is used since the trajectories become more linear as they move further from the nuclei. Either they will reach the detection distance, or they will be sufficiently far away from the nuclei such that the trajectories are assumed linear.

Once the nuclei positions and the total time are defined, ode45.m is used  $n$  times to call the function scatter.m, which represents the system of differential equations for the  $i^{th}$   $\alpha$ -particle. This finds the approximate trajectory for that particle. The data is then trimmed so that the trajectories end at the detector. For the first step, a data array is preallocated to store the trajectory data for all  $n$   $\alpha$ -particles. Since ode45.m uses a variable step size routine, one large array cannot be preallocated due to the fact that some trajectories may need more steps than others. To maintain efficiency, the size of the data is increased to fit the data set for each particle as needed. A data "marker",  $\pi\sqrt{3}$ , is placed into the data array to signify the end of the actual data, and where the preallocated data begins. This marker is used later to extract the data for plotting.

As discussed in Section 3.2.3, ODE45.m is used due to its efficient routine. The adaptive step size of the Dormand-Prince embedded pair method increases efficiency by taking larger steps when the error is below a set tolerance. The Dormand-Prince(4,5) embedded pair method uses a fourth order method, along with a fifth order method to approximate the solution at each step. These two solutions, shown in Section 3.2.3, are then subtracted to give a better estimate of the error of that step. This error is then compared to a set relative error tolerance,  $Tol$  to find the next step size,

$$\Delta t_{i+1} = \Delta t_i \left( \frac{Tol}{err_i} \right)^{\frac{1}{5}}. \quad (3.22)$$

This shows how the Dormand-Prince embedded pair method changes the step size. Advanced routines, like ODE45.m, also use techniques such as local extrapolation while finding the numerical solution [7]. Since the force on the  $\alpha$ -particles gets larger the closer to the nuclei it gets, more time steps are needed to avoid large errors at closer distances. The sudden increase in force causes the trajectories to change significantly, therefore, a finer time step is needed to accurately compute the rapidly changing positions during that period of scattering. This is even more evident in looking at the log-log plot of the time step versus the magnitude of the  $x$ -position of an  $\alpha$ -particle in Figure 3.1. As the particle moves closer to the origin, where the nuclei are located, the step size remains relatively small until the particle moves away again when the time step increase. Since the time step is related to the error in each iteration and the error is related to the  $x$ -position, the relationship shown in Figure 3.1 is expected.

Table 3.4 shows the total time to run AlphaScat.m for both 'Atom' and 'Foil' type experiments. For both the experiments, the runtime is directly proportional to the number of  $\alpha$ -particles. This is expected since the system size is directly proportional to the number of particles. Comparing (3.12) with (3.11), we divide the runtimes by the number of nuclei,  $N = 441$ , to account for the need to sum the  $N$  terms in (3.12). This information, seen in Table 3.5, shows how much more efficient the variable step size method is compared to the single step size method. The average run time per  $\alpha$ -particle per nuclei for the 'Foil' experiment is  $1.97 \times 10^{-4}s$ , which is about 300 times faster than the 'Atom' experiments average of  $6.15 \times 10^{-2}s$ .

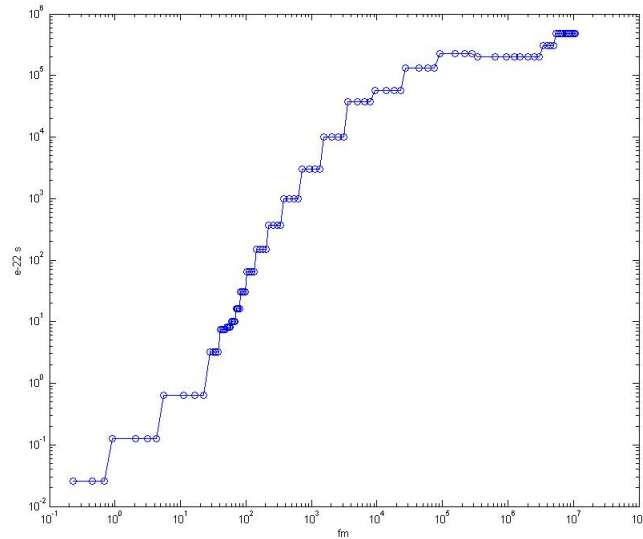


Figure 3.1: This figure, time step size versus the magnitude of the  $x$ -position, shows how the step size changes as an  $\alpha$ -particle moves through the foil.

Number of Particles	'Foil', 441 Nuclei, (s)	'Atom', 1 Nuclei, (s)
1	0.14	0.06
2	0.20	0.13
3	0.23	0.19
7	0.56	0.44
13	1.03	0.78
31	2.67	1.89
47	3.87	2.85
97	7.74	5.94
199	15.40	12.10
397	31.00	24.40
797	62.90	48.50
997	80.54	61.20

Table 3.4: This table shows the run times for both the 'Atom' experiments and 'Foil' experiments.

# of Particles, $n$	'Foil', Time/ $n/N$ ( $\times 10^{-4}$ s)	'Atom', Time/ $n/N$ ( $\times 10^{-2}$ s)
1	3.17	6.30
2	2.29	6.25
3	1.77	6.23
7	1.82	6.24
13	1.80	6.00
31	1.95	6.09
47	1.87	6.06
97	1.81	6.12
199	1.75	6.08
397	1.77	6.15
797	1.79	6.09
997	1.83	6.14

Table 3.5: This shows the times versus particle for each experiment depicted in Table 3.4.

### 3.3.3 AlphaCount.m and AlphaCount.m

AlphaCount.m is used after running AlphaScat.m to collect the trajectory data. This function has two possible arguments (AlphaCount(FileName,ddT)). The first, which must be entered, is the data file that contains the data from AlphaScat. This file is loaded so that the data can be used to find the angular distribution. If the data file is from an 'Atom' type experiments, AlphaCount trims the trajectory data using the same method used in AlphaScat.m for the 'Foil' data. After trimming the data the count distribution is found based on the second argument,  $ddT$ . This is used as the angular step size to count the number of particles within a certain angular interval. The default step size is  $0.02radians$ , which in most cases provides clear results. For the 'Atom' Type experiment the range of angles goes from 0 to  $2\pi$  starting from the  $+x$ -axis, moving counter clockwise. For 'Foil' type experiments the range is only from 0 to  $\frac{\pi}{2}$  and  $\frac{3\pi}{2}$  to  $2\pi$ . This range is similar to the range available with the actual lab setup. AlphaCount.m provides the data that AlphaPlot.m uses to show the correlation between the number of scattered particles and  $\frac{1}{\sin(\frac{\theta}{2})}$ . After calculating this distribution, a new data file is saved containing all the information.

AlphaPlot.m compiles the data calculated by AlphaScat.m and AlphaCount.m to build figures that graphically represent the data. This function uses between one and six to create up to four figures (AlphaPlot(FileName, Trajectories, Magnitudes, Energies, Angles, PARTs)). The first argument, FileName, determines which data file gets loaded. The last five optional arguments determine the data that will be represented. If the data file loaded is from a 'Foil' experiment only the trajectory data and the angle data can be plotted. However, AlphaPlot.m creates up to four figures for 'Atom' data files, including the trajectory and angular distribution figures. The other two show the distance, speed, acceleration, kinetic energy, and potential energy versus time, as well as the total energy versus initiate distance for all  $n$   $\alpha$ -particles. The angular distribution plots are scaled so that the largest count is reported as 100. This scaling factor is  $\frac{100}{\max(Count)}$ . If the last argument, PARTs, is used as  $PARTs = [i,j]$ , then only the data for particles  $i$  through  $j$  will be plotted. These plots are shown in Figures 3.2 to 3.7.

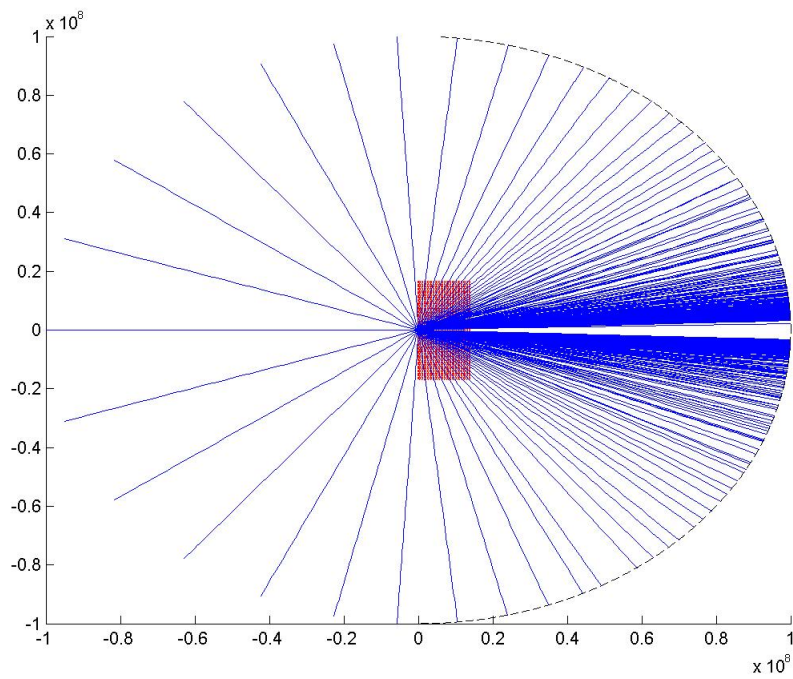


Figure 3.2: This is an example of a 'Foil' experiment trajectories plot, where 499 particles are incident upon a 47 layers of 97 Gold nuclei.

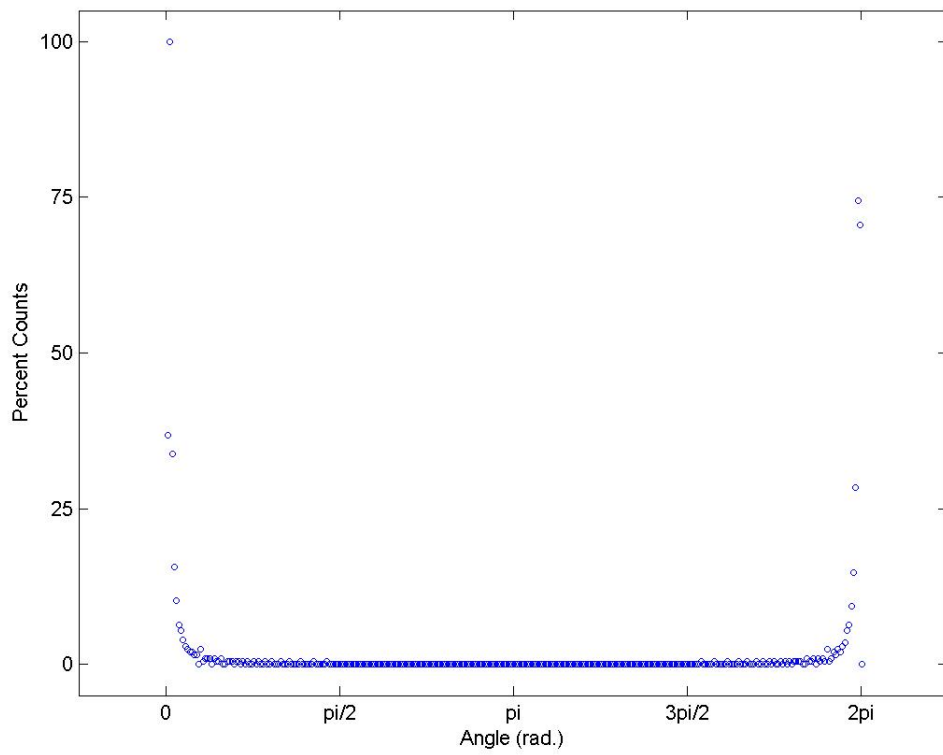


Figure 3.3: This is an example of a 'Foil' experiment angle distribution plot, where 997 particles are incident upon a 21 layers of 21 Gold nuclei.

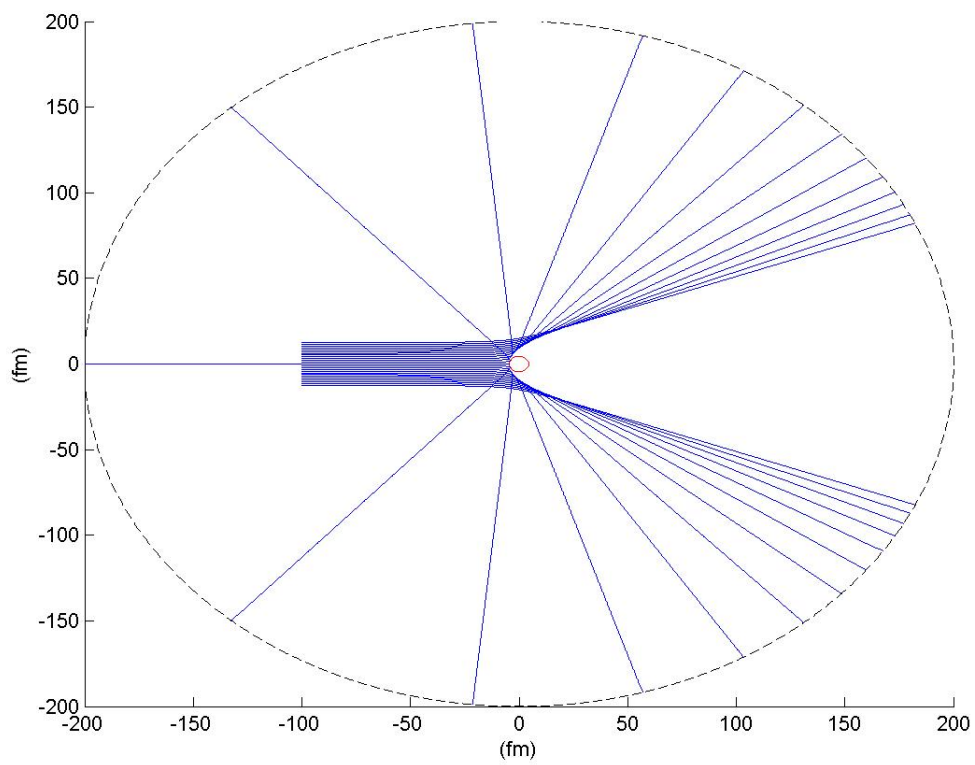


Figure 3.4: This is an example of a 'Atom' experiment trajectories plot, where 25 particles are incident upon an Aluminum nucleus.

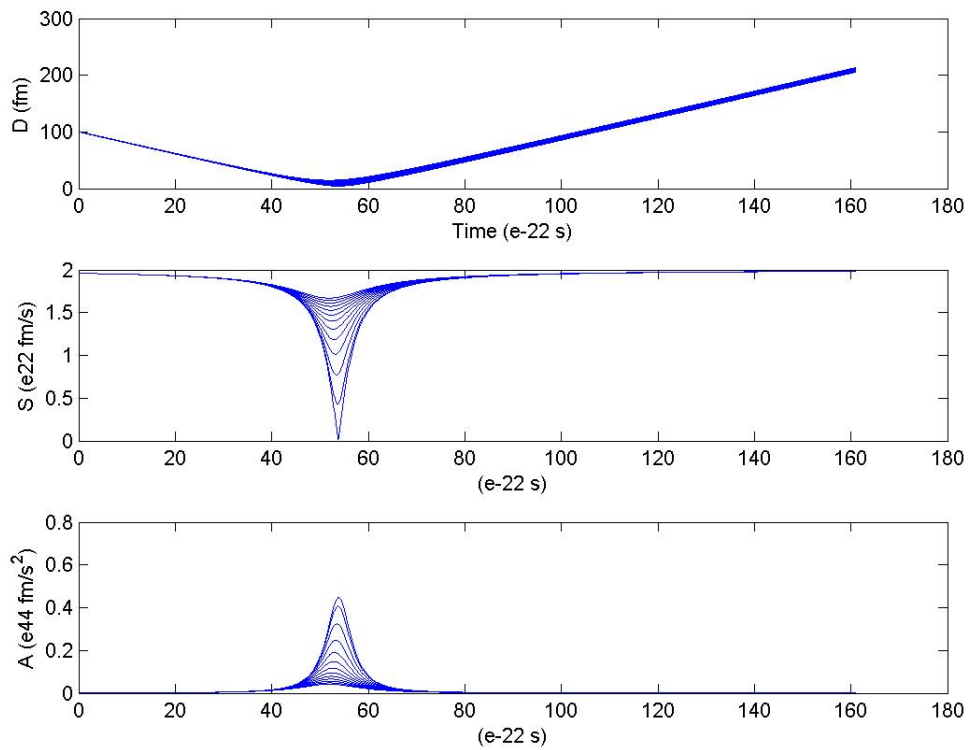


Figure 3.5: This is an example of a 'Atom' experiment magnitudes plot, where 25 particles are incident upon an Aluminum nucleus.

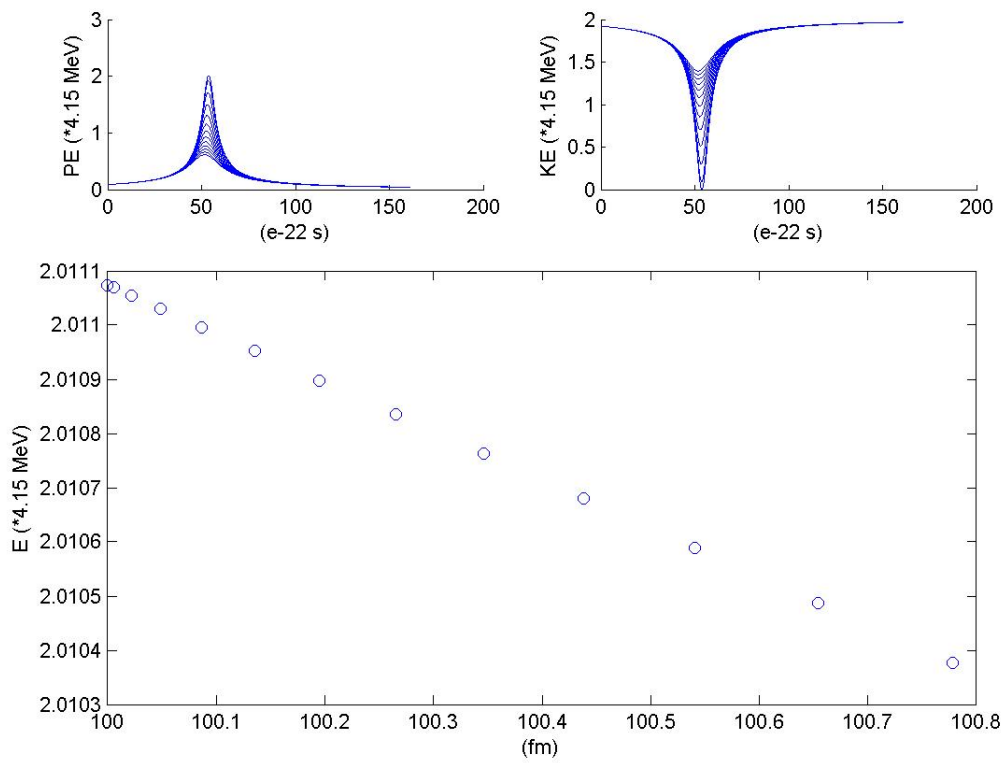


Figure 3.6: This is an example of a 'Atom' experiment energies plot, where 25 particles are incident upon an Aluminum nucleus.



## 3.4 Numerical Rutherford Scattering Experiment Procedure

There are many different aspects of Rutherford's experiment that can be investigated with the MATLAB code presented. This is a proposed procedure that explicitly describes how to investigate several of these aspects. The results from the 'Foil' experiment are analyzed later in Section 4.3.

### 3.4.1 'Atom' Numerical Experiment

AlphaScat('Atom', Target, n)

AlphaCount(FileName)

AlphaPlot(FileName, Trajectories, Magnitudes, Energies, Angles)

- **Purpose:** To investigate the relationship between the number of scattered  $\alpha$ -particles and the atomic number of the target, the number of incident particles, and the scattering angle.
- **Collecting Data** For different targets, run AlphaScat with several values for  $n$  while keeping the other values constant (Ex. AlphaScat('Atom', 'Al', 25)).
- **Count the Particles** To get the angular distribution of the number of particles scattered run AlphaCount with the data files previously created by AlphaScat (Ex. AlphaCount('AlAtom25')).
- **Recall Data for Analysis** To obtain the number of particles scattered, the data must be loaded from the data file. The MATLAB function load(FileName, 'dTheta', 'Count') will load the data for the number of particles (Count) scattered at different angular intervals (dTheta). This should be interpreted as the number of particles with a scattering angle between  $d\theta_i$  and  $d\theta_i - dT$  is  $Count_i$ . In this instance  $dT = 0.02$  by default and  $i = 1, \dots, 315$ ; however,  $dT$  can be varied which would lead to a different maximum  $i = \lceil \frac{2\pi}{dT} \rceil$ . AlphaPlot.m plots the data that the previous two functions calculated (Ex. AlphaPlot('AlAtom25dT 10E-2')). AlphaPlot(FileName) will produce four figures, Trajectories, Magnitudes, Energies, and Angles. These figures aid in the understanding of the motion of the particles and show the relationship between the scattering angle and the number of particles counted.

### 3.4.2 'Foil' Numerical Experiment

AlphaScat('Foil', Target, n)

AlphaCount(FileName)

AlphaPlot(FileName, Trajectories, 'off', 'off', Angles)

- **Purpose:** To investigate the relationship between the number of scattered  $\alpha$ -particles and the atomic number of the target, the thickness and width of the foil, the number of incident particles, and the scattering angle.
- **Collecting Data** For different targets, run AlphaScat changing the variables  $n$ ,  $layers$ , and  $N$  while keeping the other values constant (Ex. AlphaScat('Atom', 'Al', 25, 1,  $10^8$ , 21, 31)).
- **Count the Particles** To get the angular distribution of the number of particles scattered run AlphaCount with the data files previously created by AlphaScat (Ex. AlphaCount('21-31AlFoil25')).

- **Recall Data for Analysis** To obtain the number of particles scattered, the data must be loaded from the data file. The MATLAB function `load(FileName, 'dTheta', 'Count')` will load the data for the number of particles (Count) scattered at different angular intervals (dTheta). This should be interpreted as the number of particles with a scattering angle between  $d\theta_i$  and  $d\theta_i - dT$  is  $Count_i$ . In this instance  $dT = 0.02$  by default and  $i = 1, \dots, 315$ ; however,  $dT$  can be varied which would lead to a different maximum  $i = \lceil \frac{2\pi}{dT} \rceil$ . `AlphaPlot.m` plots the data that the previous two functions calculated (Ex. `AlphaPlot('AlAtom25dT 10E-2')`). `AlphaPlot(FileName)` will produce two figures, Trajectories, and Angles. These figures aid in the understanding of the motion of the particles and show the relationship between the scattering angle and the number of particles counted.

### 3.5 GeLi Detection

In this section we will detail our work with the Germanium-Lithium (GeLi) gamma ray detection device. We will detail the setup and running procedure as well as the calibration. We have tested various samples for gamma radiation, including soil from around the WPI campus.

GeLi detection requires a very intricate setup in order to correctly monitor a wide variety of energy levels. Liquid nitrogen, or LN2 as it is commonly known, is necessary for the operation of the gamma ray detector. The liquid nitrogen keeps the GeLi crystal at a low enough temperature to remove the background radiation so the device can detect lower energies of gamma rays. For this reason, the liquid nitrogen must be constantly replaced in a process of transferring it from dewar to dewar. The process involves bringing one dewar to the LN2 tank and carefully filling one portable dewar with a diffusing hose. Once the dewar is filled, the tank must be closed. It is important to wear a thick work glove as everything involved in the process will become very cold. Once the portable dewar is filled, it can then be brought to the detector where, by use of the plastic hose provided, it can fill the dewar of the detector. It is important to stop the flow every now and then to build pressure in the dewar. Once the detector dewar is full, the portable dewar should be left slightly open so that any remaining LN2 can heat up and exit the dewar as a gas.

Before gathering data from naturally occurring sources of gamma ray emissions, a baseline and efficiency level for the detector must be known. By gathering a baseline and efficiency level, any data collected can be accurately represented without the bias of the detector. To determine these necessary calibration factors, the detector was run empty, with a known multi-nuclide source and with an empty plastic jar to be used with natural soil samples. Running the empty detector for twenty hours would yield enough data to form a base line; similarly, running an empty plastic jar for nineteen hours yields a baseline for the soil samples. To determine an efficiency level, the multi-nuclide source had to be tested against its data sheet, and so similar conditions had to be maintained. The multi-nuclide source was run for fifty hours to produce comparable data.

By taking the known amount of original counts for the isotopes in this sample, as well as the half lives, and the amount of days since the original count was taken, we are able to calculate the expected counts using the equation

$$ExpectedCountRate = OriginalCountRate \times (1/2)^{\frac{\#days}{half-life}}. \quad (3.23)$$

This equation will provide us with the count rates that we should expect to see from the sample.

The date of the original source data was 7/1/2006 and the date of our collection was 10/13/2008. From this we decided that there are 835 days from the original source date, and using this we were able to calculate the number of half lives in the table. By comparing these with the actual data taken we were able to find an efficiency curve by graphing the energy levels in keV versus the efficiency. While there were supposed to

Isotope	1/2 life (days)	Energy(keV)	Original Counts/s	# of Halfives	Expected Counts/s	Measured Counts/s	Efficiency
Cd-109	462.600	88.04	327.0	1.805	93.58	9.96	10.64
Co-57	271.790	122.07	207.5	3.072	24.67	4.44	18.00
Ce-139	137.640	165.85	371.3	6.067	5.54	0.58	10.47
Sn-113	115.090	391.71	1197	7.255	7.84	0.41	5.23
Cs-137	11019.400	661.62	1332	0.076	1263.84	37.76	2.99
Yt-88	106.630	898.02	3271	7.831	14.37	0.28	1.95
Co-60	1925.600	1173.23	1823	0.434	1349.74	20.02	1.48
Co-60	1925.600	1332.51	1825	0.434	1351.22	17.53	1.30
Yt-88	106.630	1836.01	3459	7.831	15.19	0.14	0.92

Table 3.6: MultiNuclide Test Data - 50 Hours

be Hg-203 and the Sr-85 peaks, we found that they were too far decayed to be noticeable and therefore they have been left out of our data.

By taking the data from Table 3.7 we are able to graph a curve representing the expected curve we have seen in the small amount of documentation we were able to find for the GeLi detector. The efficiency greatly decays as you increase in energy level. This can be seen in Figure 3.8.

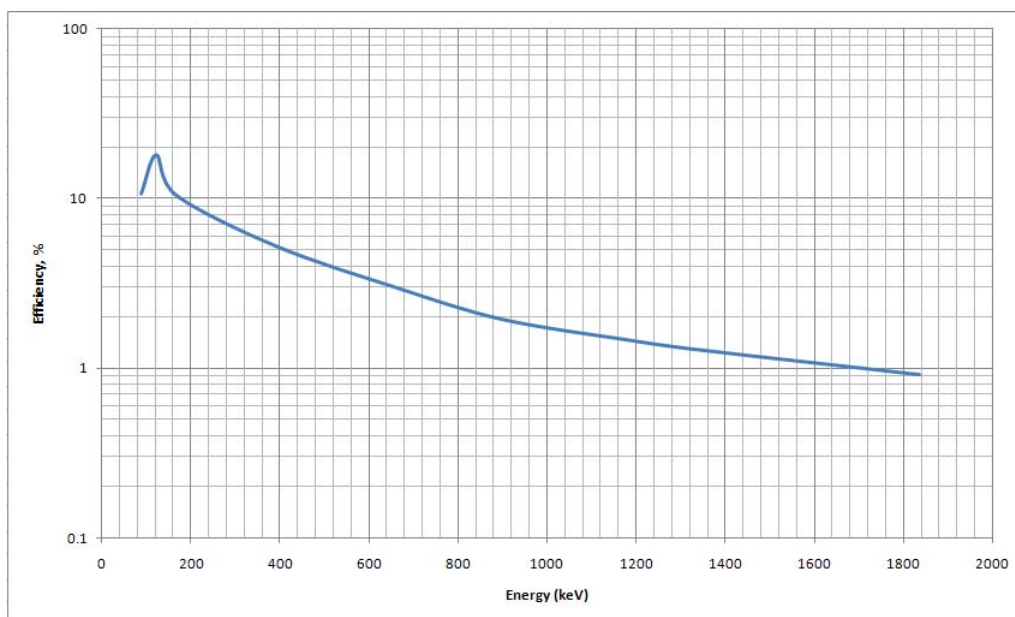


Figure 3.8: Measured Efficiency Curve for GeLi Detector.

To perform a full test of the detectors capabilities, soil samples were collected across the campus. Having divided the campus into eighteen quadrants, a sample of the soil in each quadrant was collected. Some of the samples came from depths of up to eleven centimeters, while the turf sample and the baseball field sample were top soil samples. Some of the samples included rocks, mulch and organic matter such as grass and roots, but all those factors will be taken into account in the analysis of their gamma ray emissions ray measurements. The mapped out quadrants may be seen in the appendix. In order to ensure accurate results from these samples, we first did a control test with an empty sample container and saved the results. Each of the soil samples was then tested for a 5 hour period. The results per hour were modified based on the control and this data was analyzed. A map of the locations soil samples were taken can be seen in Figure 3.9.

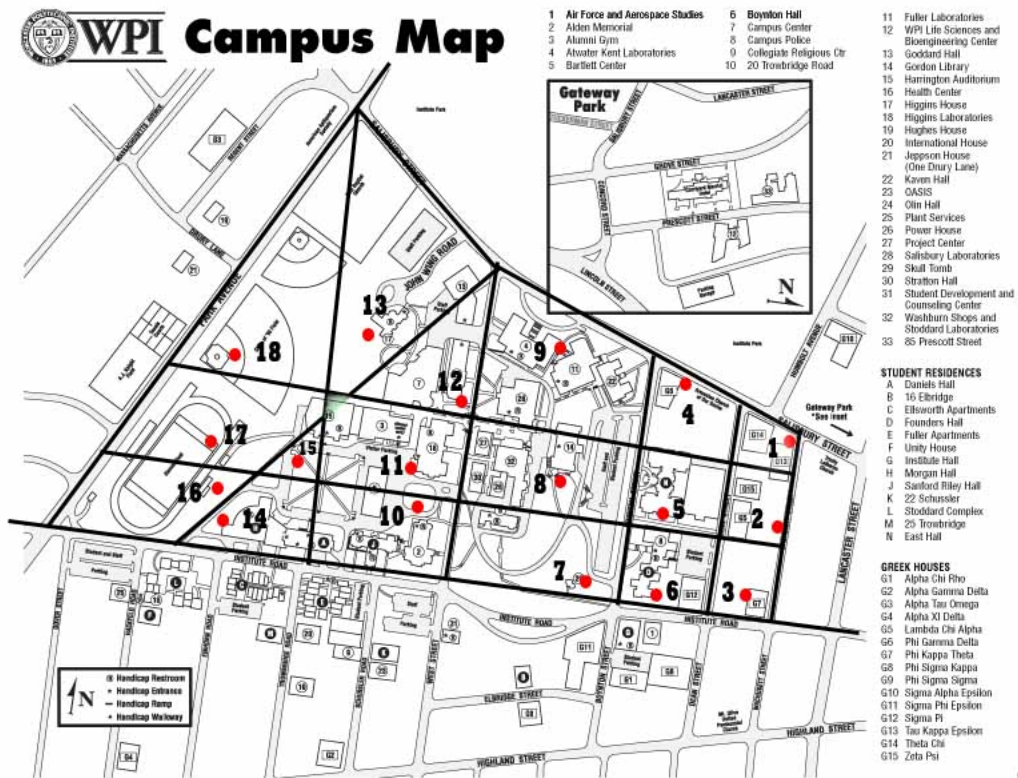


Figure 3.9: Soil Sample Locations

Sample	Location
1	Corner of Salisbury and Wachusett Streets (9 cm down)
2	Stump in front of 59 Wachusett St. (11 cm down)
3	Back door of Phi Kappa Theta House (8 cm down)
4	Back of Founders SE Corner (7 cm down)
5	East Hall by Founders Side Entrance (11 cm down)
6	Sidewalk in front of statute (12 cm down)
7	NE Corner of Skull Tomb (10cm down)
8	By garbage can (8 cm down)
9	Fuller path (9 cm down)
10	Edge of Mulch (7 cm down)
11	Underneath light post (7 cm down)a
12	Underneath vent by 1958 cornerstone (7 cm down)
13	Behind rock wall near 4 split tree (11 cm down)
14	Flower bed behind DAKA dining hall (10 cm down)
15	Big Tree mulch bed (5 cm down)
16	Top of Hill near locked gate (7 cm down)
17	Turf sample (Top Soil)
18	Second Base Sand of Baseball Field (Top Soil)

After speaking with graduate student, Marco Kaltofen, of WPI, we were briefed in some possible methods to clear the background radiation we were getting in our lab space. The lab where our detector is located has very poor ventilation and the basement is surrounded by concrete. This causes there to be increased levels of radon detected in the experiment. Mr. Kaltofen suggested that we use some type of inert gas to purge the test chamber, as well as vacuum cleaning it. We attempted to flush the air out of the chamber using CO<sub>2</sub> produced by dry ice, and then vacuumed and cleaned the entire chamber. After retesting some of our initial samples it showed that our attempts were not effective and the same background peaks still remained.

The samples were dried in order to ensure that there was minimal water content in them. In order to do this we placed them in disposable muffin trays and heated them in an oven at 550 degrees until they were as dry as possible. By eliminating the water we can now to get an accurate mass reading to use in radiation level calculations.

In addition to all the soil samples taken, Mr. Kaltofen provided us with unique samples of silt from the Columbia River, sediment from the Ganges River, goat's teeth from a location of high radiation in Russia, a plastic machine button from the Chernobyl Reactor explosion, and some samples from Los Alamos. These samples were also analyzed to find noticeable radiation peaks.

# Chapter 4

## Analysis

In this chapter, we present and analyze the collected data from both the numerical Rutherford scattering experiment as well as the GeLi gamma ray detection. Here, the radiation detected from the WPI soil samples are determined to be well within the national averages, while data from several international samples reveal interesting radioactive isotopes. We use the data from the numerical Rutherford scattering experiment, to verify and repeat Rutherford's original findings.

### 4.1 Total Radiation Effect

In this section, we will discuss the total radiation effect. The total radiation effect is the calculation of the total amount of radiation that would affect a human that was around the source. Through this process we will determine a way of converting the data from the GeLi detector into comparable data.

Radiation is not always harmful, but is always present. Although the ozone layer filters most of the harmful radiation from the sun, people are constantly being bombarded with radiation. Low energy radiation can have little effect on the human body, but with enough energy, the radiation is considered ionization radiation.

Ionizing radiation refers to waves or particles with enough energy to remove an electron from an atom or molecule that it has struck. Examples of ionizing radiation are alpha and beta particles and electromagnetic waves or photons, such as x-rays and gamma rays. The effects that the ionizing radiation has on the body include cell death and cell mutations that can contribute to cancer. These effects are usually associated with prolonged exposure to ionizing radiation, as single exposures to low energy radiation have minimal side effects.

When discussing the radiation given off and radiation absorbed, it is important to know the absorbed dose and the effective dose. The absorbed dose is the level of radiation given off by the source around, while the effective dose is more telling of the effect that it will have on anything in the area. The unit of the absorbed dose, or total ionizing dose, is a gray, or a joule per kilogram. This unit is very different from the sievert, also a joule per kilogram, which is the unit of effective radiation [15]. The effective radiation takes into account two important scaling factors and thus must have different units to denote the difference dose.

The two major scaling factors are a quality factor,  $Q$ , that is dependent on the type of ionizing radiation and a scaling factor,  $N$ , dependant on the type of biomaterial that is absorbing the radiation. For the quality factor,  $\alpha$ -particles are rated at  $Q = 20$ , protons are given  $Q = 5$ , neutrons are rated from  $Q = 5$  to  $Q = 20$  and photons have  $Q = 1$ . This relative quality factors demonstrate the penetrating and destructive power of

these radiation sources. For the biological scaling factor,  $N$ , can range for various organisms, but humans are commonly rated at  $N = 1$  [16].

In the context of our experiments, the data measured by the GeLi detector is given in counts per channel, where channels refer to various energy levels that gamma rays could have. To make better use of this data, we must convert it to the total amount of energy given off by a soil sample. To do this, we multiplied the energy of each channel by the number of counts for each channel and then sum all of these energies across the total number of channels. This equation represented by:

$$E_i = 0.409i + 17.92. \quad (4.1)$$

Since this equation was determined by a best fit line of gathered data, it is slightly off from the actual channel to energy conversion. The actual conversion is not perfectly linear and therefore a certain amount of error is incurred by this linear assumption. To determine the accuracy of this assumption we found the error relative to the theoretical relationship. Figure 4.1 shows a plot of this error function. Here you can see that the error is very high, but it drops below 3% after the first 150 channels. Since the beginning channels do not often have important values, we can simply accept the error and assume linearity.

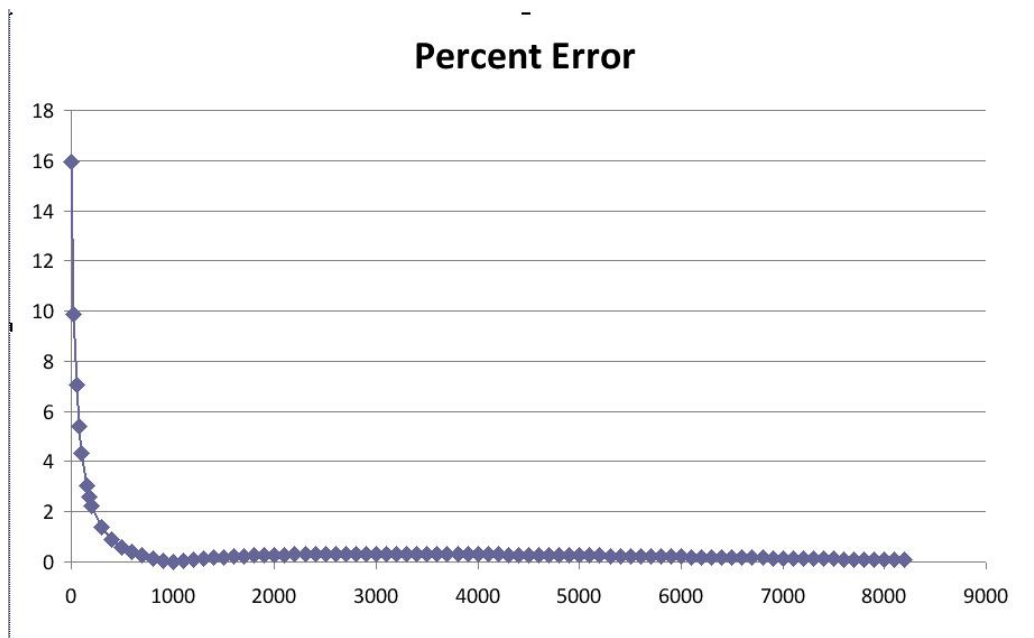


Figure 4.1: Graph of percent error in the linear assumption of energy conversion.

The equation to calculate the total energy,  $E_t$  emitted from all 8,190 channels is

$$E_t = \sum_{i=0}^{8190} C_i E_i = \sum_{i=0}^{8190} C_i (0.409i + 17.92) keV, \quad (4.2)$$

where  $C_i$  is the number of counts for the channel, and  $E_i$  refers to the energy per channel which is a constant determined by the program used to read and represent the GeLi data. This total energy emitted is then converted from kilo-electron volts to joules and it represents the total emitted radiation from the source measured. This source, however, is not the total amount of soil a person would encounter, at any given time.

To determine the amount of energy that would be emitted by the amount of soil a person would walk over, we must multiply by a scaling factor that represents the volume of soil a person would encounter divided by the volume of the sample soil size [13],

$$E'_t = \left( \frac{\frac{W^2}{4\pi} x}{\pi \left( \frac{d^2}{4} \right) h} \right) \left( 1.60218 \times 10^{-16} \frac{J}{keV} \right) E_t = \left( \frac{W^2 x}{\pi^2 d^2 h} \right) \left( 1.60218 \times 10^{-16} \frac{J}{keV} \right) E_t. \quad (4.3)$$

Equation (4.3) is represented using  $W$  as the average waist size of a man,  $d$  as the diameter of the sample jar,  $x$  as the depth of contributing soil, and  $h$  as the height of the sample jar. The waist size is used to predict the average cross sectional area of soil that a person is exposed to. While the largest portion of the human body is larger than the waist (on average), the waist serves as a good median of body sizes. The purpose of this is to find the best area over which the cross section of mass is distributed. The second major issue of determining the amount of contributing soil is to find the depth of soil contributing. This can be found using the Beer-Lambert Law. This law shows that unlike alpha and beta particles, the mass-less gamma particles are scattered and absorbed by the photoelectric effect, Compton scattering and pair production. Therefore, the intensity of the photon stream will fall off exponentially. The Beer-Lambert Law can be rearranged to give

$$\begin{aligned} x_i &= \left( \frac{\rho}{\mu} \right)_{iSoil} \frac{1}{\rho_{soil}} \ln \left( \frac{I_0}{I} \right) \\ &= \left[ \rho_w \omega_w \left( \frac{\mu}{\rho} \right)_{ww} + \rho_a \omega_a \left( \frac{\mu}{\rho} \right)_{wa} + \rho_c \omega_c \left( \frac{\mu}{\rho} \right)_{wc} + \rho_s \omega_s \left( \frac{\mu}{\rho} \right)_{ws} \right]^{-1} \ln \left( \frac{I_0}{I} \right), \end{aligned} \quad (4.4)$$

where  $\rho$  is the density of the material,  $\mu$  is its mass attenuation coefficient, and  $w$  is the weighting factor, or the composition percentage for each material.

In (4.4), the relationship of density to mass attenuation coefficient for soil is found using the natural cubic spline of data collected by the National Institute of Standards and Technology and is a function that is related to the energy  $E_i$ . This function is then multiplied by the natural log of the ratio of initial intensity to final intensity. To determine the depth at which radiation would not make it to the surface and therefore not contribute to the total ionizing radiation, then a ratio of 10, or a depth at which the final intensity is only one tenth of the initial intensity is to be used.

In order to determine the ratio of the density and the mass attenuation coefficient for soil, we must understand the soil composition. The ideal soil is supposed to contain 25% air, 25% water, 16.7% organic material and 33.3% minerals. For the purposes of our experimentation, the organic material is assumed to be entirely carbon, as organic life is carbon based, and the minerals are assumed to be silicon. This simplification allows us to use the weighted average for data to find both the density and the ratio of density to mass attenuation coefficient. Using the National Institute of Standards and Technology data, we accurately create a function. This can be used to create a complete look at the total energy,

$$E'_t = \frac{\left( \frac{W^2 \ln(10)}{\pi^2 d^2 h} \right) \left( 1.60218 \times 10^{-16} \frac{J}{keV} \right) \sum_{i=0}^{8190} C_i (0.409i + 17.92)}{\left[ \rho_w \omega_w \left( \frac{\mu}{\rho} \right)_{ww} + \rho_a \omega_a \left( \frac{\mu}{\rho} \right)_{wa} + \rho_c \omega_c \left( \frac{\mu}{\rho} \right)_{wc} + \rho_s \omega_s \left( \frac{\mu}{\rho} \right)_{ws} \right]}. \quad (4.5)$$

This would yield the total energy emitted by the soil, but to find the absorbed dose, one must take the total emitted energy and divide by the mass of the object that is in the path of emissions,  $m$ , or the average mass

of a human male in the US in this case. Therefore, the complete equation of absorbed dose would be given by the following:

$$\Gamma_A = \frac{\left(\frac{W^2 \ln(10)}{\pi^2 d^2 hm}\right) (1.60218 \times 10^{-16} \frac{J}{keV}) \sum_{i=0}^{8190} C_i (0.409i + 17.92)}{\left[\rho_w \omega_w \left(\frac{\mu}{\rho}\right)_{ww} + \rho_a \omega_a \left(\frac{\mu}{\rho}\right)_{wa} + \rho_c \omega_c \left(\frac{\mu}{\rho}\right)_{wc} + \rho_s \omega_s \left(\frac{\mu}{\rho}\right)_{ws}\right]}. \quad (4.6)$$

And therefore the effective dose will be equal to:

$$\Gamma_E = QN\Gamma_A. \quad (4.7)$$

This equation can be simplified further for the context of this lab. For gamma ray emission, as with all photons, the quality factor is one. Furthermore, if one uses the a full human as the object absorbing the radiation, then the scaling factor is equal to one as well and the effective dose is equal to the absorbed dose

While (4.6) is correct for the ideal detector, the GeLi detector is not a perfect one. Using the multi-nuclide source, we were able to create the efficiency curve for the machine. Because the device is only efficient for energies up to and including 3000 keV, only those counts within channels 0 to 7291. Since we have the efficiency of the device as a function of the energy, we can take the collected counts for each energy level and divide by the efficiency for the energy,  $U_i$ . The final version of the equation will then be as follows:

$$\Gamma_A = \frac{\left(\frac{W^2 \ln(10)}{\pi^2 d^2 hm}\right) (1.60218 \times 10^{-16} \frac{J}{keV}) \sum_{i=0}^{7192} \frac{C_i}{U_i} (0.409i + 17.92)}{\left[\rho_w \omega_w \left(\frac{\mu}{\rho}\right)_{ww} + \rho_a \omega_a \left(\frac{\mu}{\rho}\right)_{wa} + \rho_c \omega_c \left(\frac{\mu}{\rho}\right)_{wc} + \rho_s \omega_s \left(\frac{\mu}{\rho}\right)_{ws}\right]}. \quad (4.8)$$

While the final effective doses are lower once efficiency is taken into account, it is necessary to use these efficiency coefficients. We must also take into account the various other parameters of the equation. For the average person, we are using a waist size of 32 inches, average mass of 78.017 kilograms, and soil samples that are 1.920 inches in diameter and 1.127 inches in height, and finally the density and mass attenuation data from the NIST (National Institute of Standards and Technology) [11].

The data represented in the chart below shows the total effective doses from soil found around campus. As can be expected, the samples are similar since the soil samples are from a relatively close proximity and there has been little radioactive activity on campus. While one might assume that the highest radioactivity would be found in soil near to Washburn Shops, where the nuclear reactor was once housed, the high point of activity is found in area 12, at the corner of Olin Hall nearest the fountain. The second lowest levels of radioactivity can be found in the rubber of the new WPI turf. The least radioactive soil, however, was found outside East Hall.

The WPI average is 1.555 mSv in one year, if a person were to only stand on campus soil without ever sitting or lying down. According to the Oak Ridge National Laboratory which adapted data from the Savannah River Site Environmental Report of 1993, the average human in the United States absorbs  $3mSv$  in one year from all background radiation sources, including soil, air, solar radiation and microwave radiation. This means that while Olin Hall has higher levels of radiation, it is still less than two thirds of the national average of all sources of radiation. Furthermore, in the same report, the Oak Ridge National Laboratory states that the effective dose of an upper gastro-intestinal X-ray is 2.2 mSv [12]. This means that if you get one stomach X-ray, you have already absorbed more ionizing radiation that if you were to stand outside Olin for an entire year.

The data set does illustrate the necessity for the efficiency of the machine to be taken into account. The average WPI soil effective dose, without the efficiency coefficients, is well over the national average at 3.242

mSv. This number is without taking into account solar radiation, natural radon in the air and every other radiation we expose ourselves too.

While this data is very reasonable, it must be said that several assumptions were taken along the way. It was assumed that humans are all the same size, and that they consist of cylinders that are the circumference of their waist with the mass evenly distributed and at no time is any more of their body exposed to the ground. It was also assumed that no amount of radiation was lost in the course of the human body, as height was not factored into the depth of soil. The soil was assumed to be a perfect mixture, as was mentioned above, where all organic material consisted entirely of carbon and all minerals consisted entirely of silicon. Finally, in our graphical representation of radiation levels across campus, we assumed that all soil within a large area would be the same level of radioactivity when, in actuality, it would be a gradient function.

A more detailed soil analysis could determine exactly what the soil was comprised of and create a much better function of depth with respect to the energy of the gamma ray. This could either increase or decrease the amount of soil that would be taken into account and change the total energy. Furthermore, one could have come up with a better model of average cross sectional area that is exposed to the ground at a given moment. Finally one could take many more soil samples across the entire campus and create a seamless map of the radiation, however, this process would have been far too time consuming for this project. Figure 4.1 contains all of the data for each site, and Figure 4.2 shows a map of the WPI Campus and the radiation levels in each region based on the above analysis. Figure 4.3 shows the effective doses of radiation absorbed by the average person from each of the sample locations and Figure 3.4 shows the efficient effective radiation absorbed by a person, which corrects the data using the efficiency curve for the GeLi detector.

## 4.2 Radioactive Object Results

In this section, we will discuss the results of the international irradiated objects given by Mr. Kaltofen. We will attempt to determine peaks of radioactive isotopes within the object. We will also try to interpret these results in the context of the sample.

When analyzing the WPI soil samples, none of the samples were made of any one particular radioactive isotope and therefore, peak analysis could not be done. The same, however, cannot be said about the samples from Chernobyl, Ganges River, Columbia River, Russian goat's teeth, or Los Alamos. Within these samples, although the overall radiation from the source is low, they have large peaks that can be identified and explained. Through the use of the identifying markers of the MAESTRO program, as well as a table of nuclear isotopes when MAESTRO was too far off, these peaks are determined.

One of the constants from all of the samples is the peaks of lead throughout the samples and the large total effective dose from each sample. The lead peaks can easily be explained by the shielding surrounding the GeLi detector. Any sample within the GeLi detector is bound to be influenced by the lead shielding that is over several inches thick. Similarly, Chernobyl and Los Alamos and other areas where testing is done, are typically surrounded by lead at most times.

The other constant in all the data is a low total effective dose from the samples. This is easily explained by the size of the samples. All of the dirt samples are much smaller than the amount of dirt a person would be exposed to. For their size, these samples are radioactive, but well within safe limits.

For the Chernobyl button, taken from a panel at the Chernobyl power plant after its meltdown, the data shows the large amount of Cesium and a peak of lead. The Cesium found can be explained by the large amounts of cesium deposited after the explosion. When the Chernobyl accident took place, Cesium was released into the air and became the largest nuclear isotope found within the site surrounding the Chernobyl station. While the total effective dose of the Cesium from the Chernobyl button is very low, one must

Sample Number	Effective Dose (mSv/s)	Effective Dose (mSv/year)	Efficient Effective Dose (mSv/s)	Efficient Effective Dose (mSv/year)	Average WPI (mSv/year)	Efficient Average (mSv/year)	Average US from All Sources (mSv/year)
1	5.71787E-08	1.80319	4.85925E-08	1.53241	3.24177	1.55510	3.00
2	7.8192E-08	2.46586	5.13209E-08	1.61846	3.24177	1.55510	3.00
3	8.25902E-08	2.60456	5.07782E-08	1.60134	3.24177	1.55510	3.00
4	1.04246E-07	3.28751	5.31937E-08	1.67752	3.24177	1.55510	3.00
5	5.30261E-08	1.67223	4.29304E-08	1.35385	3.24177	1.55510	3.00
6	7.25557E-08	2.28812	4.54694E-08	1.43392	3.24177	1.55510	3.00
7	7.06809E-08	2.22899	4.80675E-08	1.51586	3.24177	1.55510	3.00
8	7.69051E-08	2.42528	4.44688E-08	1.40237	3.24177	1.55510	3.00
9	9.75426E-08	3.07610	5.38323E-08	1.69766	3.24177	1.55510	3.00
10	6.48237E-08	2.04428	4.6714E-08	1.47317	3.24177	1.55510	3.00
11	8.76887E-08	2.76535	5.31945E-08	1.67754	3.24177	1.55510	3.00
12	1.04019E-07	3.28033	5.46756E-08	1.72425	3.24177	1.55510	3.00
13	1.10417E-07	3.48210	5.07664E-08	1.60097	3.24177	1.55510	3.00
14	2.23795E-07	7.05761	5.23634E-08	1.65133	3.24177	1.55510	3.00
15	9.00652E-08	2.84030	5.01057E-08	1.58013	3.24177	1.55510	3.00
16	6.76696E-08	2.13403	4.89325E-08	1.54313	3.24177	1.55510	3.00
17	3.47376E-07	10.95484	4.40159E-08	1.38809	3.24177	1.55510	3.00
18	6.1554E-08	1.94117	4.81903E-08	1.51973	3.24177	1.55510	3.00

Table 4.1: Calculated Dirt Sample Data

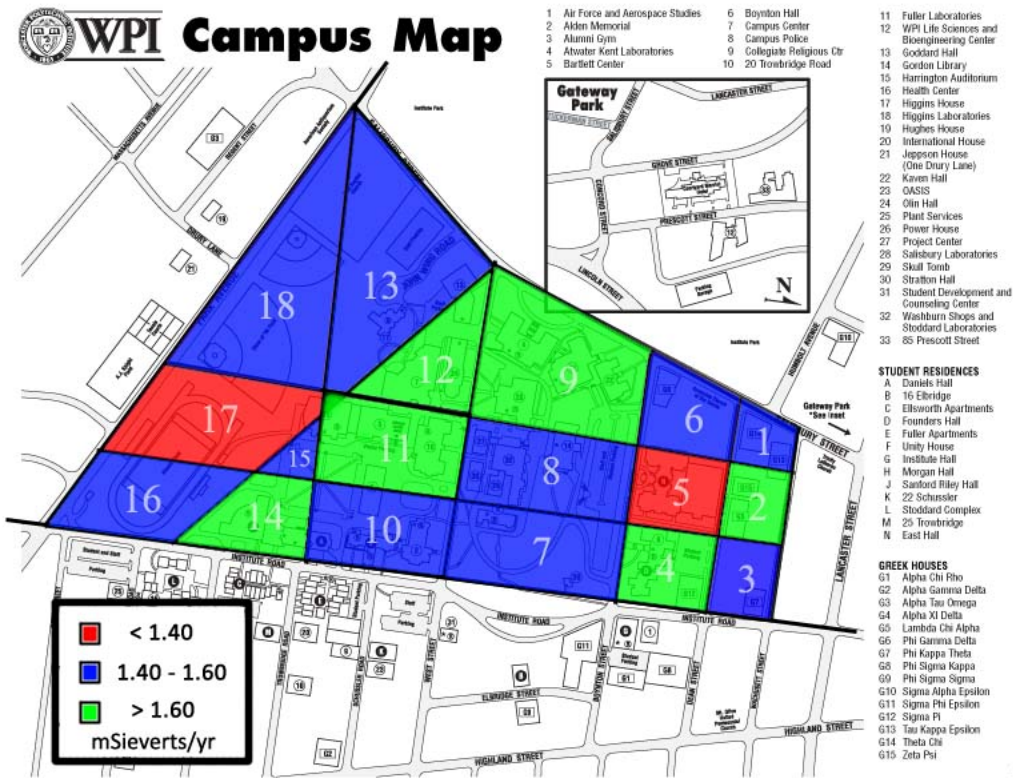


Figure 4.2: Radiation Levels around WPI Campus in mSieverts. The average yearly total from external radiation is 3.00

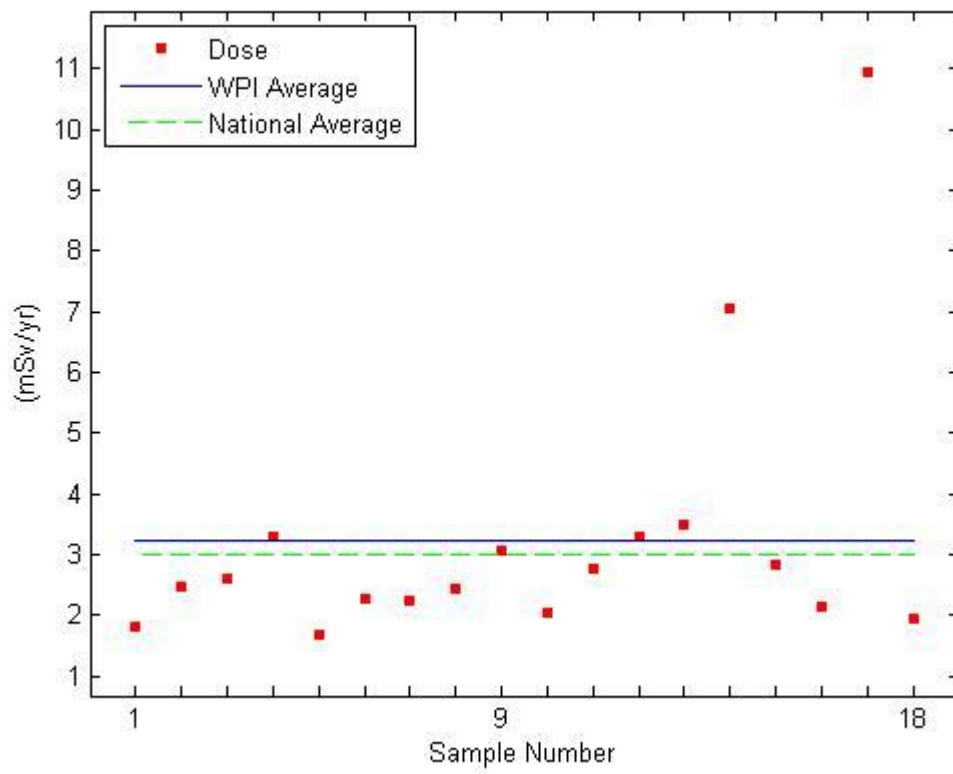


Figure 4.3: Effective doses of radiation before correction for each area along with national and WPI averages.

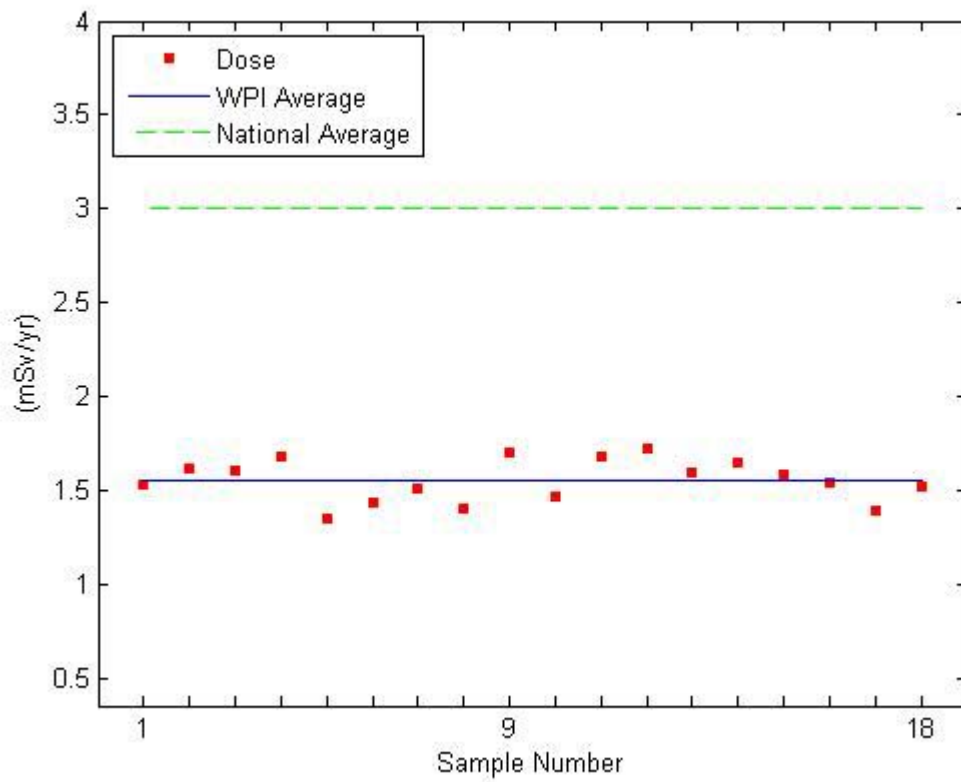


Figure 4.4: Actual Radiation absorbed by a person using efficiency corrections along with national and WPI averages.

remember that with a half life of approximately 30 years, and that the event happened over 20 years ago, there is little more than half the Cesium still left on the button. Also, this button itself is relatively small in size (about one square inch), but for its size, it represents one thousandth of the amount of radiation received annually from all background radiation sources. This means that if you had a 3 foot by 5 foot dinner table made of these buttons, you would take in 7.63 mSv annually, or over twice the amount of radiation you would take in from natural radiation or nearly 4 more stomach X-rays a year.

The next samples to analyze were the silt from the Ganges River and the Columbia River. Both rivers share in common that they run next to nuclear testing facilities. These facilities through testing, mishandling of samples or mishandling of waste have contaminated the river with radioactive isotopes in their silt. Both rivers had a large amount of Uranium-233, a common radioactive isotope used in nuclear weapons and early nuclear reactors. Both samples also have a large amount of lead that can be explained by either the shielding around the GeLi detector or shielding that was around the site. For the Columbia River silt, the other main isotope is Potassium-40. The Potassium-40 found is easily understood because K-40 is a naturally occurring gamma ray emitter. For the Ganges River silt, the other main isotope is Bismuth-207. Although Bismuth-207 is not naturally occurring, it is often created by proton radiation of lead sources. This would mean that any alpha radiation hitting the lead shielding of the test center, or possibly the lead in the silt already, would have created Bismuth-207 as a byproduct. All of the isotopes within these samples can be explained and therefore, the program is reliable.

With the Los Alamos samples, labeled “LAO 1175”, “Mesa Soil”, “Takedu Solods” and “Trailer Dust” the most prevalent isotope found was always Uranium. This isotope is most easily explained through the history of the site. Los Alamos was the site where J Robert Oppenheimer and his team set about the task of creating the first atomic bomb. Here they experimented with and utilized Uranium for their work. It makes sense that Uranium, from either testing or mishandling ended up in the soil below the work station. Again the isotopes K-40 and Bi-207 are both found throughout some of the samples. Again, Potassium-40 is a naturally occurring radioactive isotope and the Bismuth-207 is created anytime alpha particles hit the lead shielding. The other main isotopes that can be identified are Cesium-136, Neptunium-237, Tantalum-182, Bismuth-214, Selenium-75, and Europium-152. These are all byproducts of nuclear production or decay. For instance, Np-237 is a byproduct of plutonium production, which occurred at Los Alamos for the production of nuclear weaponry. Similarly, Eu-152 is a product of fission of U-235, the nuclear isotope that underwent fission in a nuclear explosion. Bismuth-214 on the other hand is created in a step of the decay of Radon-222 (another byproduct of U-235 fission) to stable Lead-206. Lastly, Tantalum-182 is a metal found naturally in the earth and was found in the soil of Los Alamos.

Because almost every peak identified by the MAESTRO program can be explained based on what the sample is, the program is accurate. The errors in the program can be solved by checking the half life of any peak identified. If the half life is not on the order of years, then it is not likely to be the radioactive isotope. Whenever using this program, you can identify and analyze the radioactive isotopes found in samples.

### **4.3 Rutherford Theoretical Data Analysis**

In this section we will discuss the data generated by the mathematical model of the Rutherford experiment. We will analyze the data for the correct relationships Rutherford discovered as well as discuss ways in which the data might differ from the real world counterpart.

With Rutherford’s equation, he concluded that the number of particles deflected and absorbed were dependant on several different variables. Those variables that are important to the mathematical model and the lab experiment itself are the angle at which the deflection is being detected, the atomic number of the

foil, the foil thickness, the foil width and the number of incident particles. The relationship between each of these variables and the counts recorded can only be determined by considering all other variables constant, therefore each variable is analyzed on its own.

The relationship between the scattering angle and the number of counts is the most complex of all the other variables. The number of estimated counts is inversely proportional to the sine of half the angle raised to the fourth power. To illustrate this data, the program model was used for Gold foil with 997 incident particles. This graph is then plotted with the graph of a constant over the sine of an angle divided by two raised to the fourth power. This is seen in Figure 4.5 with the theoretical data in a solid red line and the experimental data as the blue circles. Looking at both of these graphs, it is clear that the relationship holds true. The error in this relationship is the nature of the sine to the negative fourth power. Although the number of counts could be very high, it will never be infinite, as the other would. For this reason, the graphs will be slightly off, but this error is necessary to account for real world conditions.

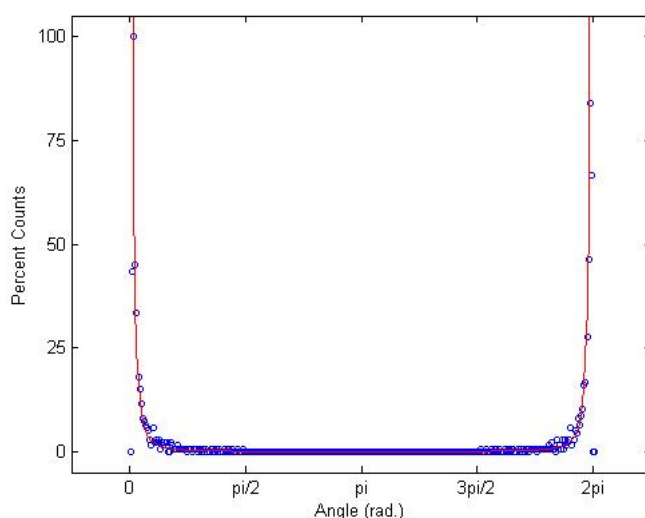


Figure 4.5: Plot of Counts per angle for 997 incident particles on Au Foil. The theoretical data is represented by the solid red line and the the experimental data is represented by the blue circles.

The second most complex relationship, according to Rutherford, is the one between the number of counts for a specific angle and the atomic number of the foil. Rutherford proved that the number of counts was proportional to the atomic number squared. The theoretical data for this is represented in Figure 4.6, with the  $x$ -values being the squared atomic number and the  $y$ -value representing the number of counts. These values were predicted by the model for a specific angle (one that is not the extremes) and for a specific number of incident particles. This graph can be seen as nearly linear. Although the graph is not perfectly linear, its error is due to the fact that the spacing between atoms was required to change. This error is due to the programming of the model and was something that could be changed to create a more accurate model given more time and a computer with much higher processing ability.

The most intuitive relationship of all that was discovered by Rutherford was that between number of incident particles and the number scattered at a specific angle. It stands to reason that the more particles fired at a target the more that are likely to be scattered off the target. One could say that this is not a relationship at all, but testing of this relationship will prove the accuracy and durability of the mathematical

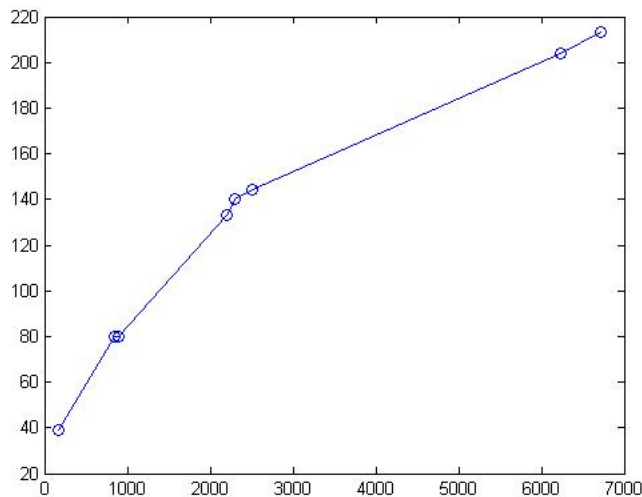


Figure 4.6: Plot of counts versus atomic number<sup>2</sup>

model. In Figure 4.7 the  $x$ -values are the number of incident particles, the  $y$ -values represent the number of particles that were scattered at a particular angle and the different colors are used to represent foils of different elements. Almost every line can be seen to be linearly upward, as would be expected. The error found in the experiment is due in large part to the simplicity with which the model had to be made. As discussed earlier, since the computers used were limited in their processing ability, some experiments and data collected therefore had to be curtailed. Although the data is imperfect, the relationship still holds true.

Almost as intuitive as the number of incident particles, one would also expect a correlation between the thickness of the foil and the number of counts at a specific angle. Knowing the theory behind scattering is that a particle tries to move through a foil, but along the way, it runs into the atoms of the foil and are pushed away from the trajectory they would have had if there had been no atoms. It makes sense then, that the more layers of atoms the particles must travel through, the less likely it becomes that the particle will come through unaltered in course. Rutherford found that the number of counts made at a specific angle was directly proportional to the thickness of the foil. The data generated by this mathematical model in Figure 4.8, but can be seen as nearly horizontal. This data would indicate that there is no relationship between counts and thickness; however, this is another flaw in the model. The fundamental flaw in the model that explains this is the number of particles coming out the side of the foil. Below the graph is the trajectory of 449 particles incident on gold foil that is 29 and 47 atoms thick respectively. These trajectories show that a large number of particles are coming out at  $90^\circ$  and beyond, with the respect to the normal. In a real laboratory experiment, the width of the foil would stop all particles from coming out the side and thus all particles would be reflected within  $180^\circ$ . If the program could be run regardless of the length of computing time, then the thickness and width would be on the order of centimeters instead of picometers to account for this error.

This leads to the last variable to be determined, the width of the foil. Rutherford's final equation that describes all the relationships he found makes no mention of foil thickness. Although, as it was discussed above, the foil should be in the order of centimeters thick to account for particles coming off the side, the data below was still kept at the picometer scale. In the graph below, the  $x$ -values are the width of the foil

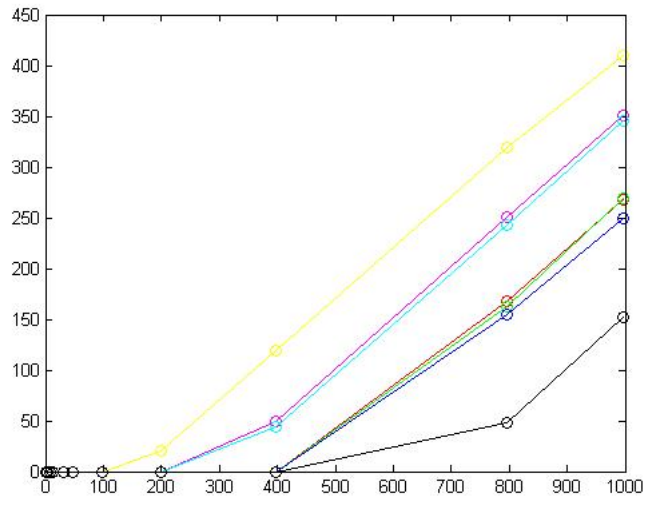


Figure 4.7: Plot of counts versus number of incident particles for all different foils.

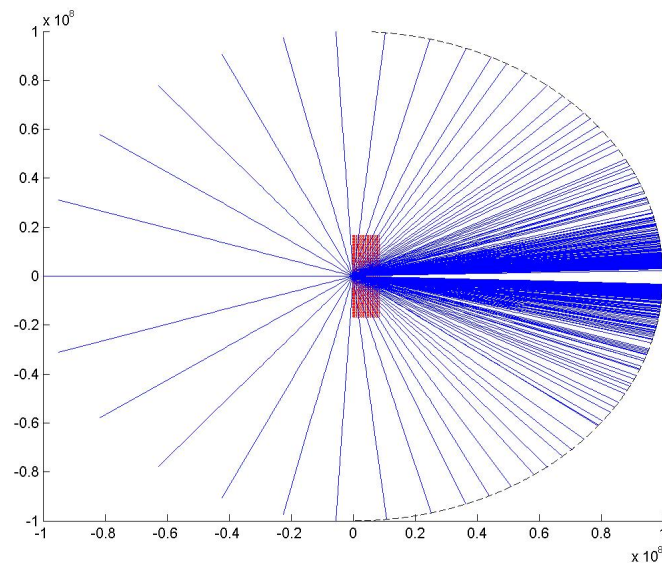


Figure 4.8: Trajectory of particles for 449 incident particles on Au foil that is 29 atoms thick.

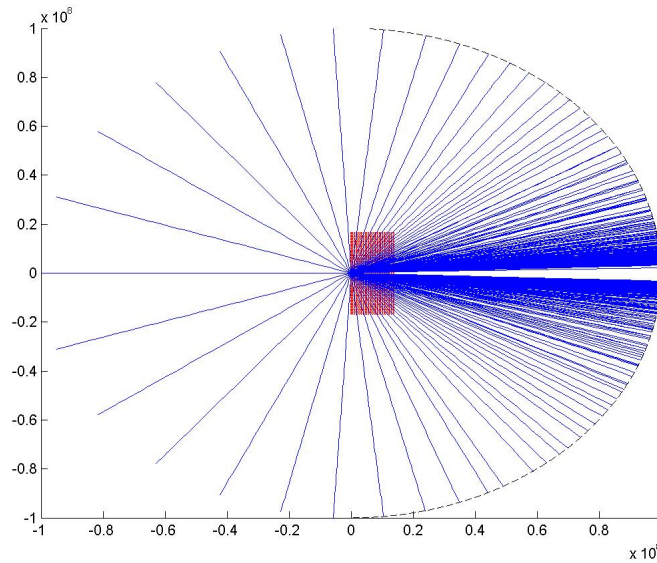


Figure 4.9: Trajectory of particles for 449 incident particles on Au foil that is 47 atoms thick.

in atoms and the y-values are the number of counts made at that specific angle, where each color represents different foils. These plots can be seen to be nearly horizontal, and therefore the independence of the two variables can be confirmed. Below the graph, there are two trajectories of 499 incident particles for gold foil of 37 and 79 atoms wide respectively. Again, very little difference can be seen between them, indicating the accuracy of the relationship.

This model is not a perfect model of the Rutherford scattering experiment. It only operates in two dimensions, instead of the three we live in. The program is limited by the computer's memory and the allotted time for the experiment. All this understood, it is still in keeping with the relationships that Rutherford himself discovered. Because of its ability to maintain the relationships, within a reasonable error, this model can be used to predict the number of counts that would be recorded for a set experiment. If the Rutherford experiment had been working, we could assess the error associated in this model by comparing it against tested data, however, this was not possible.

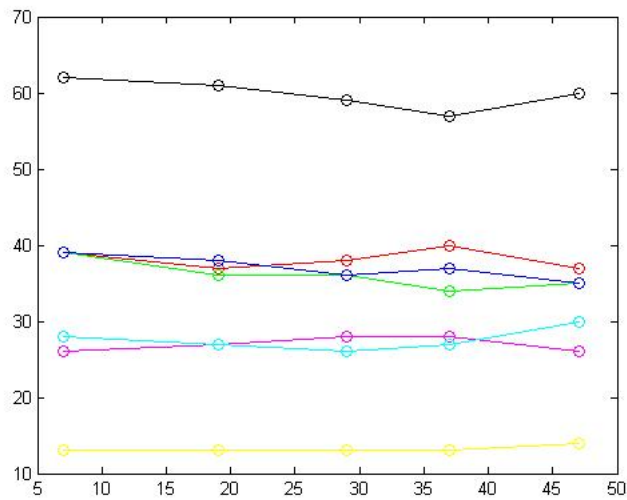


Figure 4.10: Plot of counts versus thickness for all foils.

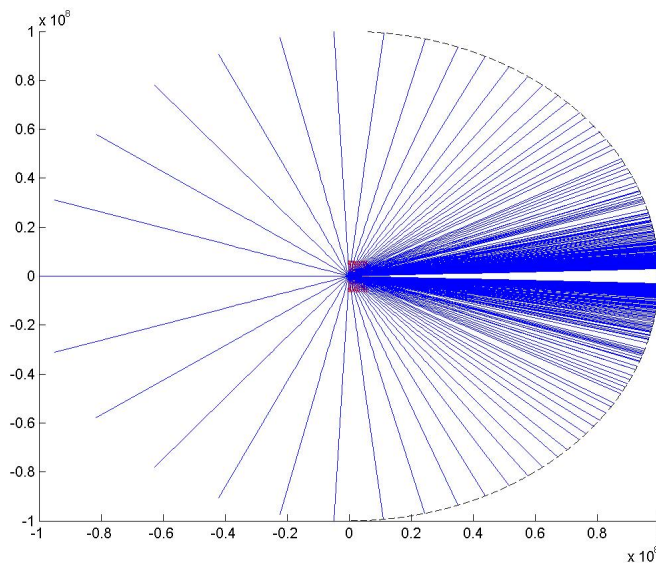


Figure 4.11: Trajectory of particles for 499 incident particles on Au that is 37 atoms wide.

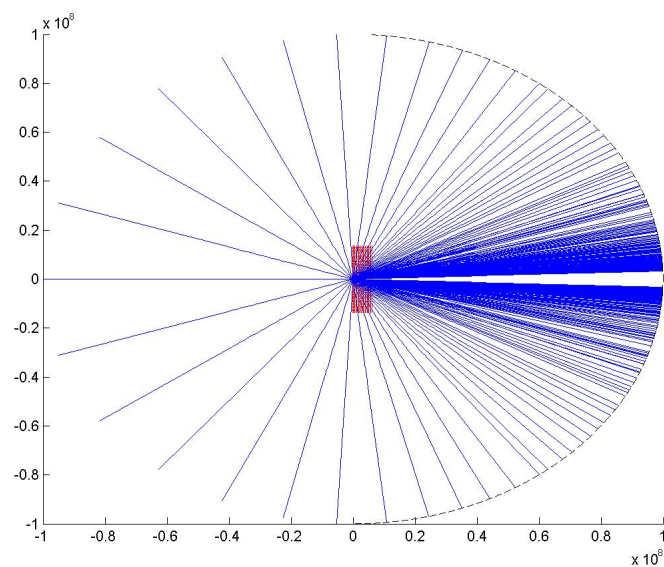


Figure 4.12: Trajectory of particles for 499 incident particles on Au that is 79 atoms wide.

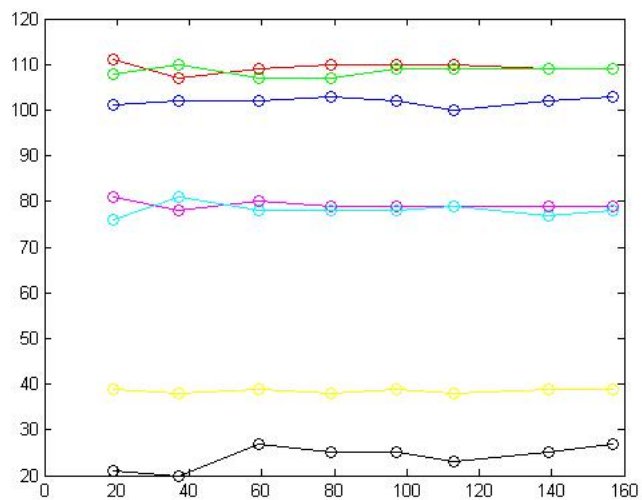


Figure 4.13: Plot of counts versus width for all foils.

## Chapter 5

# Conclusions

In this chapter, we will explain what we have accomplished and determine steps that can be made in the future on this project. We will analyze any errors or assumptions that we might have made. Finally we evaluate whether or not we have achieved our goals.

Through our physical work with the Rutherford scattering device we were able to get it almost fully operational. The device is set and there are procedures ready to be run once it is fully operational. The device is in need of a new  $\alpha$ -particle detector which must be further researched. The detector is a surface barrier detector with a 25 mm<sup>2</sup> detection area. Once this is replaced data may be once again collected to repeat Rutherford's classic experiment. While the device was unable to be fully repaired, we created a laboratory procedure that can be run to help students fully understand the principles behind the Rutherford alpha scattering experiment.

After this data has been collected, it may be compared with the mathematical representation of the Alpha Scattering experiment created in MATLAB. The MATLAB program should provide an accurate mathematical model of the scattering experiment created by Rutherford. It models the path of particles shot at a nucleus, as well as particles shot at layers of nuclei and models the scattering caused by this. The possible problems that may arise from this numerical experiment are that the code at its fastest still takes a lot of processor time to compute close to real world results. This is evident in the analysis of the count dependence on thickness. It would be beneficial to examine the relationships other than just those that are verified using the lab setup. The numerical experiment uses two methods of numerical modeling, the classical fourth order Runge Kutta method and the Dormand-Prince(4,5) embedded pair method (through ODE45.m). An investigation into more advanced routines, such as a higher order embedded pair would prove useful in developing a more accurate experiment. Ultimately the numerical experiment is limited to the computer processing time available, and inherently the level of technology available to the student carrying out the experiment. While the Dormand-Prince method proved to be much more efficient than the classical Runge Kutta method, any other routine that increases the efficiency and maintains the accuracy of the experiment would be invaluable. Adjusting the model assumptions, such as how the nuclei positions are defined, might yield results that more closely resemble lab results. This numerical experiment is not only used as an investigation into Rutherford scattering but also as a study and comparison of various mathematical methods. Being able to compare the physical data with the predicted mathematical data will give students a further understanding of the scientific principles involved.

In terms of the GeLi detector we were able to provide an analysis of soil samples from various regions around the WPI Campus, as well as analyze some samples from radioactive hot spots around the world. We were also able to right up a step by step procedure on how to run the GeLi detector, replace its nitrogen, and

interpret the data that it provides. The GeLi detector provides students with a way to further understand the nature of gamma ray emission and detection. It is an easy to use device that will allow students to gain experience in identify radioactive peaks based on the emitted energy levels, as well as how to identify peaks through background radiation.

While the GeLi detector provides analysis of a wide range of energy levels, it is not a perfect analysis device. Because it was located in the basement of Olin Hall, surrounded by concrete and in a room with no ventilation, a lot of the data collected was contaminated by radiation in the air and coming from the surroundings. We were unable to successfully purge the air from the testing chamber and therefore there were always noticeable radon peaks in our data. In addition all of this contamination created a large amount of noise in our graphs, which cause some small radiation peaks to go uninterpretable. In the future it would be ideal to create some way to have the samples analyzed in a vacuum and clear radiation environment because the detector is so sensitive.

## Chapter 6

# Appendices

### 6.1 Alpha Scattering Experiment Setup in Pictures



Figure 6.1: Full setup of the Rutherford Scattering Experiment. On the left there is a standard Ortec electronic counter. In the middle is the control box for the setup. There is a switch for rotating the sample wheel, and a switch for moving the detector through a range of angles.

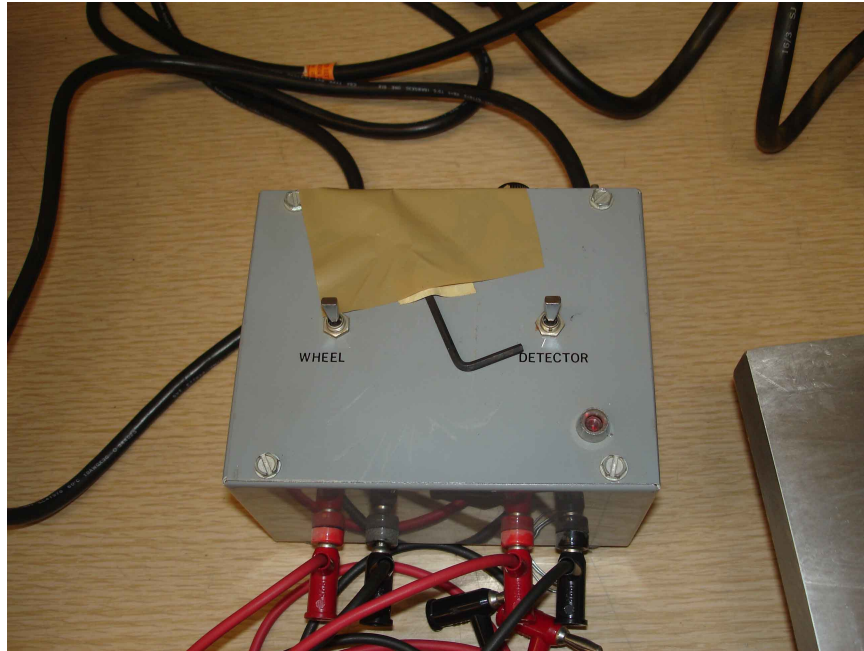


Figure 6.2: Rutherford Control Switch. The left switch rotates the thin film wheel, while the right switch moves the detector through a range of angles.



Figure 6.3: The counter and control box are connected to the main section of the experiment setup via cables into the following connector.

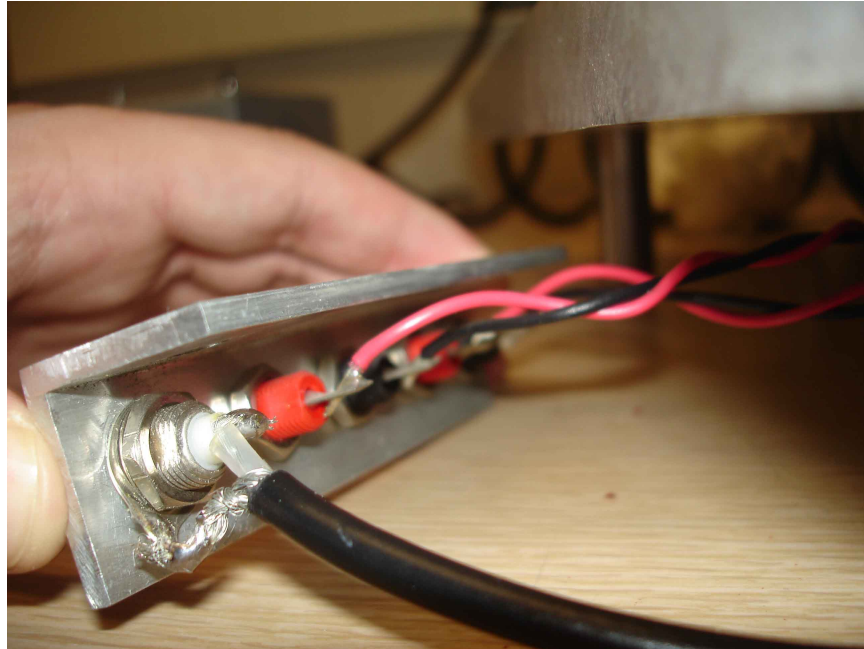


Figure 6.4: The back part of this connector shown below, is connected to the main detector housing, and the wiring on the back was removed and re-soldered to ensure that it is working.



Figure 6.5: These connections are connected into the vacuum chamber through a contact plate on the under side seen here.

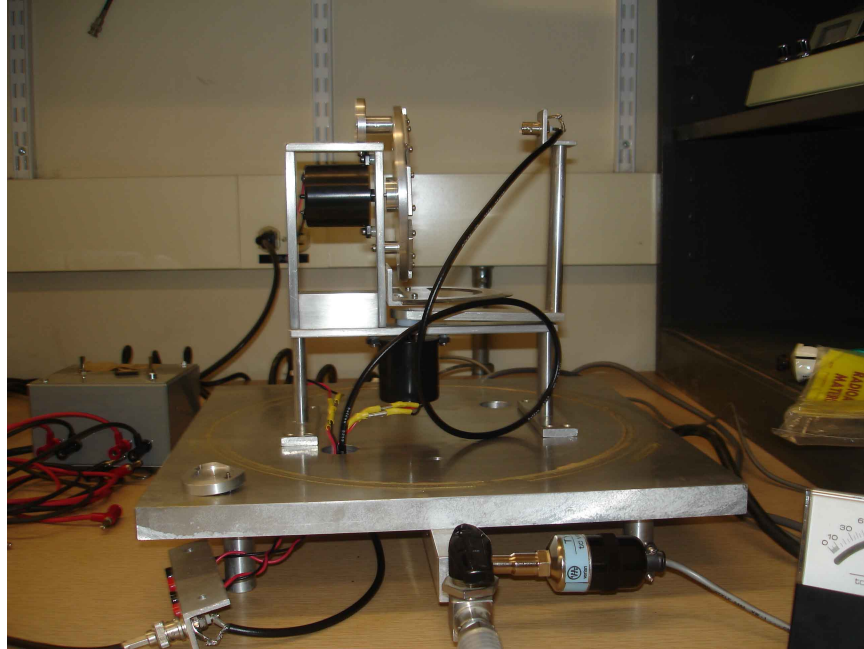


Figure 6.6: All the connections lead to the main region of the connector which contains a wheel to hold thin material samples, a detector to detect alpha rays, and a holder for the alpha ray sample.

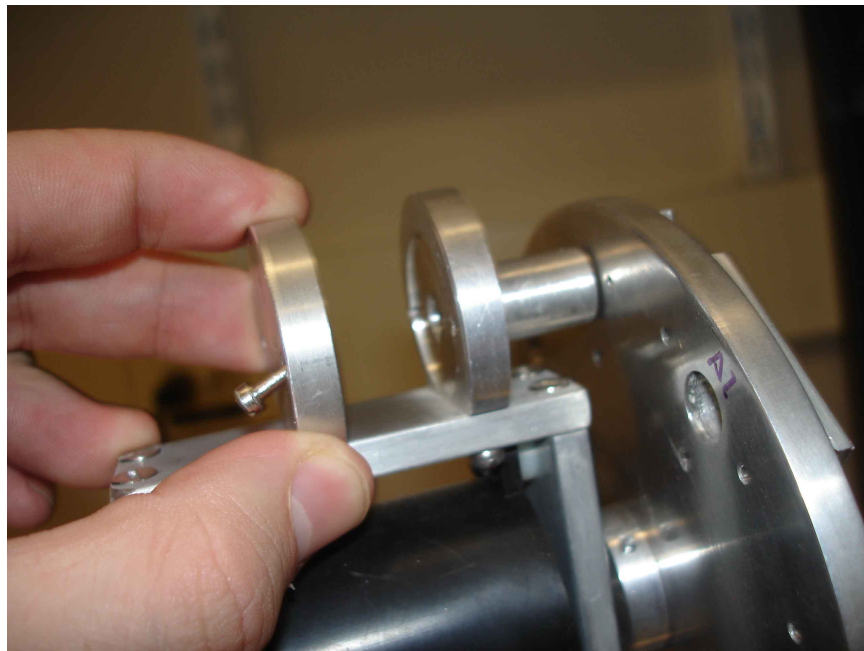


Figure 6.7: The Sample is held in place by this plate with two screws to project the  $\alpha$ -particles directly forward through the thin film wheel.



Figure 6.8: The sample wheel seen here is used to hold thin material films a few atoms thick in order to measure the deflection created by the nuclei of the atom. In addition the protractor is used in relation to the detector arm to determine the angle of deflection being measured.



Figure 6.9: The detector connections were also re-soldered to ensure that they were working properly.



Figure 6.10: This is connected to the previous region via a BNC connection and registers when an  $\alpha$ -particle hits it. This is the section of the device that we have determined to be malfunctioning.



Figure 6.11: When the entire device is assembled a bell jar is placed over the detection devices, and a light dampening cover is placed on top of that. The setup is hooked to a vacuum pump and a vacuum is created in order to ensure that there are no loose particles floating around.

## 6.2 Alpha Scattering Lab Procedure

### 6.2.1 Rutherford Scattering Experiment

In order to begin the Rutherford Scattering experiment you will need some small Alpha Ray sources. Point sources encased in a plastic 1 inch diameter disk are suggested. Ensure that the device is fully operational by powering up all the equipment and testing it out. Make sure that the wheel turning mechanism and the angular movement of the detector are both functional. Next, place the bell jar over the device and test out the vacuum pump until you are able to ensure that a viable vacuum is reached in the chamber and it cannot be removed by normal means. Once all of these devices are working take an alpha sample and mount it to the device such that the source is pointed through the hole and towards the detector. Make sure the detector is facing directly at the source (zero deflection angle), and take some base counts. Take some counts at other angles as well to see that there should be no deflection effect.

Now it is time to begin the experiment. To begin you will need some thin sheets of material such as pure Al, pure Au, etc, just a few atoms thick. The experiment wheel has slots for these to be mounted so that the alpha particles may be shot through the screen. By repeating the initial test experiment you should see a decrease in the particles that are able to go through un-deflected. Conduct further tests at equal angular distributions to the left and right side of the normal. These should allow you to see an angular distribution of deflection which is based upon the deflection caused by the nuclei of the material through which the particles are traveling. By testing this through different known sources, an understanding should be developed about how the mass and charge of the nuclei affect the rate of deflection. To test this understanding the experimenter should then use some films of unknown concentrations of materials to determine the approximate atomic distribution through the material based upon the scattering. This test can be conducted with other pure films, or mixed films can be attempted for a greater degree of difficulty.

### 6.2.2 Alpha Detector Experimental Procedure

The purpose of this laboratory experiment would be to take students through Rutherford's thought process and help them to determine the relationships he found. Students could use a known foil, to determine the relationship between deflection angles and foil thickness and foil type. Students could then apply this relationship to an unknown foil in an attempt to determine its thickness and foil type. Furthermore, this exercise would illustrate the importance of error analysis and efficient laboratory and testing skills.

#### Setup of Experiment

In setting up the experiment, the first steps must be safety precautions. Start by checking the bell jar for cracks or bubbles. Under the vacuum you will be working with, any crack or bubble could break and the glass bell jar will shatter. Second, make sure that the belt on the vacuum pump is facing a wall. When the pump is turned on, the belt will rotate very rapidly, and any loose clothing could get caught. Finally, the plugs in the side of the Alpha Scattering base are soldered on to the device. Do not touch the back of the plugs together for fear of electric shock. As with all laboratory experiments, it is good practice to never work alone. In the event that an accident occurs, it is always best to have a partner there to assist you. Following all safety precautions, one must start by hooking the wheel and detector control box to the apparatus base using red wires as positive and black as negative. Using the controller, move the detector to the 90° mark, or directly in front of the alpha source, at the same time, move the wheel to an open hole with no foil. Next, using the provided BNC cable, attach the apparatus base to the ORTEC counting device. Finally, applying a layer of vacuum grease to the bell jar, place the jar over the apparatus and attach the vacuum pump to the

device. Turn the pump on and create a vacuum. Once the vacuum is achieved, seal off the apparatus and place the black box over the bell jar. Set the ORTEC counter to a specific time step and measure the amount of counts given at 90° with no obstruction. Repeat this several times for the same time step until you have a statistically relevant average for the number of base counts. Throughout the course of the experiment, you must use the same time step to make sure that all data is comparable. Rutherford's experiment does not take in to account a rate of particles detected, thus only counts over the same time step will be directly comparable.

### Known Foil Testing

Once you have established a base count level, remove the black box again and turn the wheel so that the gold foil of known thickness is in the path of the beam. Move the detector to the 0° mark, cover the bell jar with the box and record the number of counts for the same time step as before. Again, repeat this step until you have statistically relevant data. Once you have completed this, remove the box and move the detector by some angle and measure the number of counts again. Repeat this through all 180° of the detector sweep path. Pay close attention to the wheel to make sure that it does not rotate during measurements. This should be performed for the silver, tin, aluminum and copper foils of known thickness. Record the thickness for each of these foils as well as the atomic number. Using the Rutherford equation, you must verify the relationships he discovered.

$$N(\theta) = C \frac{(N_i n L Z^2)}{\sin^4 \frac{\theta}{2}} \quad (6.1)$$

In his equation,  $N_i$  is used to represent the number of incident particles (which is the base count found earlier),  $n$  is used as the number of particles per cubic meter or the particle density of the foil,  $L$  is the thickness of the foil in meters,  $Z$  is the atomic number of the foil and  $\theta$  is the angle at which the measurement is taken. In Rutherford's original equation, the number of particles is dependent on the distance the detector is from the alpha source, the permittivity of free space and the kinetic energy of the alpha source, however, these are all constant in the

For the five foils, plot the number of counts made versus the sine of half the angle raised to the fourth power. For all foils, are the plots linear? Why not? Add error bars and determine if it is now linear. What do the slopes of these plots represent? Given the base count and the thickness, as well as the slope of the plot, can you come up with a relationship of  $n$  and  $Z$  for each foil?

### Unknown Foil Testing

To truly test the relationships determined above, you must also prove that it can work with some unknown data. For this reason, two of the foils in the wheel are considered unknowns. The first is known in composition, but unknown in thickness. The second is of known thickness, but unknown in composition. For this reason, we have established a relationship between the particle density of a foil and the atomic number of a foil.

Once you have measured all of the known foils, you must move the wheel to the foil of known composition, but unknown thickness. For this foil, again measure the counts at different angles, varying the angles and recording the data. Using the same laboratory practices as above, take several measurements for each angle to establish a statistical average and an error for each point. Plot the number of counts against the sine of half the angle raised to the fourth power again to determine if the function is linear. Using the slope, of the line, determine the thickness of the foil. How does the data compare to the foil of the same composition, but

different thickness? Add the plot of the same composition but different thickness to this plot? What is the relationship between the slopes? What is the relationship between the known thickness of the original foil and the experimental thickness of our unknown foil?

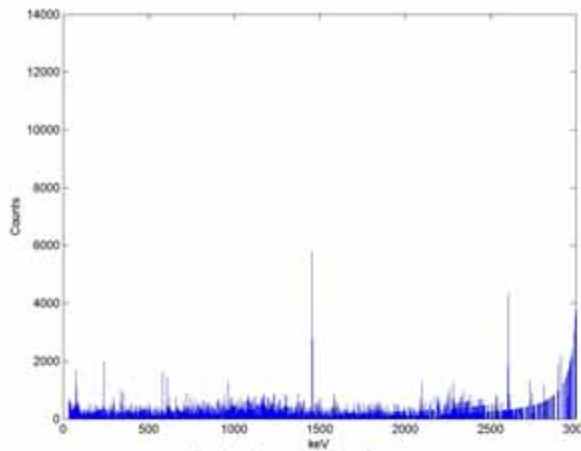
Lastly, move the wheel to the final foil, the foil of known thickness and unknown composition. Using the same laboratory technique, sweep out a full  $180^\circ$  with the detector and measure the counts along the path, being sure to take several counts at each angle to ensure a statistically accurate data set. Plot the number of counts against the sine of half the angle raised to the fourth power. Is the plot linear? What is the slope of the line? Using the slope, the thickness of the foil, and the relationship between particle density and atomic number, determine the atomic number and thereby the composition of the foil? Compare this data with the other foil of the same composition. Plotting their data on the same graph, are the plots linearly dependent?

### **Conclusion**

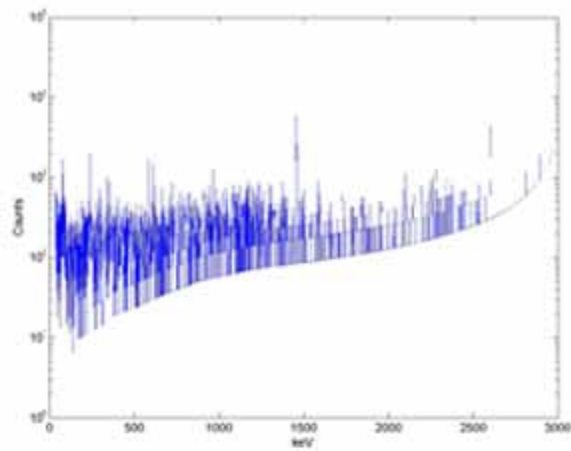
What conclusions can be drawn about Rutherford's relationships? How accurate was the data measured? Can the relationship be used on unknown? How did the theoretical unknowns match against the actual foils? Can you account for any differences between the theory and the data?

## **6.3 Dirt Sample Graphs**

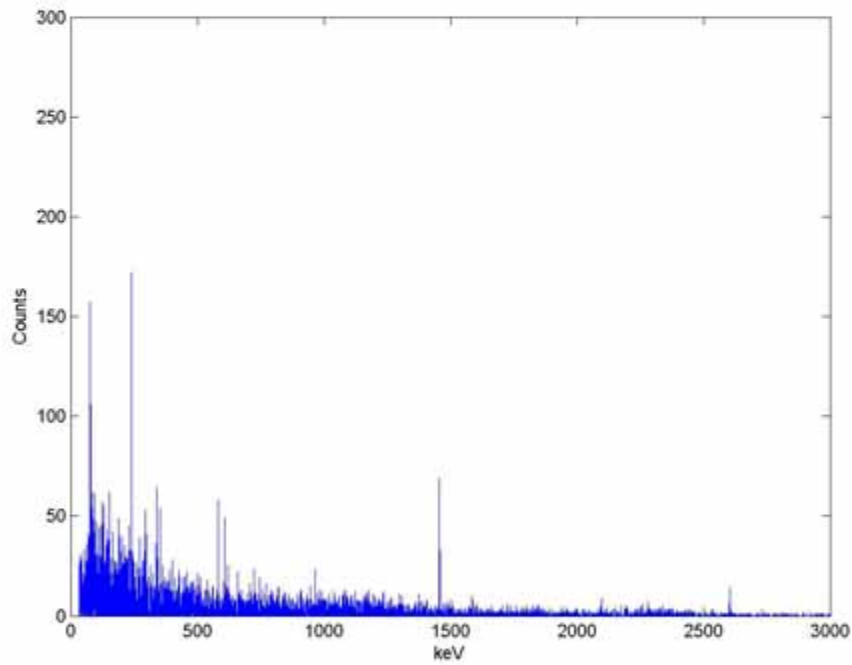
Contained here are the actual data graphs we received by using the GeLi detector. In addition there are also graphs of the correct data, which takes into account the data we obtained in the GeLi detector with no sample inside of it. The final graph is the semi-log graph of the corrected data, which allows you to see a clear noise curve in the data.



**Data Corrected using  
GeLi efficiency curve**

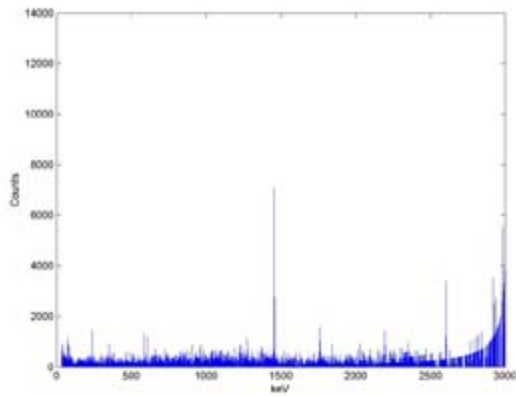


**Semi-Log of Corrected Data**

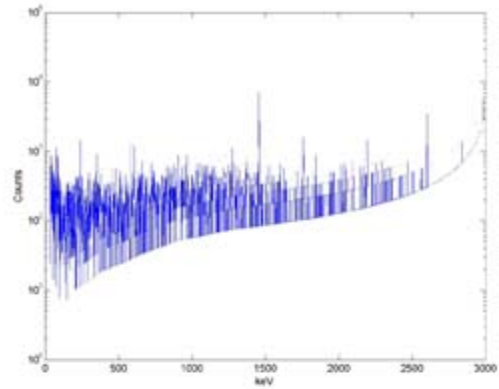


**Counts after removing background radiation**

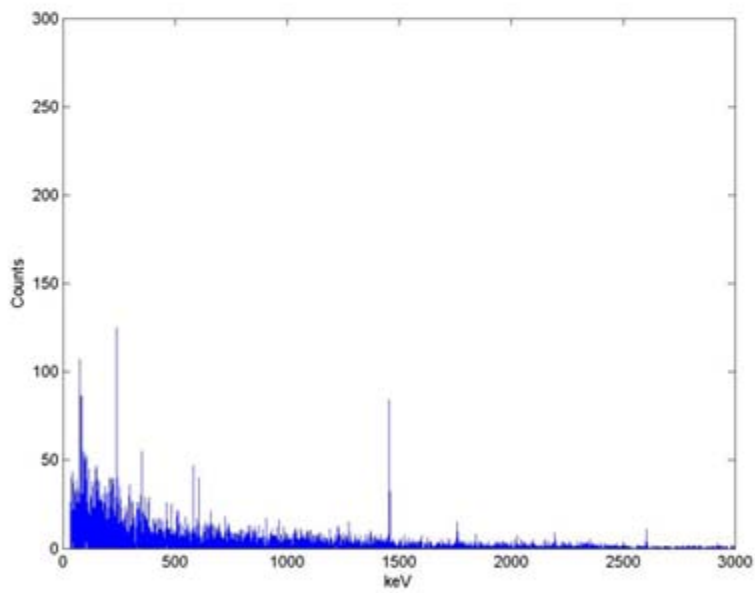
# Sample 1



**Data Corrected using  
GeLi efficiency curve**

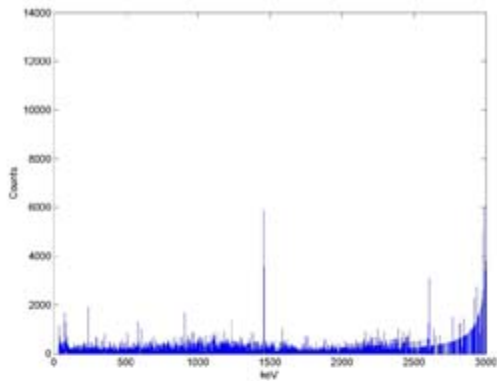


**Semi-Log of Corrected Data**

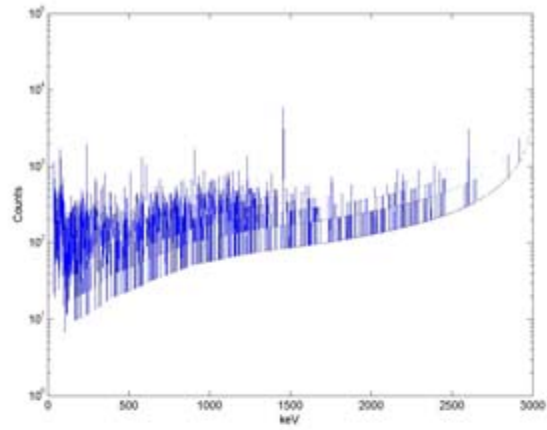


**Counts after removing background radiation**

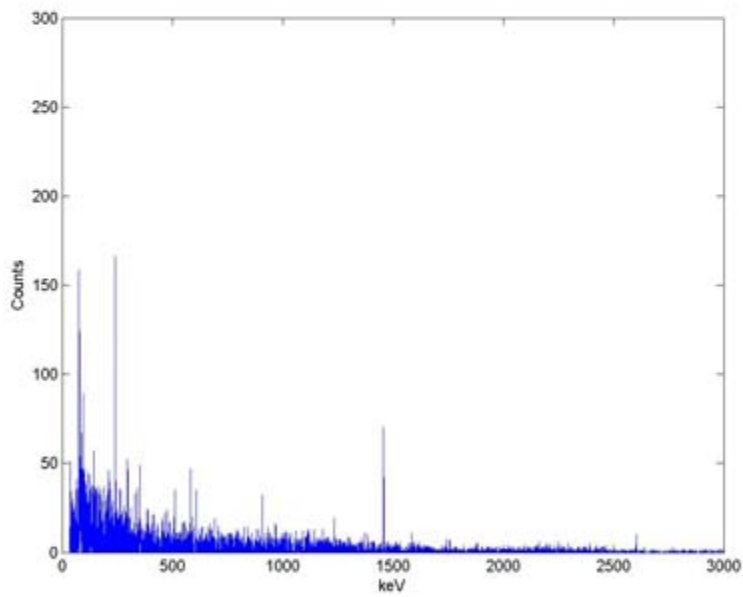
# Sample 2



**Data Corrected using  
GeLi efficiency curve**

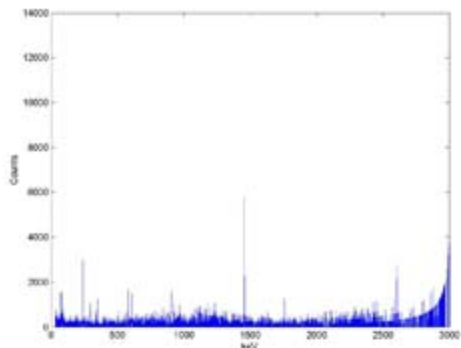


**Semi-Log of Corrected Data**

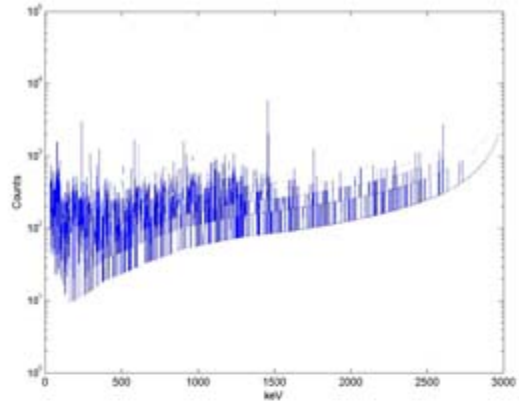


**Counts after removing background radiation**

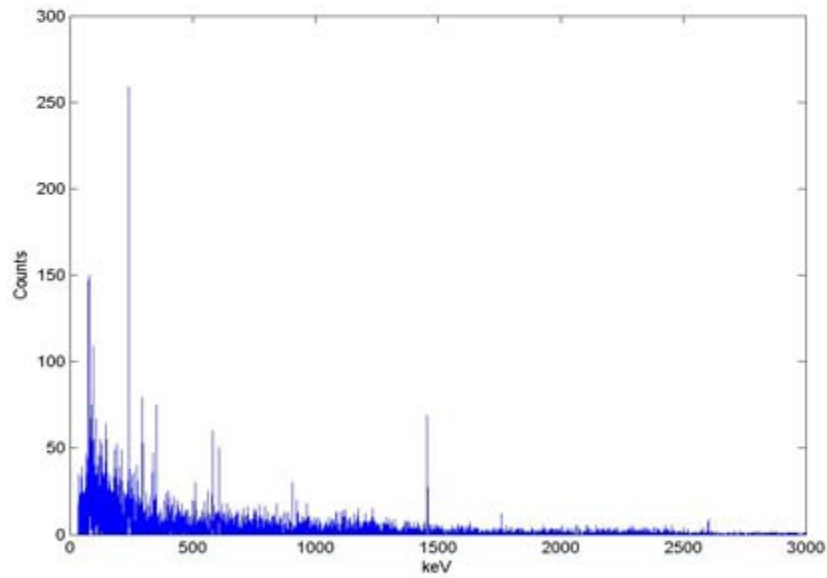
# Sample 3



**Data Corrected using  
GeLi efficiency curve**

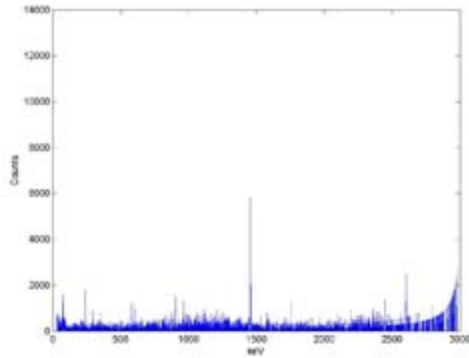


**Semi-Log of Corrected Data**

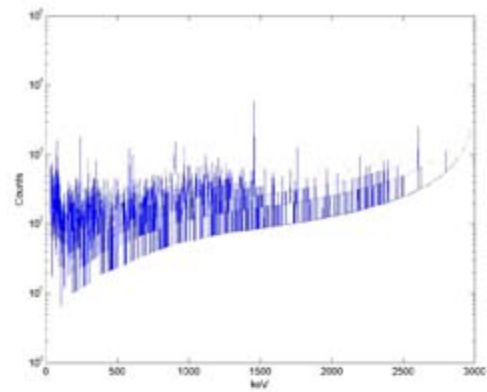


**Counts after removing background radiation**

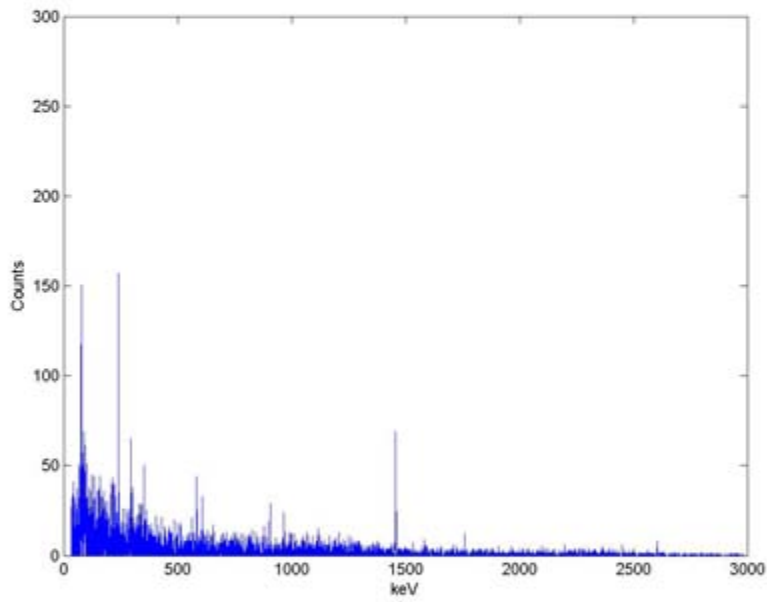
# Sample 4



**Data Corrected using  
GeLi efficiency curve**

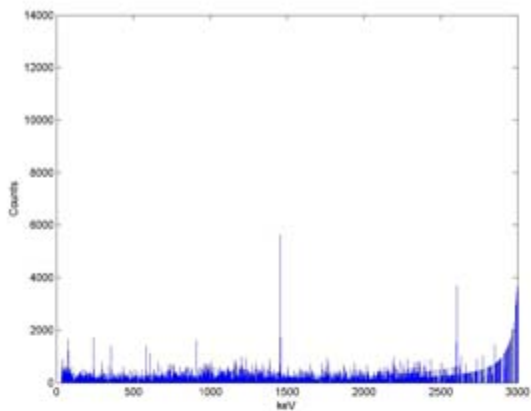


**Semi-Log of Corrected Data**

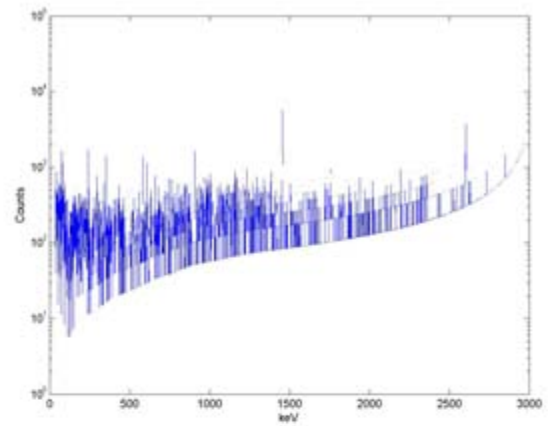


**Counts after removing background radiation**

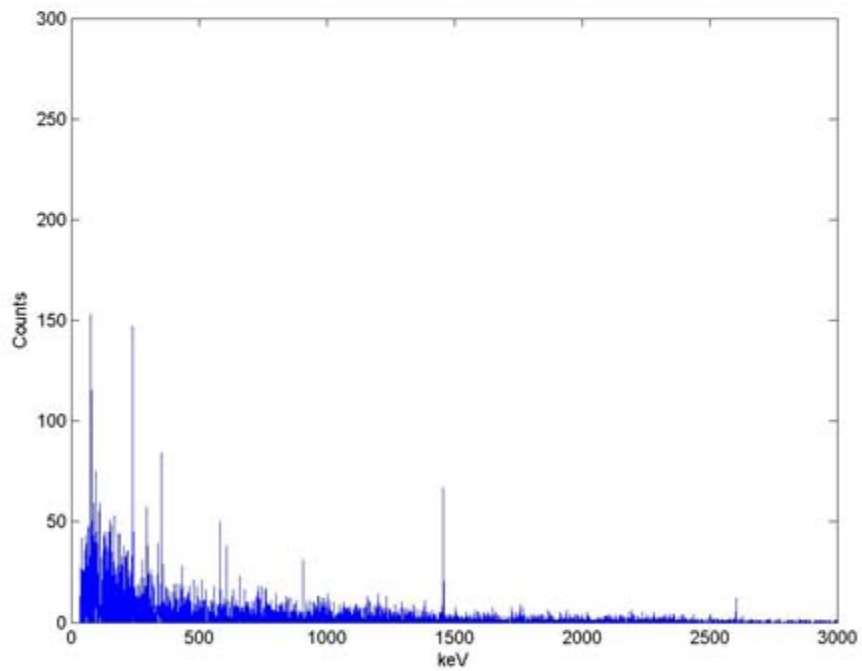
# Sample 5



**Data Corrected using  
GeLi efficiency curve**

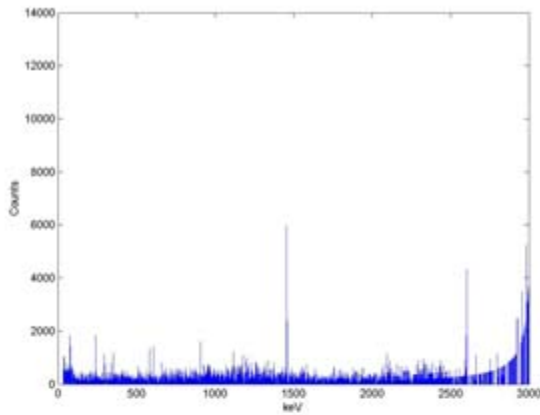


**Semi-Log of Corrected Data**

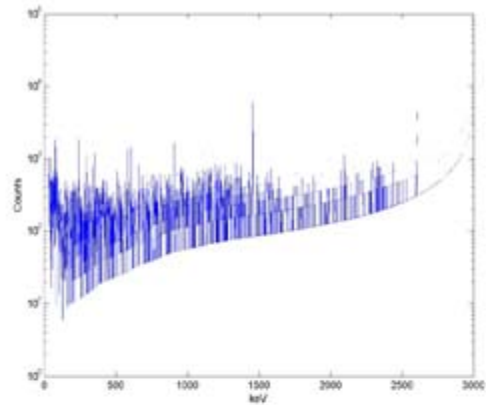


**Counts after removing background radiation**

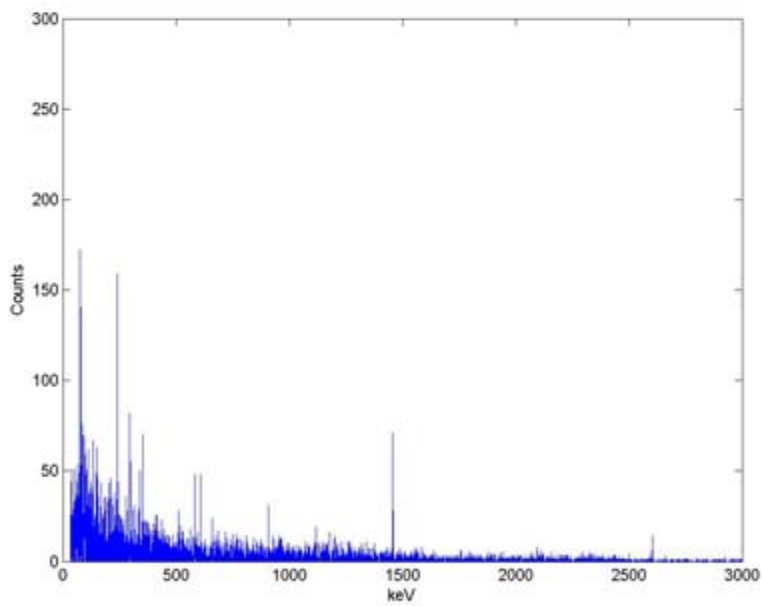
# Sample 6



**Data Corrected using  
GeLi efficiency curve**

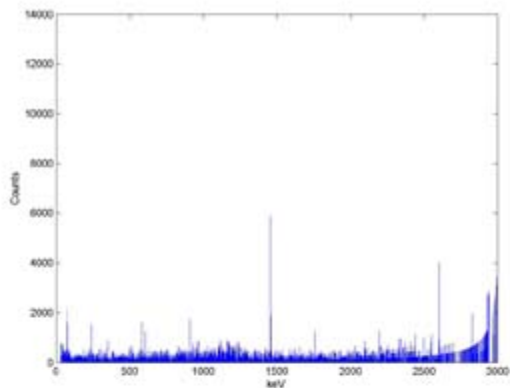


**Semi-Log of Corrected Data**

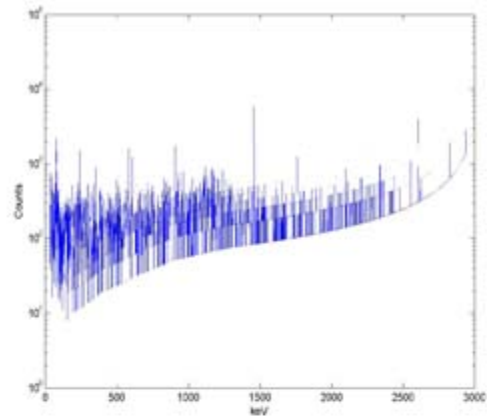


**Counts after removing background radiation**

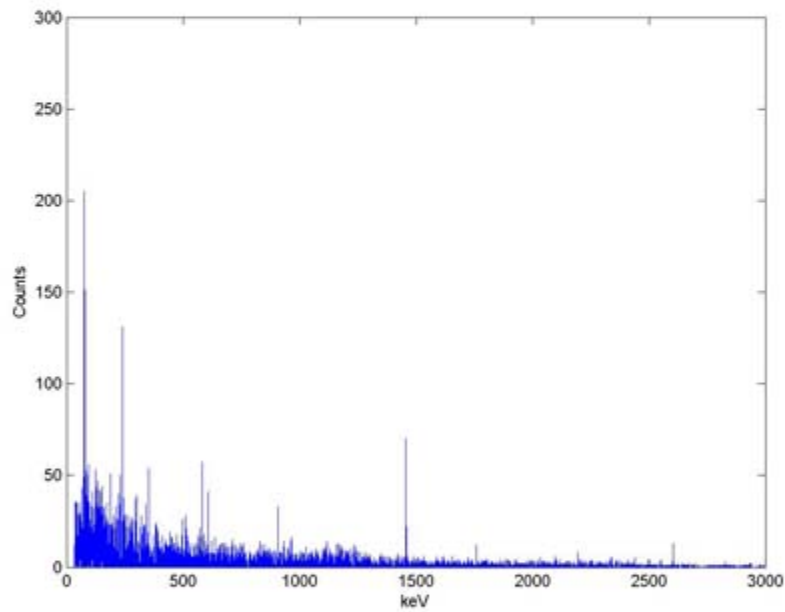
# Sample 7



**Data Corrected using  
GeLi efficiency curve**

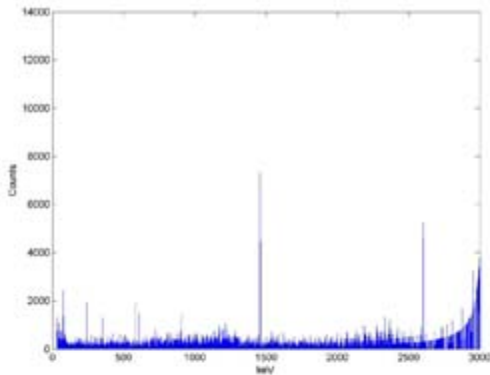


**Semi-Log of Corrected Data**

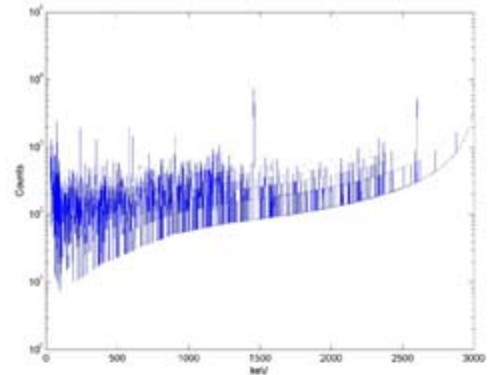


**Counts after removing background radiation**

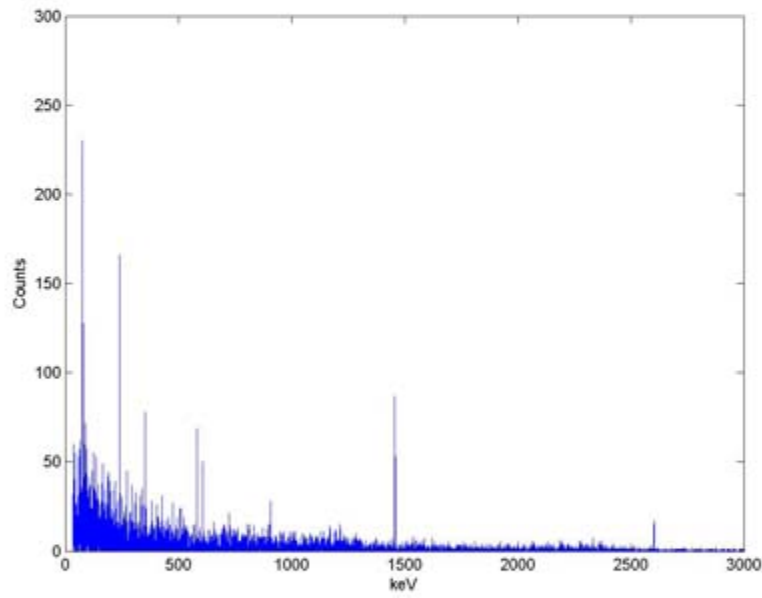
# Sample 8



**Data Corrected using  
GeLi efficiency curve**

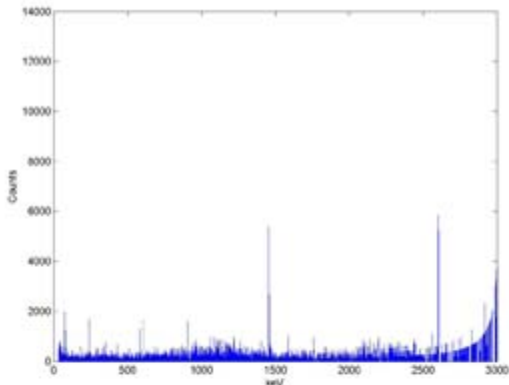


**Semi-Log of Corrected Data**

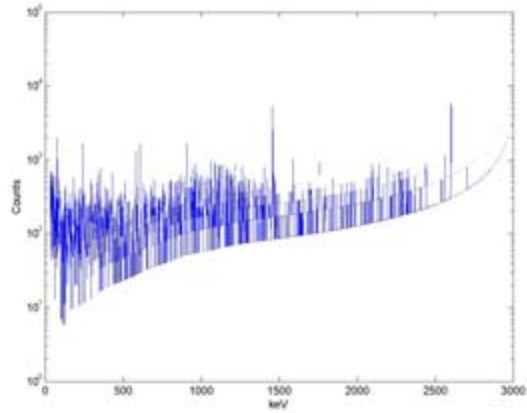


**Counts after removing background radiation**

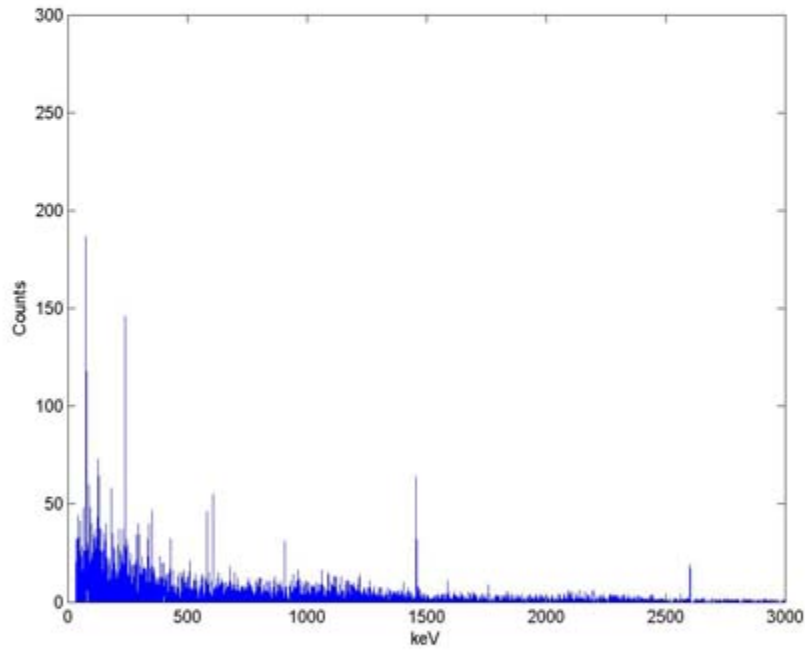
# Sample 9



**Data Corrected using  
GeLi efficiency curve**

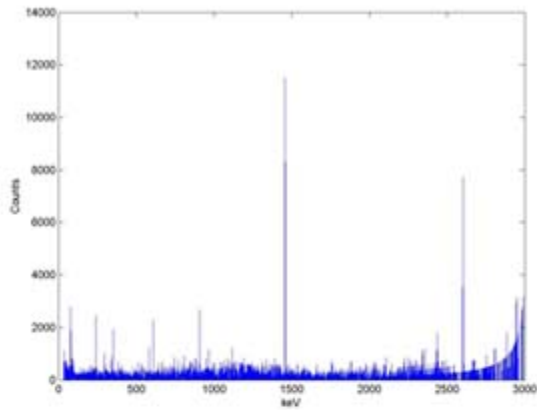


**Semi-Log of Corrected Data**

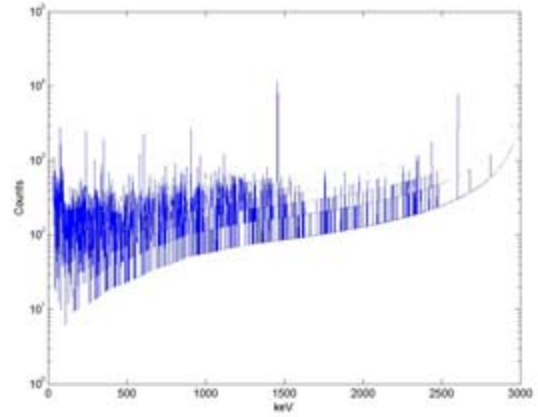


**Counts after removing background radiation**

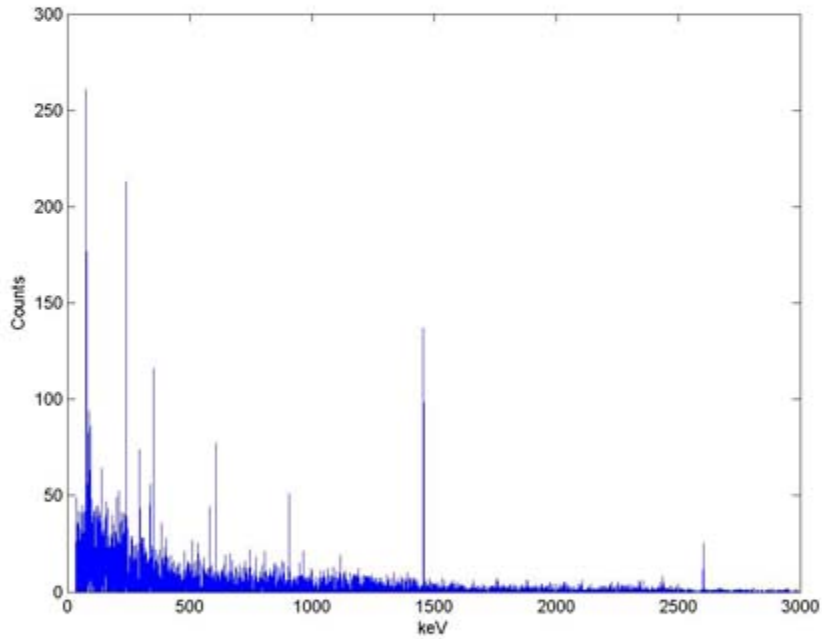
# Sample 10



**Data Corrected using  
GeLi efficiency curve**

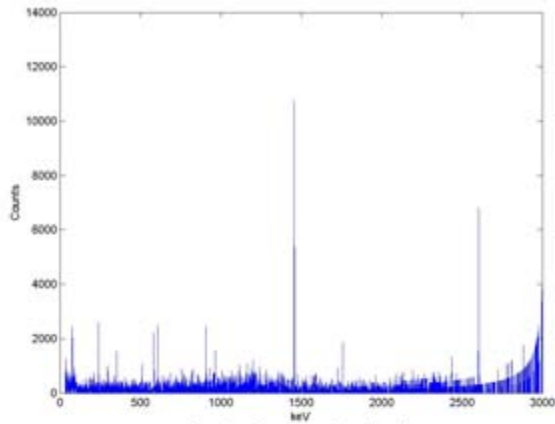


**Semi-Log of Corrected Data**

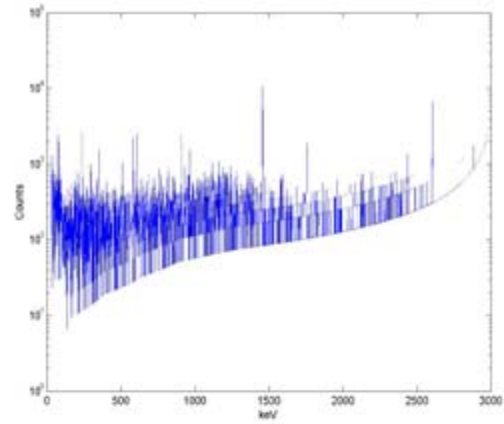


**Counts after removing background radiation**

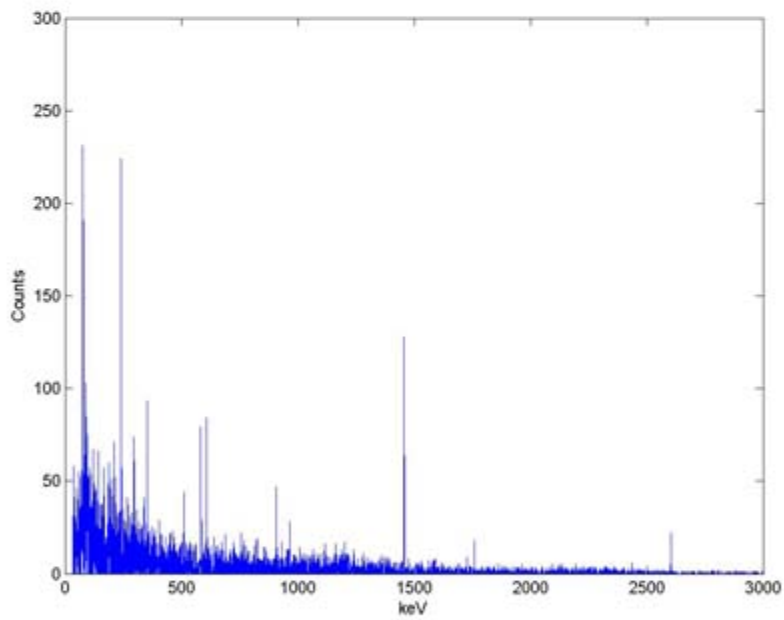
# Sample 11



**Data Corrected using  
GeLi efficiency curve**

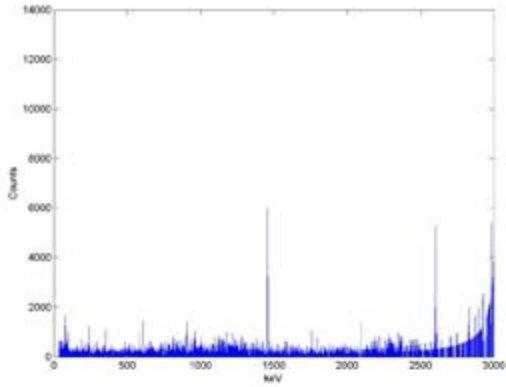


**Semi-Log of Corrected Data**

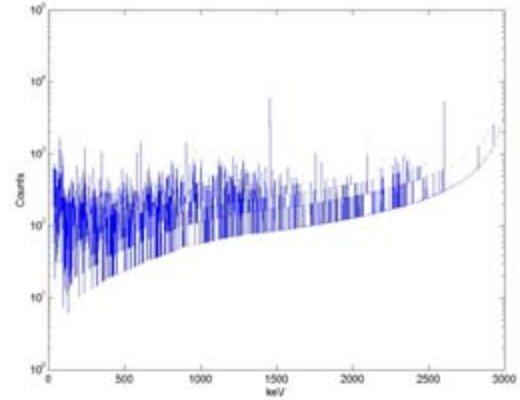


**Counts after removing background radiation**

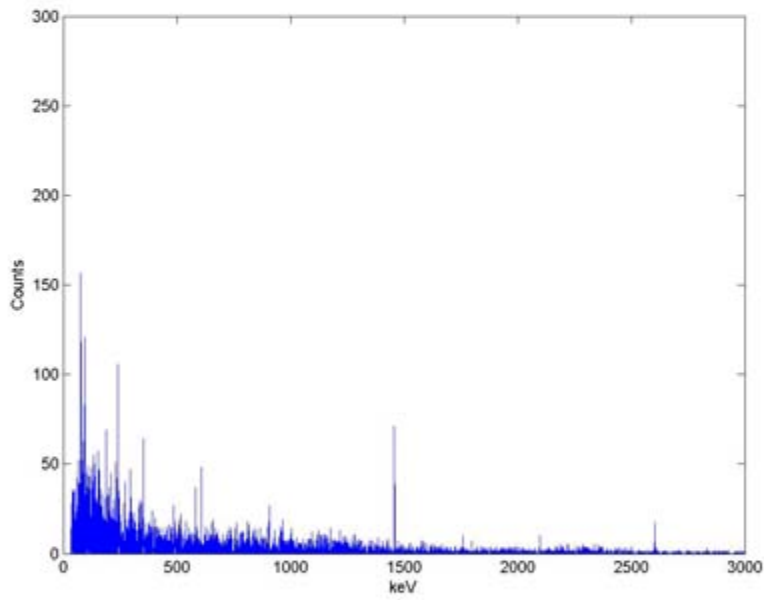
# Sample 12



**Data Corrected using  
GeLi efficiency curve**

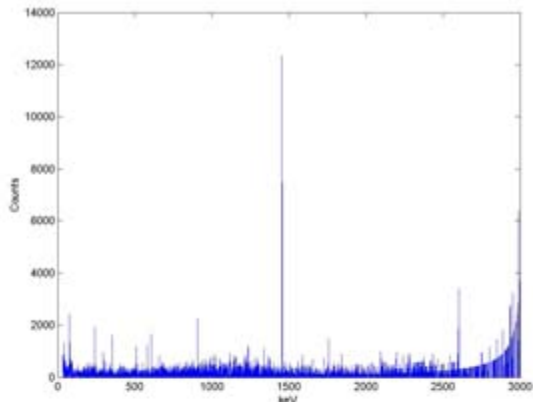


**Semi-Log of Corrected Data**

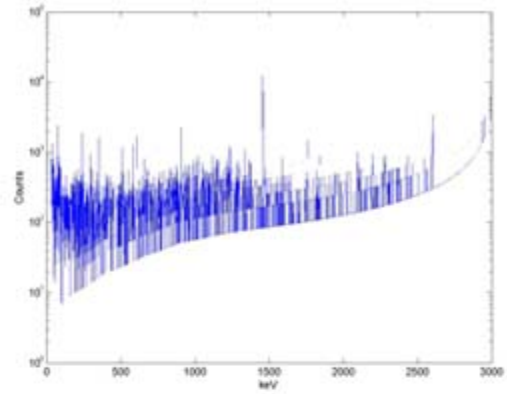


**Counts after removing background radiation**

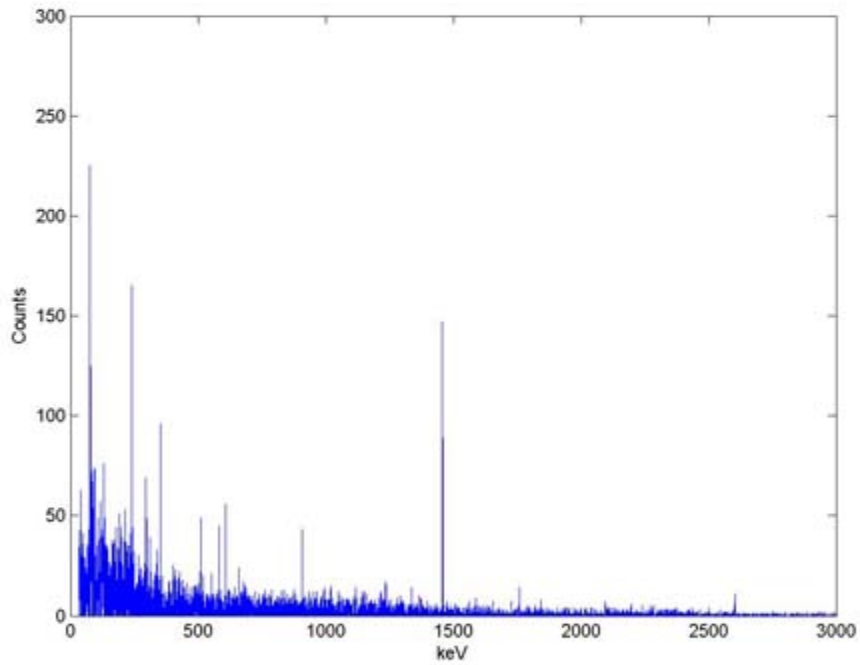
# Sample 13



**Data Corrected using  
GeLi efficiency curve**

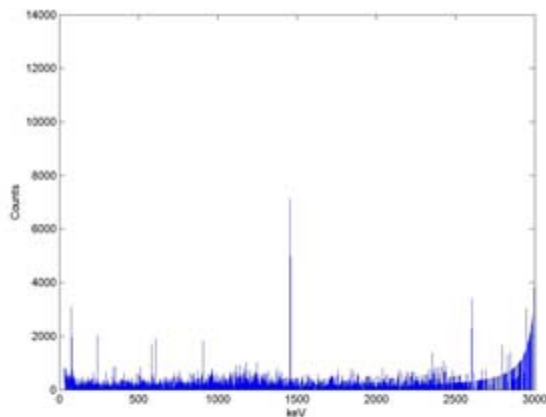


**Semi-Log of Corrected Data**

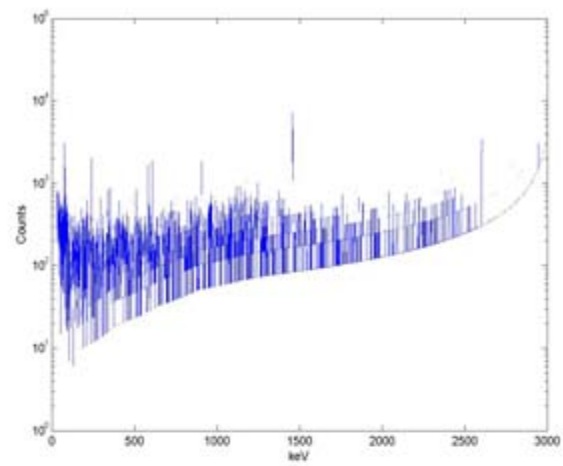


**Counts after removing background radiation**

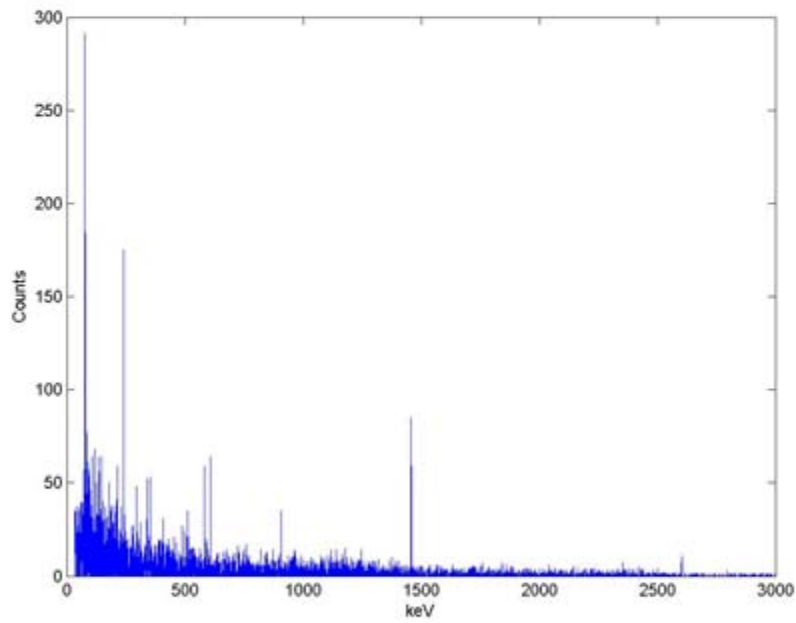
# Sample 14



**Data Corrected using  
GeLi efficiency curve**

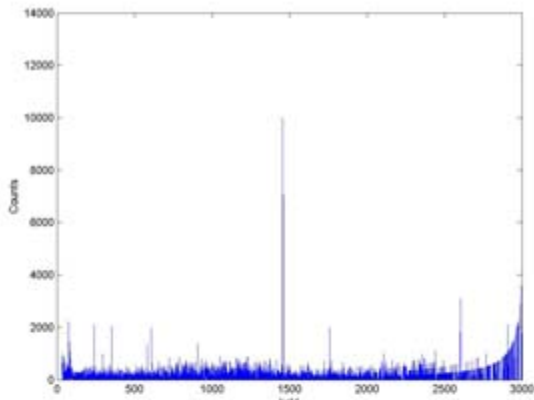


**Semi-Log of Corrected Data**

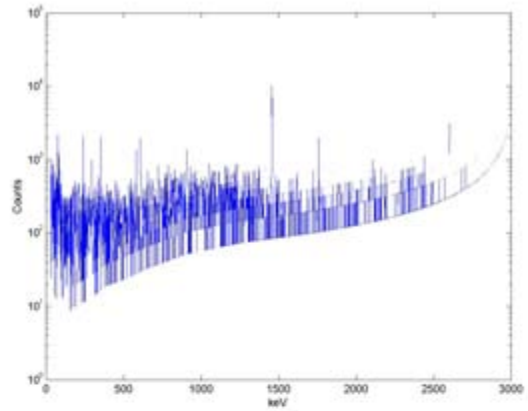


**Counts after removing background radiation**

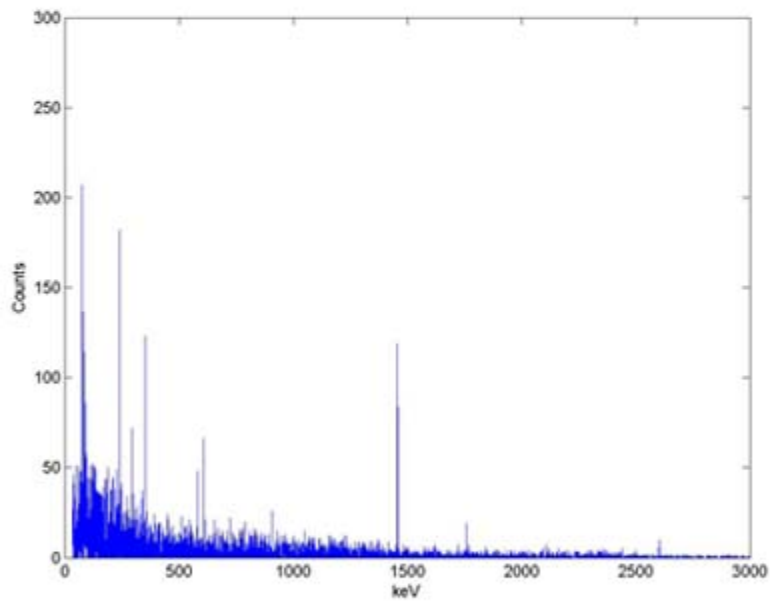
# Sample 15



**Data Corrected using  
GeLi efficiency curve**

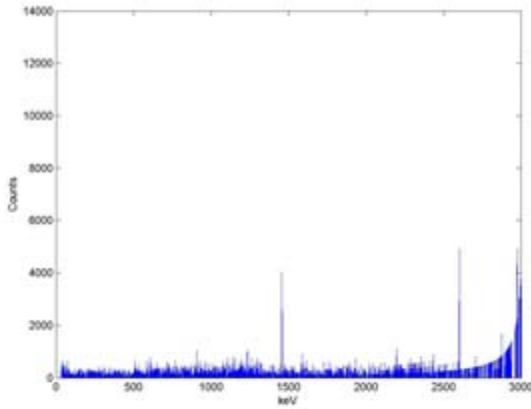


**Semi-Log of Corrected Data**

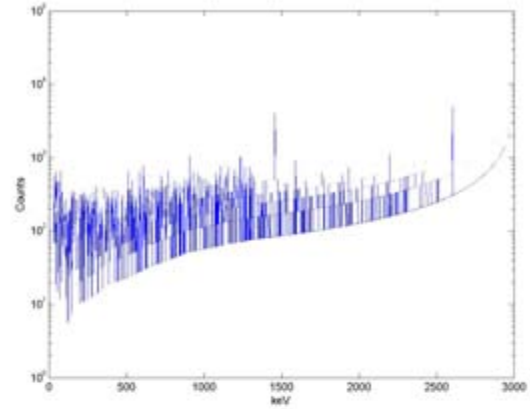


**Counts after removing background radiation**

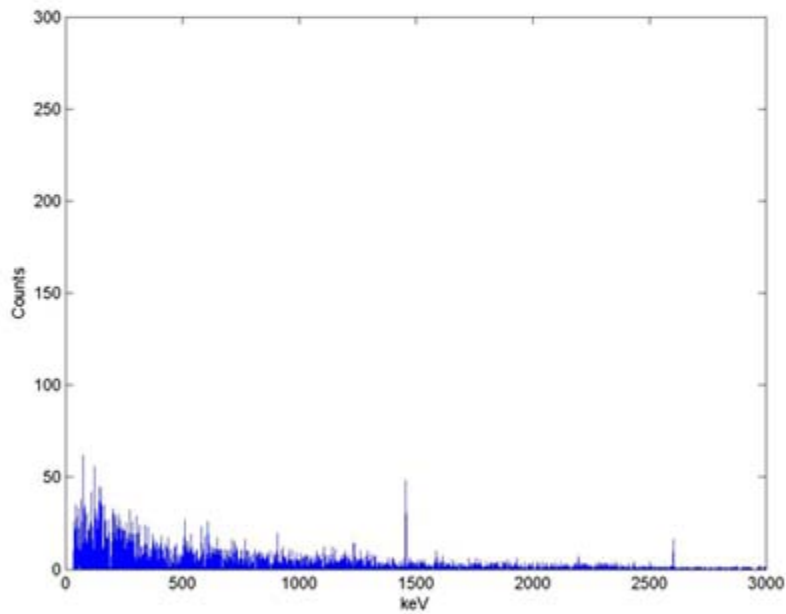
# Sample 16



**Data Corrected using  
GeLi efficiency curve**

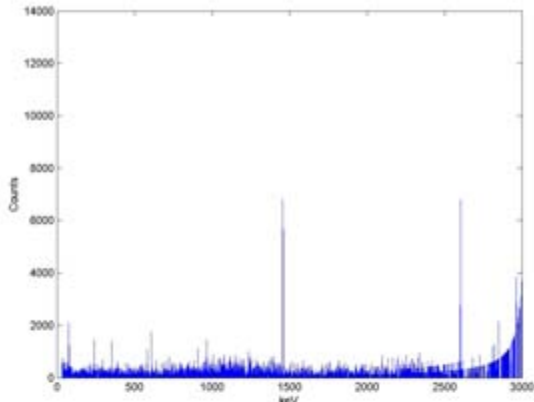


**Semi-Log of Corrected Data**

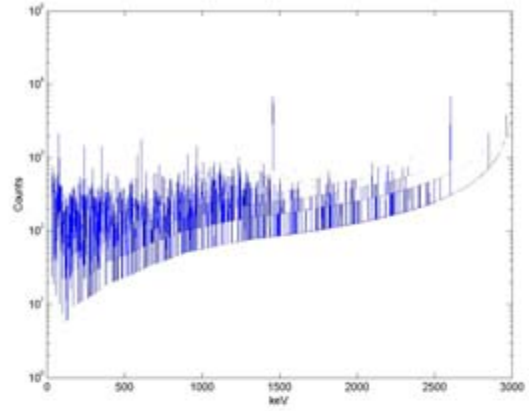


**Counts after removing background radiation**

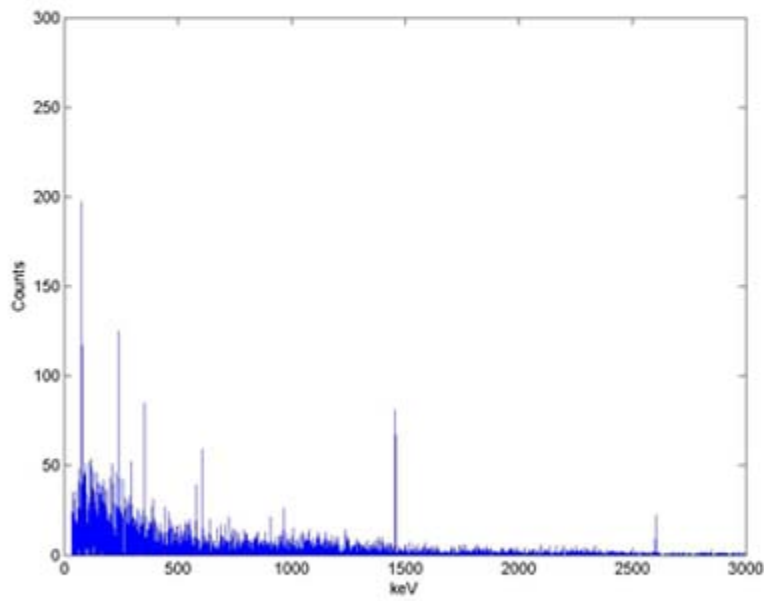
# Sample 17



**Data Corrected using  
GeLi efficiency curve**



**Semi-Log of Corrected Data**



**Counts after removing background radiation**

# Sample 18

## 6.4 GeLi Instructions

Turn on Physics laboratory computer named FERMI, using the username guest and the password guest. While the computer is loading, use the Canberra control panel to turn the device on. First, on the board labeled Model 2000, turn the master power switch on. Check the third blade labeled LN2 Monitor. Flip the switch to activate, if the H.V. Off light is on, then the device is out of LN2 and the high voltage supply will not work. At this time, you must refill the LN2 supply (for instructions on this, see section). Then move to the second blade labeled H.V. Power Supply Model 3105. This blade controls the high voltage power for the device. Turn the blade on by flipping the switch at the bottom of the blade, and then very slowly turn the knob up from zero to 3500V. Make sure that the display above shows 3.5 kV. Once this has been completed, the device is running and ready to go.

Once the computer has loaded, open the program on the desktop labeled MAESTRO for Windows. Once open, you will see the following setup. From there, go to the “Acquire” menu and select “MCB Properties”. Click on the tab that reads “Presets” and you will see the following. In the box labeled “Real Time”, input the amount of time you want the sample to run for in seconds then click close.

Now you are ready to measure for a sample. Open the hatch for the GeLi detector and place your sample on the red detection face, trying to center the sample as best as possible. When placing a sample inside the chamber, never place the sample in direct contact with the detector. Always have either a plastic bag or plastic container to separate the two, as this will prevent portions of the sample being left behind and altering later data. Once the sample is inside, close the latch back up and hit the green button labeled “GO” on your tool bar. The sample is now running and you may already see some counts being measured.

Once the data has finished running, you will want to save it. First go to File and select Settings. You will see the following interface. For your first save, make sure that ASCII .Spe Data is selected. From there go to File and select Save As. Find the folder in which you want to save your data, name the file, then set the file type to Real SPC. This version of the file can be opened again using the MAESTRO program should you wish to explore the data more closely. Once you have done that, go back to File and Save As. From there, find the folder you want and change the file type to All Files, now name the file and add .txt to the end of the file. You have now successfully saved the data. From here you can go to Acquire, select Clear and repeat the steps for all of your samples.

Once you are finished, you must shut down the GeLi detector by turning the High Voltage Control knob down to zero and then turning the High Voltage Control Blade off. Then turn off the LN2 monitor blade and finally turn off the Power Control Blade. You must then make sure to copy all of your .txt files onto a floppy disk. Once you have the files on your personal computer, you must change the files to either .xls or .csv for use in either excel or MATLAB. These files still contain some non-numerical data at the beginning and end, but by deleting those rows, you will be left with one column. This column lists the number of counts where each row represents a different channel. These channels start at 0 and end at 8190. To convert from channel to emission power, you may follow the equation provided in the analysis section of this project.

## 6.5 Radioactive Sample Data

There are some noticeable peaks in the data for the various samples we were able to inspect courtesy of graduate student Marco Kaltofen. First is that of the button from the Chernobyl Reactor meltdown. The data can be seen below.

Channel	Energy (keV)	Energy (J)	Net Counts	Effective Dose (mSv/s)	Isotope
1571	660.46	1.05817E-13	115	2.92911E-12	Cs-137
1570	660.05	1.05752E-13	110	2.79832E-12	Cs-137
1572	660.87	1.05883E-13	70	1.78513E-12	Cs-137
1569	659.64	1.05686E-13	62	1.57525E-12	Cs-137
1573	661.28	1.05948E-13	23	5.87262E-13	Cs-137
1568	659.23	1.05621E-13	14	3.55264E-13	Cs-137
145	77.23	1.23728E-14	26	2.43157E-14	Pb-214
Total Efficient Effective Dose (mSv/s)				1.12045E-10	
Total Efficient Effective Dose (mSv/y)				0.003533442	

Table 6.1: Peak data for Chernobyl button.

Channel	Energy (keV)	Energy (J)	Net Counts	Effective Dose (mSv/s)	Isotope
3520	1457.60	2.33533E-13	22	3.07209E-12	K-40
3522	1458.42	2.33664E-13	19	2.65622E-12	K-40
151	79.68	1.27660E-14	45	4.20809E-14	Pb-214
145	77.23	1.23728E-14	32	2.99271E-14	Pb-214
819	352.89	5.65394E-14	29	1.93363E-13	Pb-214
818	352.48	5.64738E-14	28	1.86183E-13	Pb-214
144	76.82	1.23073E-14	26	2.4316E-14	Pb-214
150	79.27	1.27005E-14	24	2.24434E-14	Pb-214
817	352.07	5.64083E-14	20	1.32623E-13	Pb-214
146	77.63	1.24383E-14	17	1.58984E-14	Pb-214
543	240.01	3.84534E-14	62	1.9542E-13	U-233
544	240.42	3.85189E-14	57	1.80166E-13	U-233
542	239.60	3.83878E-14	44	1.38296E-13	U-233
545	240.83	3.85844E-14	27	8.55815E-14	U-233
Total Efficient Effective Dose (mSv/s)				1.36849E-10	
Total Efficient Effective Dose (mSv/y)				0.004315656	

Table 6.2: Peak data for the Columbia River sand sample.

Channel	Energy (keV)	Energy (J)	Net Counts	Effective Dose (mSv/s)	Isotope
145	77.23	1.23728E-14	266	2.48769E-14	Bi-207
151	79.68	1.27660E-14	201	1.87961E-14	Bi-207
152	80.09	1.28315E-14	119	1.11278E-14	Bi-207
150	79.27	1.27005E-14	108	1.00995E-14	Bi-207
144	76.82	1.23073E-14	94	8.79117E-15	Bi-207
175	89.50	1.43387E-14	84	7.69774E-15	Bi-207
176	89.90	1.44042E-14	82	7.48832E-15	Bi-207
146	77.63	1.24383E-14	81	7.57512E-15	Bi-207
143	76.41	1.22417E-14	78	7.29496E-15	Bi-207
819	352.89	5.65394E-14	181	1.20685E-13	Pb-214
818	352.48	5.64738E-14	169	1.12374E-13	Pb-214
543	240.01	3.84534E-14	219	6.90274E-14	U-233
544	240.42	3.85189E-14	170	5.37336E-14	U-233
545	240.83	3.85844E-14	110	3.48665E-14	U-233
542	239.60	3.83878E-14	91	2.86022E-14	U-233
Total Efficient Effective Dose (mSv/s)				1.15786E-10	
Total Efficient Effective Dose (mSv/y)				0.003651436	

Table 6.3: Peak data for the Ganges River sediment sample.

Channel	Energy (keV)	Energy (J)	Net Counts	Effective Dose (mSv/s)	Isotope
145	77.23	1.23728E-14	43	2.01072E-14	Bi-207
146	77.63	1.24383E-14	33	1.54308E-14	Bi-207
1444	608.52	9.74950E-14	27	2.78148E-13	Bi-214
1443	608.11	9.74295E-14	18	1.85121E-13	Bi-214
150	79.27	1.27005E-14	30	1.40271E-14	Pb-214
151	79.68	1.27660E-14	29	1.35594E-14	Pb-214
152	80.09	1.28315E-14	29	1.35591E-14	Pb-214
149	78.86	1.26349E-14	22	1.02868E-14	Pb-214
543	240.01	3.84534E-14	52	8.19504E-14	U-233
542	239.60	3.83878E-14	31	4.8718E-14	U-233
544	240.42	3.85189E-14	26	4.10904E-14	U-233
452	202.79	3.24902E-14	18	2.17786E-14	U-233
Total Efficient Effective Dose (mSv/s)				1.05814E-10	
Total Efficient Effective Dose (mSv/y)				0.003336943	

Table 6.4: Peak data for the LAO 1175 sample from Los Alamos.

Channel	Energy (keV)	Energy (J)	Net Counts	Effective Dose (mSv/s)	Isotope
145	77.23	1.23728E-14	26	1.21579E-14	Bi-207
143	76.41	1.22417E-14	16	7.48201E-15	Bi-207
125	69.05	1.10622E-14	18	8.41998E-15	Cs-136
3519	1457.19	2.33468E-13	17	1.18631E-12	K-40
188	94.81	1.51906E-14	29	1.27467E-14	Np-237
151	79.68	1.27660E-14	31	1.44945E-14	Pb-214
175	89.50	1.43387E-14	18	8.24758E-15	Pb-214
208	102.99	1.65011E-14	21	8.75401E-15	Ta-182
543	240.01	3.84534E-14	27	4.25512E-14	U-235
192	96.45	1.54527E-14	19	8.25522E-15	U-235
542	239.60	3.83878E-14	17	2.67163E-14	U-235
Total Efficient Effective Dose (mSv/s)				1.02411E-10	
Total Efficient Effective Dose (mSv/y)				0.003229627	

Table 6.5: Peak data for the mesa soil sample from Los Alamos.

Channel	Energy (keV)	Energy (J)	Net Counts	Effective Dose (mSv/s)	Isotope
1444	608.52	9.74950E-14	32	3.29657E-13	Bi-214
1443	608.11	9.74295E-14	25	2.57112E-13	Bi-214
3519	1457.19	2.33468E-13	39	2.72154E-12	K-40
188	94.81	1.51906E-14	39	1.71421E-14	Np-237
189	95.22	1.52561E-14	35	1.53381E-14	Np-237
145	77.23	1.23728E-14	102	4.76963E-14	Pb-214
151	79.68	1.27660E-14	90	4.20809E-14	Pb-214
818	352.48	5.64738E-14	76	2.52676E-13	Pb-214
819	352.89	5.65394E-14	62	2.06698E-13	Pb-214
681	296.45	4.74964E-14	55	1.26323E-13	Pb-214
150	79.27	1.27005E-14	51	2.38461E-14	Pb-214
146	77.63	1.24383E-14	47	2.19772E-14	Pb-214
680	296.04	4.74308E-14	47	1.07659E-13	Pb-214
175	89.50	1.43387E-14	43	1.97026E-14	Pb-214
152	80.09	1.28315E-14	42	1.96374E-14	Pb-214
820	353.30	5.66049E-14	34	1.13663E-13	Pb-214
144	76.82	1.23073E-14	32	1.49637E-14	Pb-214
682	296.86	4.75619E-14	31	7.13915E-14	Pb-214
551	243.28	3.89776E-14	30	4.83511E-14	Pb-214
817	352.07	5.64083E-14	30	9.9467E-14	Pb-214
143	76.41	1.22417E-14	28	1.30935E-14	Pb-214
257	123.03	1.97121E-14	30	1.19537E-14	Se-75
543	240.01	3.84534E-14	94	1.48141E-13	U-233
544	240.42	3.85189E-14	82	1.29593E-13	U-233
542	239.60	3.83878E-14	41	6.44334E-14	U-233
545	240.83	3.85844E-14	38	6.0224E-14	U-233
	Total Efficient Effective Dose (mSv/s)			1.51394E-10	
	Total Efficient Effective Dose (mSv/y)			0.00477436	

Table 6.6: Peak data for Takedu Solods sample from Los Alamos.

Channel	Energy (keV)	Energy (J)	Net Counts	Effective Dose (mSv/s)	Isotope
145	77.23	1.23728E-14	23	1.0755E-14	Bi-207
110	62.91	1.00793E-14	25	1.16983E-14	Eu-155
3516	1455.96	2.33271E-13	28	1.95081E-12	K-40
3514	1455.15	2.33140E-13	21	1.46155E-12	K-40
3518	1456.78	2.33402E-13	19	1.32517E-12	K-40
3515	1455.56	2.33206E-13	18	1.25342E-12	K-40
818	352.48	5.64738E-14	27	8.97666E-14	Pb-214
151	79.68	1.27660E-14	25	1.16891E-14	Pb-214
543	240.01	3.84534E-14	35	5.51589E-14	U-233
544	240.42	3.85189E-14	32	5.05728E-14	U-233
542	239.60	3.83878E-14	22	3.4574E-14	U-233
545	240.83	3.85844E-14	17	2.69423E-14	U-233
182	92.36	1.47974E-14	24	1.07449E-14	U-235
	Total Efficient Effective Dose (mSv/s)			1.07679E-10	
	Total Efficient Effective Dose (mSv/y)			0.003395766	

Table 6.7: Peak data for trailer dust sample from Los Alamos.

## 6.6 MATLAB Code

### 6.6.1 AlphaScat.m

```
0001 function C=AlphaScat(Exper, Target, n, AlphaDensity, Xdet,...
0002 layers, N, x0, vx0, FileName)
0003 %   AlphaScat is the first of three functions that model various alpha
0004 %   scattering experiments. AlphaScat calculates the data for the
0005 %   specified experiment, which is determined by the arguments. This
0006 %   data is saved so that it may be accessed by AlphaCount and/or
0007 %   AlphaPlot.
0008 %   This model reproduces experimental results similar to those obtained by
0009 %   Earnest Rutherford and others who have performed alpha scattering
0010 %   experiments. Using numerical methods, particularly the classical
0011 %   fourth order Runge Kutta method and Dormand-Prince (4,5) embedded
0012 %   pair method (through the use of MATLAB's ODE45.m), this program
0013 %   helps investigate the interaction between alpha particles and
0014 %   specific materials listed below.
0015 %
0016 %           -----Target_Characteristics-----
0017 %           |_Atomic_Number_|_Seperation_|_Material_|_Symbol_|
0018 %           |      13      |    236    | Aluminum |  Al  |
0019 %           |      29      |    290    |  Copper  |  Cu  |
0020 %           |      30      |    284    |   Zinc   |  Zn  |
0021 %           |      47      |    330    |  Silver  |  Ag  |
0022 %           |      48      |    322    | Cadmium  |  Cd  |
0023 %           |      50      |    290    |   Tin    |  Sn  |
0024 %           |      79      |    348    |   Gold   |  Au  |
0025 %           |      82      |    308    |   Lead   |  Pb  |
0026 %           ~~~~~
0027 %
0028 %   To investigate the interactions between alpha particles and a single
0029 %   nucleus of one of the materials listed above (Ex. AlphaScat,
0030 %   AlphaScat('Atom','Pb')), the classical Runge Kutta method is used
0031 %   with a fixed time step.
0032 %   To investigate the interactions between alpha particles and a thin
0033 %   foil, (Ex. AlphaScat('Foil','Al')) ODE45.m is used due to its
0034 %   efficient use of the Dormand-Prince embedded pair method. This
0035 %   approach involves a variable time step; therefore, more data can be
0036 %   approximated.
0037 %
0038 %   !! Required !! (Not included with MATLAB packages.):
0039 %   scatter.m - AlphaScat.m calls this function when using ODE45.m for
0040 %   the 'Foil' experiments.
0041 %
0042 %   '' Optional '' (Recommended. Not included with MATLAB packages):
```

0043 %       AlphaCount.m - Function used (after running AlphaScat.m) to  
0044 %                count particles at different angular intervals.  
0045 %       AlphaPlot.m - Function used (after running AlphaScat.m or  
0046 %                AlphaCount.m) to build figures that graphically represent  
0047 %                what is occurring during the experiment.  
0048 %  
0049 %   INPUTS:  
0050 %  
0051 %       NOTE: If the experiment is 'Atom' then there are only 7 arguments.  
0052 %                AlphaScat(Exper, Target, n, AlphaDensity, Xdet, layers, x0,  
0053 %                vx0, FileName)  
0054 %  
0055 %       Exper - 'Atom' or 'Foil' (default, 'Atom'). This input  
0056 %                specifies the experiment type of experiment that  
0057 %                will be performed.  
0058 %  
0059 %       Target - 'Al', 'Cu', 'Zn', 'Ag', 'Cd', 'Sn', 'Au', or 'Pb'  
0060 %                (default, 'Au'). This input specifies the target  
0061 %                material. See table above for details.  
0062 %  
0063 %       n - This integer input specifies the number of alpha  
0064 %                particles incident to the target. (default, 101).  
0065 %  
0066 %       AlphaDensity - This input determines the initial separation in  
0067 %                between the alpha particles (default, 1). The  
0068 %                separation is  $n/\text{AlphaDensity}$  ranging from  
0069 %                 $-n/(2\text{AlphaDensity})$  to  $n/(2\text{AlphaDensity})$   
0070 %                Ex. If AlphaDensity=5 and n=10, then the 10 initial x  
0071 %                positions would be equally spaced by 1 between -1  
0072 %                and 1.  
0073 %  
0074 %       Xdet - This specifies how far away the 'detector' is from the  
0075 %                origin (default,  $10^8$  for 'Foil' 200 for 'Atom').  
0076 %  
0077 %       layers - This specifies how many layers of target nuclei are in  
0078 %                the foil (default, 21).  
0079 %  
0080 %       N - This specifies how many nuclei are in each layer (default,  
0081 %                21).  
0082 %  
0083 %       x0 - This specifies the initial x-position of the alpha  
0084 %                particles (default, 1.96).  
0085 %  
0086 %       vx0 - This specifies the initial velocity of the alpha  
0087 %                particles in the x-direction (default, 1.96).

```

0088 %
0089 %           FileName - FileName specifies the name of the data file that
0090 %                   AlphaScat will create (.mat format).
0091 %
0092 %           Default File Names
0093 %                   Ex. Exper='Atom', Target='Au', n=101 then
0094 %                   FileName='AuAtom101'
0095 %                   Ex. Exper='Foil', Target='Au', n=101, layers=21, n=31,
0096 %                   FileName='21-31AuFoil101'
0097 %
0098 %           NOTE: AlphaScat can be run with or with out arguments as long as
0099 %                   the arguments entered in are in the order stated above.
0100 %                   Arguments that are left out are set to the default values
0101 %                   listed above.
0102 %
0103 %
0104 %   OUTPUTS:
0105 %           C - This is the total time taken to run AlphaScat.
0106 %
0107 %
0108 format long
0109 C=clock;
0110 %% Check Arguments
0111 if nargin > 10
0112 error('Too many arguments.')
```

```

0113 elseif nargin==10
0114 if strcmp(Exper,'Atom')==1
0115 error('Too many arguments, for the Atom experiment.')
```

```

0116 end
0117 elseif nargin < 10
0118 if nargin==9
0119 if strcmp(Exper,'Atom')==1
0120 error('Too many arguments, for the Atom experiment.')
```

```

0121 end
0122 end
0123 FileName=1;
0124 if nargin < 9
0125 vx0=1.96;
0126 if nargin < 8
0127 x0=-100;
0128 if nargin < 7
0129 if nargin < 6
0130 if nargin < 5
0131 if nargin < 4
0132 AlphaDensity=1;

```

```

0133 if nargin <3
0134 n=101;
0135 if nargin < 2
0136 Target='Au';
0137 if nargin <1
0138 display('Experiment not chosen.');
```

```

0139 display('Defaults chosen instead.');
```

```

0140 Exper='Atom';
0141 end
0142 end
0143 end
0144 end
0145 if strcmp(Exper,'Atom')==1
0146 Xdet=200;
0147 elseif strcmp(Exper,'Foil')==1
0148 Xdet=10^8;
0149 end
0150 end
0151 layers=21;
0152 else
0153 if strcmp(Exper,'Atom')
0154 x0=layers;
0155 end
0156 end
0157 N=21;
0158 else
0159 if strcmp(Exper,'Atom')
0160 vx0=N;
0161 x0=layers;
0162 end
0163 end
0164 else
0165 if strcmp(Exper,'Atom')
0166 FileName=x0;
0167 vx0=N;
0168 x0=layers;
0169 end
0170 end
0171 end
0172 end
0173 %% Assign Experiment Parameters
0174 %
0175 %   Define Target characteristics
0176 %
0177 Tar=[13 236;...      % Aluminum,  Al
```

```

0178 29 290;...      % Copper,      Cu
0179 30 284;...      % Zinc,        Zn
0180 47 330;...      % Silver,       Ag
0181 48 322;...      % Cadmium,      Cd
0182 50 290;...      % Tin,          Sn
0183 79 348;...      % Gold,         Au
0184 82 308];        % Lead,         Pb
0185 if strcmp(Target,'Al')==1
0186 Z=Tar(1,1);
0187 sep=Tar(1,2)*10^3;
0188 elseif strcmp(Target,'Cu')==1
0189 Z=Tar(2,1);
0190 sep=Tar(2,2)*10^3;
0191 elseif strcmp(Target,'Zn')==1
0192 Z=Tar(3,1);
0193 sep=Tar(3,2)*10^3;
0194 elseif strcmp(Target,'Ag')==1
0195 Z=Tar(4,1);
0196 sep=Tar(4,2)*10^3;
0197 elseif strcmp(Target,'Cd')==1
0198 Z=Tar(5,1);
0199 sep=Tar(5,2)*10^3;
0200 elseif strcmp(Target,'Sn')==1
0201 Z=Tar(6,1);
0202 sep=Tar(6,2)*10^3;
0203 elseif strcmp(Target,'Au')==1
0204 Z=Tar(7,1);
0205 sep=Tar(7,2)*10^3;
0206 elseif strcmp(Target,'Pb')==1
0207 Z=Tar(8,1);
0208 sep=Tar(8,2)*10^3;
0209 else
0210 display('No element match for Target.');
```

```

0211 display('Gold (Au) chosen by default.');
```

```

0212 Target='Au';
0213 Z=Tar(7,1);
0214 sep=Tar(7,2)*10^3;
0215 end
0216 %
0217 %   Define experiment type.
0218 %
0219 if strcmp(Exper,'Atom')==1
0220 EXP=1;
0221 if Xdet>=10^3
0222 display('Warning. Xdet may be too large.');
```

```

0223 display('Program may take longer than expected to complete.');
```

```

0224 end
```

```

0225 elseif strcmp(Exper,'Foil')==1
```

```

0226 EXP=2;
```

```

0227 if N<layers
```

```

0228 display('Foil is thicker than it is wide.');
```

```

0229 display('Consider increasing the width.')
```

```

0230 end
```

```

0231 if Xdet<=.1*layers*sqrt(3)*sep
```

```

0232 display('Warning. Xdet may be too small.');
```

```

0233 display('Xdet too close to the foil.');
```

```

0234 end
```

```

0235 else
```

```

0236 display('Experiment not chosen correctly.');
```

```

0237 display('Single atom experiment chosen by default.');
```

```

0238 Exper='Atom';
```

```

0239 EXP=1;
```

```

0240 Xdet=200;
```

```

0241 end
```

```

0242 if Xdet<=1.1*norm([n/(2*AlphaDensity),x0])
```

```

0243 display('Please choose new inputs')
```

```

0244 error('Some initial positions are outside the detectors range.')
```

```

0245 end
```

```

0246 %
```

```

0247 %   Define file name, if it not specified.
```

```

0248 %
```

```

0249 if FileName==1
```

```

0250 if EXP==1
```

```

0251 FileName=[Target Exper int2str(n)];
```

```

0252 else
```

```

0253 FileName=[int2str(layers),'-',int2str(N),...
```

```

0254 Target,Exper,int2str(n)];
```

```

0255 end
```

```

0256 end
```

```

0257 %% Constants and fixed variables
```

```

0258 z=2; % Number of protons in an alpha particle
```

```

0259 M=6.644656*10^-27; % Mass of an alpha particle, kg
```

```

0260 e=1.602176*10^-19; % Charge of a proton, C
```

```

0261 eps=8.854188*10^-12; % Permittivity of a vacuum, (C*s)^2/(m^3*kg)
```

```

0262 B=z*Z*e^2/(4*pi*eps)/M*... % Scaling factor
```

```

0263 (10^-22)^2/(10^-15)^3;
```

```

0264 d=B/(-B/x0+1/2*vx0^2); % Distance of closest approach
```

```

0265 %% Calculate the data
```

```

0266 if EXP==1
```

```

0267 %% Single Atom Experiment
```

```

0268 %
0269 %   Define time parameters.
0270 %
0271 dt=.1;                               % Time step scaled, 1*10^-22s
0272 Time=ceil(1.05*(Xdet... % Total run time
0273         +abs(x0))/vx0);
0274 K=Time/dt;                             % Number of time steps
0275 T=linspace(0,Time,K); %#ok<NASGU> % Time data
0276 %
0277 %   Preallocate data arrays.
0278 %
0279 r=zeros(K,2,n);
0280 v=zeros(K,2,n);
0281 acc=zeros(K,2,n);
0282 rmag=zeros(K,n);
0283 vmag=zeros(K,n);
0284 amag=zeros(K,n);
0285 KE=zeros(K,n);
0286 PE=zeros(K,n);
0287 E=zeros(K,n);
0288 %
0289 %   Define x-positions for detector.
0290 %
0291 xdet=linspace(-Xdet,Xdet,1000);
0292 %
0293 %   Define initial conditions.
0294 %
0295 r(1,1,:)=x0;                           % Initial x-position
0296 r(1,2,:)=linspace(...% Initial y-positions
0297 -n/(2*AlphaDensity),n/(2*AlphaDensity),n);
0298 v(1,1,:)=vx0;                           % Initial x-velocity
0299 %
0300 %   Define initial values.
0301 %
0302 vmag(1,:)=norm(v(1,:,1));                % Speeds
0303 KE(1,:)=0.5*vmag(1,1)^2;                % Kinetic energies
0304 for j=1:n
0305   rmag(1,j)=norm(r(1,:,j));              % Distances
0306   acc(1,:,j)=...% Accelerations
0307   B/norm(r(1,:,j))^(3)*r(1,:,j);
0308   amag(1,j)=norm(acc(1,:,j));           % Acceleration magnitudes
0309   PE(1,j)=B/rmag(1,j);                  % Potential energies
0310   E(1,j)=PE(1,j)+KE(1,j);               % Total energies
0311 end
0312 %

```

```

0313 %   Solve the differential equations using RK 4th order method.
0314 %
0315 for i=2:K
0316 for j=1:n
0317 %
0318 %   Compute intermediate steps.
0319 %
0320 X=r(i-1,:,j);
0321 acc(i,:,j)=B/norm(X)^(3)*X;
0322 a=acc(i,:,j);
0323 v1=dt*a;
0324 r1=dt*v(i-1,:,j);
0325
0326 X=r(i-1,:,j)+1/2*r1;
0327 a=B/norm(X)^(3)*X;
0328 v2=dt*a;
0329 r2=dt*(v(i-1,:,j)+1/2*v1);
0330
0331 X=r(i-1,:,j)+1/2*r2;
0332 a=B/norm(X)^(3)*X;
0333 v3=dt*a;
0334 r3=dt*(v(i-1,:,j)+1/2*v2);
0335
0336 X=r(i-1,:,j)+r3;
0337 a=B/norm(X)^(3)*X;
0338 v4=dt*a;
0339 r4=dt*(v(i-1,:,j)+v3);
0340 %
0341 %   Compute ith step.
0342 %
0343 r(i,:,j)=r(i-1,:,j)+(r1+2*(r2+r3)+r4)/6;
0344 v(i,:,j)=v(i-1,:,j)+(v1+2*(v2+v3)+v4)/6;
0345 %
0346 %   Compute ith values.
0347 %
0348 rmag(i,j)=norm(r(i,:,j));
0349 PE(i,j)=B/rmag(i,j);
0350 vmag(i,j)=norm(v(i,:,j));
0351 KE(i,j)=0.5*vmag(i,j)^2;
0352 amag(i,j)=norm(acc(i,:,j));
0353 E(i,j)=PE(i,j)+KE(i,j);
0354 end
0355 end
0356 elseif EXP==2
0357 %% Foil Experiment

```

```

0358 %
0359 %   Preallocate data arrays.
0360 %
0361 Theta=zeros(n,3);
0362 r_N=zeros(layers*N,2);
0363 %
0364 %   Define initial alpha-particle y-positions.
0365 %
0366 X=linspace(-n/(2*AlphaDensity),n/(2*AlphaDensity),n);
0367 %
0368 %   Define x-positions for detector.
0369 %
0370 xdet=linspace(0,Xdet,1000);
0371 %
0372 %   Define nuclei positions.
0373 %
0374 rN=linspace(-sep*(N-1)/2,sep*(N-1)/2,N);
0375 for i=1:layers*N
0376 r_N(i,1)=floor((i-1)/N)*sqrt(3)*0.5*sep;
0377 r_N(i,2)=rN(mod(i-1,N)+1)-mod(floor((i-1)/N),2)*sep/2;
0378 end
0379 %
0380 %   Define time parameter.
0381 %
0382 Time=min([3*sqrt(3)*layers*sep+abs(x0) Xdet+abs(x0)])/vx0;
0383 %
0384 %   Solve the differential equations using MATLAB's ODE45.m
0385 %
0386 for i=1:n
0387 %
0388 %   Solves the differential equations for the ith particle.
0389 %
0390 if i==1
0391 [T,Y] = ode45(@(t,y) scatter(t,y,layers,N,sep,B),...
0392 [0 Time],[x0 X(i) vx0 0]);
0393 %
0394 %   Preallocate initial data array.
0395 %
0396 S=size(Y);
0397 R=zeros(S(1)+1,S(2)+1,n);
0398 else
0399 [T,Y] = ode45(@(t,y) scatter(t,y,layers,N,sep,B),[0 Time],[x0 X(i) vx0 0]);
0400 end
0401 %
0402 %   Trim data so that the trajectory ends at the 'detector'.

```

```

0403 %
0404 Ymag=sqrt(Y(:,1).^2+Y(:,2).^2);
0405 if max(Ymag)>=Xdet
0406 j=find(ismember(Ymag>=Xdet,1),1,'first');
0407 Y(j+1:length(Ymag),:)=[];
0408 T(j+1:length(Ymag))=[];
0409 else
0410 j=length(Y(:,1));
0411 end
0412 X1=Y(j-1,1);
0413 Y1=Y(j-1,2);
0414 X2=Y(j,1);
0415 Y2=Y(j,2);
0416 m=(Y2-Y1)/(X2-X1);
0417 b=Y1-m*X1;
0418 Xd=[(-b*m+sqrt((m^2+1)*Xdet^2-b^2))/(m^2+1),...
0419 (-b*m-sqrt((m^2+1)*Xdet^2-b^2))/(m^2+1)];
0420 if sign((X2-X1))==1
0421 Xd=max(Xd);
0422 elseif sign((X2-X1))== -1
0423 Xd=min(Xd);
0424 else
0425 Xd=X2;
0426 end
0427 Yd=m*Xd+b;
0428 Y(j,:)= [Xd Yd Y(j-1,3) Y(j-1,4)];
0429 T(j)=(sqrt(Xd^2+Yd^2)-norm(Y(j-1,1:2)))/norm(Y(j-1,3:4));
0430 %
0431 % Find the 'detectors' angle to detect ith particle.
0432 %
0433 Theta(i,1)=atan(Yd/Xd);
0434 if and(Yd>0,Xd>0)
0435 Theta(i,1)=Theta(i,1);
0436 elseif and(Yd>0,Xd<0)
0437 Theta(i,1)=Theta(i,1)+pi;
0438 elseif and(Yd<0,Xd<0)
0439 Theta(i,1)=Theta(i,1)+pi;
0440 elseif and(Yd<0,Xd>0)
0441 Theta(i,1)=Theta(i,1)+2*pi;
0442 end
0443 Theta(i,2)=sign(Xd);
0444 Theta(i,3)=j;
0445 %
0446 % Store final data for ith trajectory.
0447 %

```

```

0448 S=size(Y);
0449 Sr=size(R);
0450 if S(1)<Sr(1)
0451 T(S(1)+1:Sr(1))=0;
0452 Y(S(1)+1:Sr(1),:)=0;           % NOTE:
0453 Y(S(1)+1,:)=sqrt(3)*pi;       % sqrt(3)*pi is used here as
0454 T(S(1)+1)=sqrt(3)*pi;         % a marker to signify the end
0455 R(:,1,i)=T;                   % of the actual data for the
0456 R(:,2:S(2)+1,i)=Y;           % ith trajectory. This is
0457 elseif S(1)>Sr(1)             % done since ODE45.m may use
0458 R(Sr(1)+1:S(1)+1,,:)=0;       % a various number of steps
0459 R(Sr(1)+1,,:)=sqrt(3)*pi;    % to find the trajectories of
0460 Y(S(1)+1,:)=sqrt(3)*pi;       % different particles.
0461 T(S(1)+1)=sqrt(3)*pi;
0462 R(:,1,i)=T;
0463 R(:,2:S(2)+1,i)=Y;
0464 else
0465 Y(S(1)+1,:)=sqrt(3)*pi;
0466 T(S(1)+1)=sqrt(3)*pi;
0467 R(S(1)+1,,:)=sqrt(3)*pi;
0468 R(:,1,i)=T;
0469 R(:,2:S(2)+1,i)=Y;
0470 end
0471 end
0472 end
0473 %% Distance of Closest Approach
0474 %
0475 %   Define set of data to represent the target nuclei in the plots.
0476 %
0477 ydet1=sqrt((Xdet)^2-xdet.^2);
0478 ydet2=-ydet1; %#ok<NASGU>
0479 x=linspace(-d,d,500);
0480 y1=sqrt((d)^2-x.^2);
0481 y2=-y1; %#ok<NASGU>
0482 %% Save Final Data
0483 C=clock-C;
0484 C=((C(3)*24+C(4))*60+C(5))*60+C(6);
0485 Res=which([FileName '.mat']);
0486 while strcmp(Res,'')==0
0487 FileName2=[FileName 'c'];
0488 display([FileName ' already exists.']);
0489 display(['File renamed ' FileName2]);
0490 FileName=FileName2;
0491 Res=which([FileName '.mat']);
0492 end

```

```
0493 save([FileName '.mat'])
```

### scatter.m

```
0001 function dy = scatter(t,y,layers,N,sep,B)
0002 % scatter.m is used with AlphaScat.m to model the interactions between a
0003 % thin foil of a specified material and alpha particles. ODE45.m
0004 % calls scatter.m for each iteration of a 'Foil' experiment to solve
0005 % the system of differential equations numerically.
0006 %
0007 dy = zeros(4,1);
0008 dy(1) = y(3);
0009 dy(2) = y(4);
0010 dy(3) = 0;
0011 dy(4) = 0;
0012 r_N=zeros(layers*N,2);
0013 rN=linspace(-sep*(N-1)/2,sep*(N-1)/2,N);
0014 for i=1:layers*N
0015 r_N(i,1)=floor((i-1)/N)*sqrt(3)*0.5*sep;
0016 r_N(i,2)=rN(mod(i-1,N)+1)-mod(floor((i-1)/N),2)*sep/2;
0017 dy(3)=dy(3)+B*(y(1)-r_N(i,1))/((y(1)-r_N(i,1))^2+(y(2)-r_N(i,2))^2)^(1.5);
0018 dy(4)=dy(4)+B*(y(2)-r_N(i,2))/((y(1)-r_N(i,1))^2+(y(2)-r_N(i,2))^2)^(1.5);
0019 end
```

### 6.6.2 AlphaCount.m

```
0001 function C=AlphaCount(FileName,ddT)
0002 % AlphaCount.m is the second of three functions that are used to model
0003 % various alpha scattering experiments. AlphaCount.m accesses the
0004 % data file saved by AlphaScat.m to find the angular distributions of
0005 % the corresponding experiment. For 'Atom' experiments, the possible
0006 % angles of detection range is [0,2pi]; however, for the 'Foil'
0007 % experiment the range is only [0,pi/2] and [3pi/2,2pi). The x and y
0008 % data for 'Atom' experiment is trimmed here so that the trajectories
0009 % end at the detector. A similar method is used for the 'Foil' data,
0010 % but that occurs in AlphaScat.m.
0011 %
0012 %
0013 % INPUTS:
0014 %     FileName - This input should be the name of a data file (.mat
0015 %               format) that was created by AlphaScat.m or
0016 %               AlphaCount. The data file is loaded in order
0017 %               to sort the appropriate data.
0018 %               Ex. 'AuAtom101' or 'AuAtom101.mat'
0019 %     ddT - This input is the angle step size used to count the alpha
0020 %           particles. Therefore, the Count data should be
```

```

0021 %                               interpreted as follows,
0022 %                               Ex. If, at some angle T, Count=5 then this would mean
0023 %                               that from T-ddT to T 5 particles wer counted.
0024 %
0025 %   OUTPUTS:
0026 %       C - This is the total time taken to run AlphaCount.
0027 %
0028 %       NOTE: The new data, along with the data loaded from the file,
0029 %       FileName, is saved as a new data file (.mat format).
0030 %       Ex. If FileName='AuAtom101' and ddT=0.01 then the new
0031 %       file would be 'AuAtom101dT~10E-2'
0032 %
0033 format long
0034 Cc=clock;           % Define start time.
0035 %% Check Arguments
0036 if nargin < 2
0037 ddT=0.02;
0038 if nargin < 1
0039 error('Not enough inputs. Please provide filename.');
```

```

0040 end
0041 end
0042 %% Load Data File
0043 load(FileName)
0044 C=Cc;
0045 clear Cc
0046 dT=ddT;
0047 clear ddT
0048 %% Count for Atom Experiment or Foil Experiment
0049 if EXP==1
0050 %% Atom Experiment Data Trim and Count
0051 Theta=zeros(1,n); 0052     for i=1:n
0053 %
0054 %   Trim Data so that the trajectory ends at the detector line.
0055 %
0056 if i==1
0057 if max(max(rmag))>=Xdet
0058 [j,CC]=find(ismember(rmag>=Xdet,1),1,'first');
```

```

0059 r(j+1:length(rmag(:,i)),:,:)=[];
0060 v(j+1:length(rmag(:,i)),:,:)=[];
0061 else
0062 j=length(rmag(i));
0063 end
0064 end
0065 X1=r(j-1,1,i);
0066 Y1=r(j-1,2,i);
```

```

0067 X2=r(j,1,i);
0068 Y2=r(j,2,i);
0069 m=(Y2-Y1)/(X2-X1);
0070 b=Y1-m*X1;
0071 Xd=[(-b*m+sqrt((m^2+1)*Xdet^2-b^2))/(m^2+1),...
0072 (-b*m-sqrt((m^2+1)*Xdet^2-b^2))/(m^2+1)];
0073 if sign((X2-X1))==1
0074 Xd=max(Xd);
0075 elseif sign((X2-X1))== -1
0076 Xd=min(Xd);
0077 else
0078 Xd=X2;
0079 end
0080 Yd=m*Xd+b;
0081 r(j,1,i)=Xd;
0082 r(j,2,i)=Yd;
0083 %
0084 % Find the angles at which the alpha particle is detected.
0085 %
0086 Theta(i)=atan(Yd/Xd);
0087 if and(Yd>0,Xd>0)
0088 Theta(i)=Theta(i);
0089 elseif and(Yd>0,Xd<0)
0090 Theta(i)=Theta(i)+pi;
0091 elseif and(Yd<0,Xd<0)
0092 Theta(i)=Theta(i)+pi;
0093 elseif and(Yd<0,Xd>0)
0094 Theta(i)=Theta(i)+2*pi;
0095 end
0096 end
0097 %
0098 % Count the alpha particles.
0099 %
0100 DT=ceil(2*pi/dT);
0101 Count=zeros(1,DT);
0102 dTheta=zeros(1,DT); 0103 for i=1:DT
0104 dTheta(i)=i*dT;
0105 for j=1:n
0106 if and(Theta(j)>=(i-1)*dT,Theta(j)<(i)*dT)
0107 Count(i)=Count(i)+1;
0108 end
0109 end
0110 end
0111 elseif EXP==2
0112 %% Count Alpha Particles for 'Foil' Experiment

```

```

0113 DT=ceil(2*pi/dT);
0114 Count=zeros(1,DT);
0115 dTheta=zeros(1,DT);
0116 for i=1:DT
0117 dTheta(i)=i*dT;
0118 for j=1:n
0119 if and(and(Theta(j,1)>=(i-1)*dT,Theta(j,1)<dT*(i)),Theta(j,2)~-1)
0120 Count(i)=Count(i)+1;
0121 end
0122 end
0123 end
0124 else
0125 display('Incorrect File.');
```

```

0126 end
0127 %% Save Final Data
0128 FileName=[FileName 'dT~10E' num2str(round(log(dT)/log(10)))];
```

```

0129 Res=which([FileName '.mat']);
0130 if strcmp(Res,'')==0;
0131 FileName2=[FileName '(c)'];
0132 display([FileName ' already exists.']);
0133 display(['File renamed ' FileName2]);
0134 FileName=FileName2;
0135 end
0136 C=clock-C;
0137 C=((C(3)*24+C(4))*60+C(5))*60+C(6);
0138 save(FileName)
```

### 6.6.3 AlphaPlot.m

```

0001 function C=AlphaPlot(FileName, Trajectories, Magnitudes,...
0002 Energies, Angles, PARTs)
0003 % AlphaPlot.m is the third of three functions that are used to model
0004 % various alpha scattering experiments. AlphaPlot.m accesses the
0005 % data file saved by AlphaCount.m to build figures that graphically
0006 % show the results of the experiments. The Trajectory plots also
0007 % use red circles as a visual aid; these represent the target nuclei.
0008 % The radius of each circle is the minimum separation distance between
0009 % and alpha particle that the alpha particle, with a given initial
0010 % velocity, can reach.
0011 %
0012 %
0013 % INPUTS:
0014 % AlphaPlot(FileName)
0015 % FileName - This input should be the name of a data file (.mat
0016 % format) that was created by AlphaScat.m or
0017 % AlphaCount. The data file is loaded in order
```

0018 %                   to build the appropriate figures.  
0019 %                   Ex. 'AuAtom101' or 'AuAtom101.mat'  
0020 %  
0021 %                   AlphaPlot(FileName, Trajectories)  
0022 %                   Trajectories - This input should be either 'on' or 'off'  
0023 %                   (default, 'on'). It determines whether or not  
0024 %                   the 'Trajectories' figure will be built. This  
0025 %                   shows the path of each alpha trajectory.  
0026 %  
0027 %                   AlphaPlot(FileName, Trajectories, Magnitudes)  
0028 %                   Magnitudes - This input should be either 'on' or 'off'  
0029 %                   (default, 'on'). It determines if the  
0030 %                   'Magnitudes' figure will be built. This figure  
0031 %                   shows the plots of distance, speed, and  
0032 %                   acceleration all vs time.  
0033 %  
0034 %                   NOTE: The following two inputs are disregarded if the data  
0035 %                   file is from a 'Foil' experiment.  
0036 %  
0037 %                   AlphaPlot(FileName, Trajectories, Magnitudes,...  
0038 %                   Energies)  
0039 %                   Energies - This input should be either 'on' or 'off' (default,  
0040 %                   'on'). It determines if the 'Energies' figure  
0041 %                   will be built. This figure shows the plots of  
0042 %                   Kinetic Energy and Potential Energy both vs  
0043 %                   time; as well as, the Total Energy vs initial  
0044 %                   distance.  
0045 %  
0046 %                   AlphaPlot(FileName, Trajectories, Magnitudes,...  
0047 %                   Energies, Angles)  
0048 %                   Angles - This input should be either 'on' or 'off' (default,  
0049 %                   'on'). It determines if the 'Angles' figure  
0050 %                   will be built. This figure shows the angular  
0051 %                   distribution (Percent Counts vs Angle) of the  
0052 %                   detector 'counts'. This is scaled by  
0053 %                   100/max(Count), where max(Count) is the maximum  
0054 %                   number of alpha particles detected within a  
0055 %                   certain range dT.  
0056 %  
0057 %                   AlphaPlot(FileName, Trajectories, Magnitudes,...  
0058 %                   Energies, Angles, PARTs)  
0059 %                   PARTs - This input determines the range of data sets that will  
0060 %                   be represented by the figures, (default, [1 n]  
0061 %                   where n is loaded from file). It needs to be  
0062 %                   an integer array of length 2, the first entry

```

0063 %           will be the starting data set and the second
0064 %           will be the last data set.
0065 %           Ex. [2,5] or [2 5] or [2;5] will yield figures that
0066 %           represent the data for the 2nd to the 5th alpha
0067 %           particle.
0068 %
0069 %           NOTE: All arguments, except the FileName, can be omitted and their
0070 %           default values will be assumed.
0071 %
0072 %   OUTPUTS:
0073 %           C - This is the total time taken to run AlphaPlot.
0074 %
0075 %           NOTE: All of the figures that are built are displayed and saved in
0076 %           .jpg and .fig formats.
0077 %
0078 format long 0079
0080 Cc=clock;           % Define start time.
0081 close all          % Closes all open figures to avoid holding
0082 %   previous data.
0083 %% Check Arguments
0084 if nargin < 6
0085 PARTs='all';
0086 if nargin < 5
0087 Angles='on';
0088 if nargin < 4
0089 Energies='on';
0090 if nargin < 3
0091 Magnitudes='on';
0092 if nargin < 2
0093 Trajectories='on';
0094 if nargin < 1
0095 error(...
0096 'Not enough inputs. Please provide filename.');
```

```

0097 end
0098 end
0099 end
0100 end
0101 end
0102 end
0103 %% Load Data File
0104 load(FileName)
0105 C=Cc;
0106 clear Cc
0107 %
0108 %   Define range of alpha particle data sets used to build plots.  If the
```

```

0109 %         range is beyond the number of data sets available in the data file,
0110 %         all the sets will be used.
0111 if strcmp(PARTs,'all')==1
0112 PARTs=[1 n];
0113 elseif or(max(PARTs)>n,or(min(PARTs)<1,min(PARTs)~=PARTs(1)))
0114 PARTs=[1 n]; 0115 end
0116 %% Build Figures for the Atom Experiment or the Foil Experiment
0117 if EXP==1
0118 %% Atom Experiment Figures
0119 %
0120 %   Plot y vs. x, x vs. time, and y vs. time in figure(1).
0121 %
0122 if strcmp(Trajectories,'on')==1
0123 figure(1)
0124 hold on
0125 plot(x,y1,'r',x,y2,'r')
0126 plot(xdet,ydet1,'--k',xdet,ydet2,'--k')
0127 for j=PARTs(1):PARTs(2)
0128 plot(r(:,1,j),r(:,2,j))
0129 end
0130 xlabel('(fm)')
0131 ylabel('(fm)')
0132 %
0133 % Define filename to save figure in both .fig and .jpg file
0134 %   formats.
0135 %
0136 if or(PARTs(1)~=1,PARTs(2)~=n)
0137 Figure=[FileName 'Trajectories' ...
0138 int2str(PARTs(1)) '-' int2str(PARTs(2))];
0139 else
0140 Figure=[FileName,'Trajectories'];
0141 end
0142 Res=which([Figure '.jpg']);
0143 if strcmp(Res,'')==0;
0144 Figure2=[Figure '(c)'];
0145 display([Figure '.jpg' 'already exists.']);
0146 display(['File renamed ' Figure2 '.jpg']);
0147 Figure=Figure2;
0148 end
0149 hgsave(figure(1),Figure)
0150 Figure=[Figure '.jpg'];
0151 saveas(figure(1),Figure);
0152 end
0153 %
0154 %   Plot distance vs. time, speed vs. time, and

```

```

0155 %           acceleration vs. time in figure(2).
0156 %
0157 if strcmp(Magnitudes,'on')==1
0158 figure(2)
0159 hold on
0160 for j=PARTs(1):PARTs(2)
0161 hold on
0162 subplot(3,1,1)
0163 plot(T,rmag(:,j))
0164 hold on
0165 subplot(3,1,2)
0166 plot(T,vmag(:,j))
0167 hold on
0168 subplot(3,1,3)
0169 plot(T,amag(:,j))
0170 end
0171 subplot(3,1,1)
0172 xlabel('Time (e-22 s)')
0173 ylabel('D (fm)')
0174 subplot(3,1,2)
0175 xlabel('(e-22 s)')
0176 ylabel('S (e22 fm/s)')
0177 subplot(3,1,3)
0178 xlabel('(e-22 s)')
0179 ylabel('A (e44 fm/s^2)')
0180 %
0181 % Define filename to save figure in both .fig and .jpg file
0182 %   formats.
0183 %
0184 if or(PARTs(1)~=1,PARTs(2)~=n)
0185 Figure=[FileName 'Magnitudes' ...
0186 int2str(PARTs(1)) '-' int2str(PARTs(2))];
0187 else
0188 Figure=[FileName 'Magnitudes'];
0189 end
0190 Res=which([Figure '.jpg']);
0191 if strcmp(Res,'')==0;
0192 Figure2=[Figure '(c)'];
0193 display([Figure '.jpg' 'already exists.']);
0194 display(['File renamed ' Figure2 '.jpg']);
0195 Figure=Figure2;
0196 end
0197 hgsave(figure(2),Figure)
0198 Figure=[Figure '.jpg'];
0199 saveas(figure(2),Figure);

```

```

0200 end
0201 %
0202 %   Plot Potential energy vs. x, Kinetic energy vs. time, and
0203 %       Total Energy vs. initial distance in figure(3).
0204 %
0205 if strcmp(Energies,'on')==1
0206 figure(3)
0207 hold on
0208 for j=PARTs(1):PARTs(2)
0209 subplot(3,2,1)
0210 hold on
0211 plot(T,PE(:,j))
0212 subplot(3,2,2)
0213 hold on
0214 plot(T,KE(:,j))
0215 end
0216 subplot(3,2,[3,6])
0217 plot(rmag(1,PARTs(1):PARTs(2)),E(1,PARTs(1):PARTs(2)),'o')
0218 subplot(3,2,1)
0219 xlabel('(e-22 s)')
0220 ylabel('PE (*4.15 MeV)')
0221 subplot(3,2,2)
0222 xlabel('(e-22 s)')
0223 ylabel('KE (*4.15 MeV)')
0224 subplot(3,2,[3,6])
0225 xlabel('(fm)')
0226 ylabel('E (*4.15 MeV)')
0227 %
0228 % Define filename to save figure in both .fig and .jpg file
0229 %   formats.
0230 %
0231 if or(PARTs(1)~=1,PARTs(2)~=n)
0232 Figure=[FileName 'Energies' ...
0233 int2str(PARTs(1)) '-' int2str(PARTs(2))];
0234 else
0235 Figure=[FileName 'Energies'];
0236 end
0237 Res=which([Figure '.jpg']);
0238 if strcmp(Res,'')==0;
0239 Figure2=[Figure '(c)'];
0240 display([Figure '.jpg' 'already exists.']);
0241 display(['File renamed ' Figure2 '.jpg']);
0242 Figure=Figure2;
0243 end
0244 hgsave(figure(3),Figure)

```

```

0245 Figure=[Figure '.jpg'];
0246 saveas(figure(3),Figure);
0247 end
0248 %
0249 %   Plot angular distribution of the alpha particles intersecting the
0250 %       detectors path in figure(4).
0251 %
0252 if strcmp(Angles,'on')==1
0253 figure(4)
0254 CountMax=max(Count);
0255 plot(dTheta,Count/CountMax*100,'o','MarkerSize',3)
0256 ylim([-5 105]);
0257 set(gca,'YTick',[0 25 50 75 100]);
0258 set(gca,'YTickLabel','0','25','50','75','100');
0259 xlim([-pi/4 9*pi/4]);
0260 set(gca,'XTick',[0 pi/2 pi 3*pi/2 2*pi]);
0261 set(gca,'XTickLabel','0','pi/2','pi','3pi/2','2pi');
0262 ylabel('Counts')
0263 xlabel('Angle (rad.)')
0264 if or(PARTs(1)~=1,PARTs(2)~=n)
0265 Figure=[FileName 'Angles' ...
0266 int2str(PARTs(1)) '-' int2str(PARTs(2))];
0267 else
0268 Figure=[FileName 'Angles'];
0269 end
0270 Res=which([Figure '.jpg']);
0271 if strcmp(Res,'')==0;
0272 Figure2=[Figure '(c)'];
0273 display([Figure '.jpg' ' already exists.']);
0274 display(['File renamed ' Figure2 '.jpg']);
0275 Figure=Figure2;
0276 end
0277 hgsave(figure(4),Figure)
0278 Figure=[Figure '.jpg'];
0279 saveas(figure(4),Figure);
0280 end
0281 elseif EXP==2
0282 %% Foil Experiment Figures
0283 %
0284 %   Plot y vs. x in figure(1).
0285 %
0286 if strcmp(Trajectories,'on')==1
0287 figure(1)
0288 hold on
0289 plot(xdet,ydet1,'--k',xdet,ydet2,'--k');

```

```

0290 for j=1:layers*N
0291 plot(x+r_N(j,1),y1+r_N(j,2),'r',x+r_N(j,1),y2+r_N(j,2),'r');
0292 end
0293 for i=PARTs(1):PARTs(2)
0294 I=find(ismember(R(:,1,i),sqrt(3)*pi));
0295 Y=R(1:I-1,:,i);
0296 plot(Y(:,2),Y(:,3))
0297 end
0298 plot(xdet,ydet1,'--k',xdet,ydet2,'--k');
0299 %
0300 % Define filename to save figure in both .fig and .jpg file
0301 %   formats.
0302 %
0303 if or(PARTs(1)~=1,PARTs(2)~=n)
0304 Figure=[FileName 'Trajectories' ...
0305 int2str(PARTs(1)) '-' int2str(PARTs(2))];
0306 else
0307 Figure=[FileName 'Trajectories'];
0308 end
0309 Res=which([Figure '.jpg']);
0310 if strcmp(Res,'')==0;
0311 Figure2=[Figure '(c)'];
0312 display([Figure '.jpg' ' already exists.']);
0313 display(['File renamed ' Figure2 '.jpg']);
0314 Figure=Figure2;
0315 end
0316 hgsave(figure(1),Figure)
0317 Figure=[Figure '.jpg'];
0318 saveas(figure(1),Figure);
0319
0320 end
0321 %
0322 %   Plot angular distribution of the alpha particles intersecting the
0323 %   detectors path in figure(2).
0324 %
0325 if strcmp(Angles,'on')==1
0326 figure(2)
0327 CountMax=max(Count);
0328 plot(dTheta,Count/CountMax*100,'o','MarkerSize',3)
0329 ylim([-5 105]);
0330 set(gca,'YTick',[0 25 50 75 100]);
0331 set(gca,'YTickLabel','0','25','50','75','100');
0332 xlim([-pi/4 9*pi/4]);
0333 set(gca,'XTick',[0 pi/2 pi 3*pi/2 2*pi]);
0334 set(gca,'XTickLabel','0','pi/2','pi','3pi/2','2pi');

```

```

0335 ylabel('Percent Counts')
0336 xlabel('Angle (rad.)')
0337 %
0338 % Define filename to save figure in both .fig and .jpg file
0339 %   formats.
0340 %
0341 if or(PARTs(1)~=1,PARTs(2)~=n)
0342 Figure=[FileName 'Angles' ...
0343 int2str(PARTs(1)) '-' int2str(PARTs(2))];
0344 else
0345 Figure=[FileName 'Angles'];
0346 end
0347 Res=which([Figure '.jpg']);
0348 if strcmp(Res,'')==0;
0349 Figure2=[Figure '(c)'];
0350 display([Figure '.jpg' 'already exists.']);
0351 display(['File renamed ' Figure2 '.jpg']);
0352 Figure=Figure2;
0353 end
0354 hgsave(figure(2),Figure)
0355 Figure=[Figure '.jpg'];
0356 saveas(figure(2),Figure);
0357 end
0358 else
0359 display('Incorrect file.')
0360 end
0361 %% Calculate Total Run Time
0362 C=clock-C; 0363 C=((C(3)*24+C(4))*60+C(5))*60+C(6);

```

#### 6.6.4 Depth Calculation Code

```

0001 clear
0002 format long
0003 u=linspace(0,8191,8192);
0004 u=(17.9+u*0.409)*0.001;
0005
0006 vW=zeros(size(u));
0007 vA=zeros(size(u));
0008 vC=zeros(size(u));
0009 vS=zeros(size(u));
0010 0011 W=textread('water.txt');
0012 A=textread('air.txt');
0013 C=textread('carbon.txt');
0014 S=textread('silicon.txt');
0015
0016 pW=0.25;

```

```

0017 pA=0.25;
0018 pC=0.167;
0019 pS=0.333;
0020
0021 dW=1;
0022 dA=1.205*10(-3);
0023 dC=1.7;
0024 dS=2.33;
0025
0026 xW=W(:,1);
0027 yW=W(:,2);
0028 xA=A(:,1);
0029 yA=A(:,2);
0030 xC=C(:,1);
0031 yC=C(:,2);
0032 xS=S(:,1);
0033 yS=S(:,2);
0034
0035 for i=1:length(u)
0036 U=u(i);
0037 vW(i)=splinetx(xW,yW,U);
0038 vA(i)=splinetx(xA,yA,U);
0039 vC(i)=splinetx(xC,yC,U);
0040 vS(i)=splinetx(xS,yS,U);
0041 end
0042 v=vW*dW*pW+vA*dA*pA+vC*dC*pC+vS*dS*pS;
0043 v=1./v*log(10);
0044
0045 figure(1)
0046 loglog(u,vW,'-s',xW,yW)
0047 figure(2)
0048 plot(log(u)/log(10),log(vA)/log(10),log(xA)/log(10),log(yA)/log(10))
0049 figure(3)
0050 plot(log(u)/log(10),log(vC)/log(10),log(xC)/log(10),log(yC)/log(10))
0051 figure(4)
0052 plot(log(u)/log(10),log(vS)/log(10),log(xS)/log(10),log(yS)/log(10))
0053 figure(5)
0054 plot(log(u)/log(10),v)
0055
0056 csvwrite('depth.csv',v')

```

# Bibliography

- [1] Bethe, H A. Elementary Nuclear Theory. New York: John Wiley and Sons, 1947.
- [2] Yuan, Luke C.L. Methods of Experimental Physics. New York: Academic Press, 1961.
- [3] Dehesa, J S, J M.G. Gomez, and A Polls. Mathematical and Computational Methods in Nuclear Physics . New York: Springer-Verlag, 1984.
- [4] Krane, Kenneth S. Introductory Nuclear Physics. Hoboken, NJ: John Wiley and Sons, Inc., 1988.
- [5] Eichholz, Geoffrey G, and John W Poston. Principles of Nuclear Radiation Detection. Ann Arbor, MI: Ann Arbor Science, 1980.
- [6] Cohen, Bernard L. Concepts of Nuclear Physics. New York: McGraw-Hill, 1971.
- [7] Moler, Cleve B. Numerical Computing with MATLAB. Philadelphia, PA: Society for Industrial and Applied Mathematics, 2004.
- [8] Clementi, E. Raimondi, D. L. and Reinhart, W. P. The Journal of Chemical Physics, 1967, 47, 1300.
- [9] Rutherford, Earnest. The Scattering of  $\alpha$  and  $\beta$  Particles by Matter and the Structure of the Atom. Philosophical Magazine Series 6, Vol 21. May 1911. p. 669-688.
- [10] Geiger, H. Mardsen, E. On a Diffuse Reflection of the  $\alpha$ -Particles Proc. Roy. Soc. 1909 A vol. 82, p. 495-500
- [11] Hubble, J. Seltzer S. National Institute of Standards and Technology. Tables of X-Ray Mass Attenuation Coefficients and Mass Energy-Absorption Coefficients.  
<http://physics.nist.gov/PhysRefData/XrayMassCoef/ComTab/air.html>  
<http://physics.nist.gov/PhysRefData/XrayMassCoef/ComTab/water.html>  
<http://physics.nist.gov/PhysRefData/XrayMassCoef/ElemTab/z06.html>  
<http://physics.nist.gov/PhysRefData/XrayMassCoef/ElemTab/z14.html>
- [12] Westinghouse Savannah River Company. Savannah Environmental Report.  
<http://www.ornl.gov/sci/envrpt/aser95/tb-a-2.pdf>
- [13] United Nations Scientific Committee on the effects of Atomic Radiation. Exposures from Natural Radiation Sources. 2001 Vol 1. Annex B. <http://www.unscear.org/docs/reports/annexb.pdf> p. 92 - 108
- [14] Nave, R. Rutherford Scattering. <http://hyperphysics.phy-astr.gsu.edu/hbase/rutsa.html>

- [15] United States Nuclear Regulatory Commission. Definitions <http://www.nrc.gov/reading-rm/doc-collections/cfr/part034/part034-0003.html>
- [16] International Commission on Radiological Protection. Summary of Recommendations. <http://www.icrp.org/docs/SummaryB-scanICRP60AnnICRP1990Recs.pdf>